Assessment of Field Surface Treatments for Prolonging the Life of Steel Welded Joints Subjected to Fatigue Loading

Mark S. Van Sickle

A thesis

submitted in partial fulfillment of the

requirements for the degree of

Master of Science in Mechanical Engineering

University of Washington

2013

Committee:

Ramulu Mamidala

John Kramlich

Paul Edwards

Program Authorized to Offer Degree:

Mechanical Engineering

Table of Contents

List of Figures

List of Tables

Chapter 1 Introduction and Objectives

Off-highway trucks operate in severe conditions and over severe surfaces. It is not unusual for off-highway vehicles operating in the field to be operating in remote regions of the world, many miles away from full service fabrication facilities. The duty cycles for these trucks varies greatly. It is not possible for the truck original equipment manufacturer (OEM) to foresee all of the potential applications and payloads that will be required of the vehicle. Figure 1.1 shows an off-highway Kenworth truck used in oil field service in the Middle East. Other potential applications include mining service or severe logging service in the extreme North.

Figure 1.1 Kenworth Off-Highway Truck

In these applications the truck owner modifies the truck as needed to suit their application. In cases where a fatigue issue is discovered in the field the customer desires to have

low-cost methods to improve performance or make repairs in the field without transporting the truck to areas where complex manufacturing services may be available.

In heavy truck applications welds are commonly used to join structural steel components that are subjected to cyclical loads of high amplitude. Suspension and brake components are commonly attached to truck axles through the use of welds (Figure 1.2). Some customer applications are more severe than can be reasonably foreseen by product designers. For these severe applications it is desirable to have the ability to field treat welded structures to improve the fatigue service life. Two such fatigue treatments are hammer peening and rotary flap peening. This research will attempt to quantify structural performance benefits that can be obtained through the use of these methods.

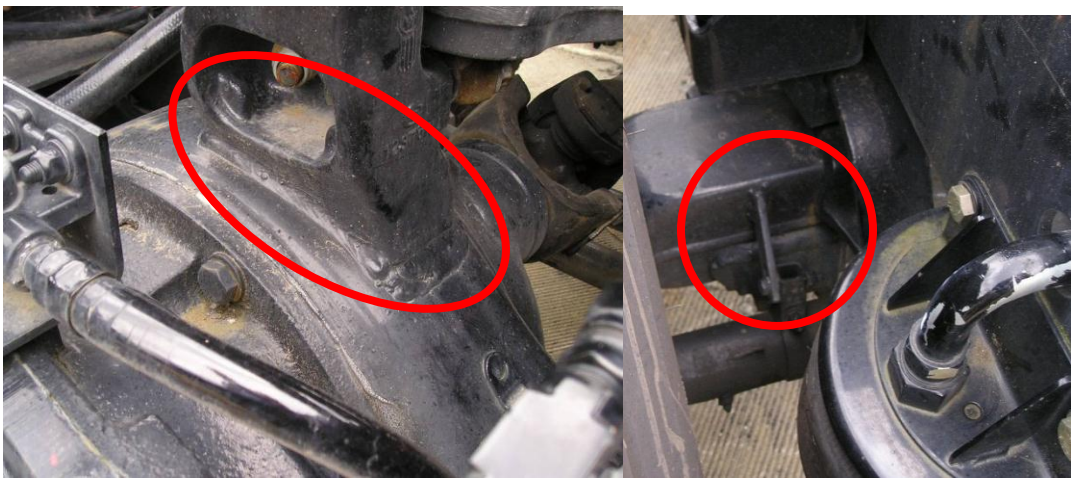

Figure 1.2 Typical Welded Joints on Truck Axle

It is desired that two objectives will be satisfied by this research. The first is to quantify the benefits of two different methods of weld peening that can be easily accomplished in the field. The second objective is to verify fatigue life predictive processes for welded structures and understand how weld peening processes impact weld fatigue life prediction.

Chapter 2 Background Information and Literature Review

2.1 Welded Structures

There is a large body of published information available regarding welded structures, shot peening, hammer peening, rotary flap peening, and methods for predicting fatigue life in welded joints. Of necessity this paper will only review a portion of the literature and will summarize relevant findings.

Welded steel structures are used widely in the truck industry. The author has observed through years of testing truck components that welded structures are more susceptible to fatigue damage than non-welded structures subjected to similar cyclical loading conditions. There are several mechanisms that contribute to the reduced fatigue life in welds. One is that heat introduced by the process of welding produces tensile stresses in the heat affected zone (HAZ). These stresses are generated both by non-uniform temperature gradients and by local elastic/plastic deformations during the welding and cooling processes (Fuchs and Stephens, 1980). These residual internal stresses may be tensile in nature across the weld itself and are detrimental to fatigue life. Maddox (edited by Macdonald, 2011) stated that these residual tensile stresses can approach material yield strength in magnitude in constrained assemblies. This occurs due to the natural expansion and contraction of the material close to the weld heat source and stresses introduced by the restraining effect of adjacent material at lower temperature (Maddox 1991).

The second mechanism that reduces fatigue performance is that the geometry of the weld itself, especially at the base, or toe, of the weld acts as a stress concentration. This concentration may behave similarly to a sharp notch, producing a likely crack initiation site. The stress concentration at the weld toe is also influenced by loading direction, and is particularly severe

when the welded assembly is loaded normal to the weld direction (Maddox, edited by Macdonald, 2011).

The third mechanism that influences welded joint fatigue life is the presence of flaws. Any one of a number of flaws can have a negative impact on weld life through the introduction of additional stress concentrations. Some of these flaws include undercutting at the toe of the weld, the creation of an abrupt weld profile with a convex shape, excessive porosity, slag inclusions, lack of fusion, and incomplete weld root penetration. Welding is a variable process. Properties in the heat affected zone (HAZ) of the parent material may differ based on temperature and speed of the weld process itself. Manual weld processes may result in different weld geometries, have different start and stop points, and varying levels of weld penetration depending on the skill of the operator. Poor welds, with partial penetration, can have significant stress concentrations at the weld root that can be even more severe than the weld toe of a weld with good penetration (Maddox 1991). A worst-case welded joint will have yield-magnitude residual tensile stresses combined with crack-like geometric discontinuities at the weld toe (Maddox, 1991). Maddox summarized three key features that influence fatigue in welded structures in his work compiled by Macdonald (2011). These three features are residual tensile stress, geometric stress concentration at the toe of the weld, and the presence of flaws due to the variations in process.

Several different options are available for improving fatigue resistance of weldments. Fuchs and Stephens (1980) list the following:

1. “Improve the actual welding procedure”.
2. “Alter the material microstructure via improved weld penetration”
3. “Reduce geometrical discontinuities”.
4. “Induce surface compressive self-stresses”

These items are inter-related, as improving the welding procedure will alter the material microstructure and reduce geometric discontinuities. This investigation will focus on weld joint processing methods that induce compressive residual surface stresses. One common method for introducing compressive surface stresses in a metal component is through the use of peening.

2.2 Peening

"Shot peening is a cold working process in which the surface of the part is bombarded with small spherical media called shot." (Metal Improvement Company, 1990) The shot acts as a peening hammer, introducing a dimple on the surface of the part and causing compressive stresses to be imparted. Peening also removes minor crack-like irregularities by dressing the surface being peened. Figure 2.1 is a sketch depicting the residual stress distribution in the sub-surface as a function of distance from the part surface for a component that has been treated by a peening process.

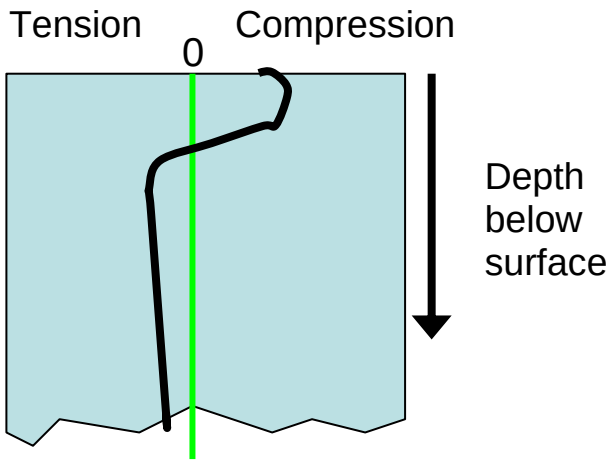

Figure 2.1 Example of Residual Stress Profile Caused by Peening.

Fatigue cracks initiate primarily at the surface of a part (Bhuvaraghan et al. 2010). This is in part because for most loaded components stresses at the surface are greater than at the

interior of the part. For this reason the introduction of compressive residual stresses can improve fatigue performance. The compressive residual stress is linearly superimposed on any tensile stresses that result from part loading. This reduces the mean stress amplitude of the fatigue loading cycle and extends the life of the peened part. This is particularly beneficial in welded joints, where there is a residual tensile stress present from the welding process. Kirkhope et al. (1999) state that the residual compressive stresses introduced by shot peening may be 70 to 80% of the yield stress of the peened material.

While compressive residual stresses are beneficial to cyclic loading, it is possible to over-peen a sample. This causes deterioration in surface integrity and reduction in fatigue strength (Bhuvaraghan et al. 2010). It is desirable to achieve a balance between maximizing the surface residual compressive stress and minimizing reduction in surface integrity. This is commonly done through the measurement of peening intensity, which is related to the amount of kinetic energy transferred from the shot to the part being peened (Miao et al. 2010). The Almen test is commonly used to quantify peening intensity.

The Almen test consists of peening a test strip made of SAE 1070 spring steel with standardized dimensions (Miao, 2010). There are various methods of securing the test strip during peening. 3M makes a magnetic Almen strip test holder that will be used for this effort. The Almen test strip is peened with controlled variables of shot speed, shot size, shot type, incidence angle, duration of peening and number of passes. The Almen strip is removed from the holder. The compressive residual stresses imparted by the peening process will have curved the test strip away from the peened surface. The resulting arc height is measured. This arc height is called the Almen intensity (3M, 2003). Target peening intensities for different materials and thicknesses have been defined in Military Specification MIL-R-81841 (1972).

In addition to intensity, coverage is an important factor in peening. Miao et al. state that coverage is defined as the ratio of area covered by peening indentations to the total treated surface area, expressed as a percentage (2010). They also state that visual inspection is the standard method for coverage evaluation. Since it is difficult to distinguish coverage as 100% is approached, 98% coverage is usually considered full coverage (Miao et al, 2010).

This research will discuss two different methods of peening: hammer peening and shot peening through the use of a rotary flap tool. These two methods are selected because they can both be performed in the field, and do not require significant tooling or equipment expense.

2.3 Hammer Peening

2.3.1 Hammer Peening Process

Hammer peening is a process in which a hardened steel rod or "hammer" is used in conjunction with a pneumatic gun to subject a material to repeated impacts. "The velocity is such that each impact produces plastic deformation of the surface, thereby inducing a compressive stress. The surfaces requiring treatment are traversed at a rate such as to give the required coverage. The process is usually applied manually to local areas of components or assemblies and is therefore subject to limitations of control" (UK Ministry of Defense, 2008). As a manual process, this method of surface impingement is subject to large variation in effectiveness based on impact hammer speed of travel, force of impact, geometry and material of the hammer, angle of impact, etc. The Almen method of peening intensity measurement was not applied to hammer peening in the literature reviewed. This is likely due to the increased depth of the layer of compressive residual stresses induced by hammer peening. Kopsov (1991) noted that hammer peening provides a significantly greater depth of residual compressive stress than

shot peening or roller peening. It is reasonable to conclude that the different stress condition and deeper plastic deformation caused by hammer peening may be incompatible with the Almen test method, which relies on measuring the curvature of a thin test strip.

Hammer peening is applied in various industrial applications, including bridges, viaducts, and off-shore oil equipment. There was no standardized method for hammer peening available for reference. Several different experiments listed key parameters to record for this process. Han, Han and Nam (2008) used an impact rate of 3,600 blows per minute (60 blows per second) using a spherical hammer tip of diameter of 6 mm. Four passes were made over the material at an undefined speed and angle. Bell, Militaru, and Braid (1995) used hammer peening settings of 2,500 blows per minute (42 blows per second) with a 12 mm hammer bit. Six peening passes were used at a tool angle of 45 degrees and a travel rate of 25 mm/sec. Maddox (1998) used hammer settings of 2800 blows per minute (47 blows per second) with a 12mm spherical hammer and four peening passes.

2.3.2 Hammer Peening Experimental Observations

Kopsov (1991) states that hammer peening has advantages over shot peening in that hammer peening can provide a greater depth of compressive residual stress compared to the depth of surface defects. Kopsov found that crack initiation was actually accelerated by a factor of 1.4 to 1.7 for hammer peened samples versus unpeened samples, varying based on the air pressure supplied to the impact tool (1991). It should be noted that Kopsov's samples were cycled at amplitudes to cause crack initiation at 10,000 to 40,000 cycles. Kopsov (1991) found that total life, including crack initiation and propagation, did increase by up to 2.7x for the hammer peened samples.

Kirkhope et al. (1999) stated that hammer peening "produces much higher improvements in fatigue strength than either shot peening or needle peening due to the large amount of cold working produced, which results in the compressive residual stresses penetrating to a greater depth in the plate." They also noted that hammer peening reduced the stress concentration at the weld toe by plastically deforming and smoothing the weld toe radius. Kirkhope et al. (1999) cited other works indicating that in some cases hammer peening of the weld has been so successful that the critical failure location has moved away from the weld and into the base material. Typical improvements in fatigue strength were presented by Kirkhope et al. in Figure 2.2. They report a fatigue strength improvement of 50 to 200% for hammer peening and 30% for shot peening.

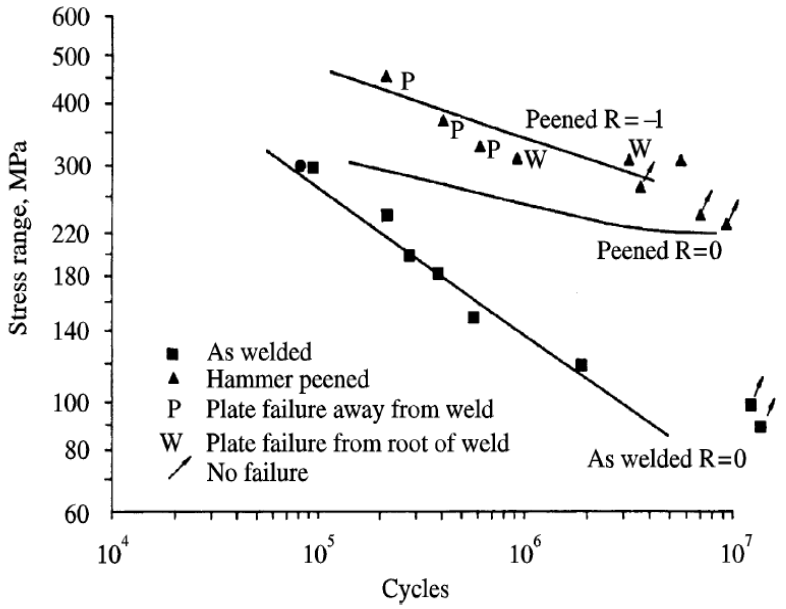

Figure 2.2 Improvement in Fatigue Strength due to Hammer Peening

(Kirkhope et al, 1999)

Maddox (1998) found in his experiment that hammer peening improved the fatigue life of welded specimens by approximately a factor of two, and that the crack initiation site moved from

the weld toe (un-peened samples) to the weld root (peened samples). Bell, Militaru and Braid (1995) found that hammer peening improved the fatigue life of welded joints by a factor of 3 for higher stress ranges and by a factor of 10 for lower stress ranges. They also found that the crack initiation site of the un-peened samples was in the weld toe, with propagation occurring through the base plate. The peened samples experienced crack initiation at the weld root, propagating through the weld throat, then through the base material (Figure 2.3).

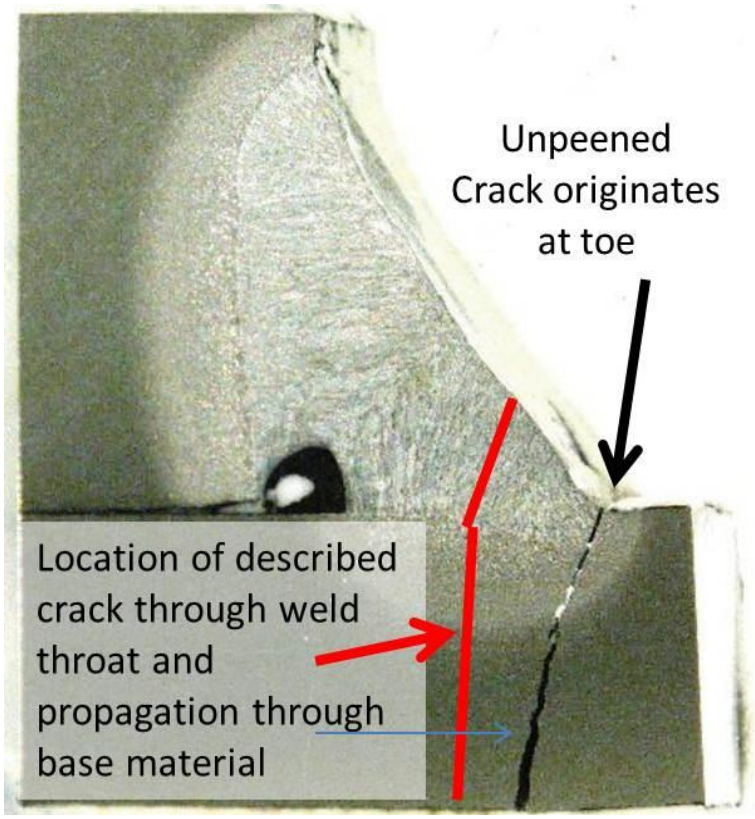

Figure 2.3 Un-Peened vs. Hammer Peened Crack Locations

Han, Han, and Nam (2008) found that the fatigue life of welded steel joints subjected to a stress range of 249 MPa was improved by approximately an order of magnitude. They also found that the fatigue strength at 2 million cycles was roughly 2 times the fatigue strength of the un-peened samples. Furthermore, they also propose that it is possible to analytically predict the fatigue life of welded joints that have been treated by hammer peening. Han et al. propose that

the fatigue life for a hammer peened welded joint can be calculated using a notch strain approach (2008). In this approach, the relation between the maximum notch stress and maximum notch strain can be calculated as follows:

$$\sigma_{max}\epsilon_{max} = \left\{ \frac{K_f S_{max}}{(1-\sigma_r)/\sigma_{max}} \right\}^2 \Big/ E$$

Where:

E = Elastic modulus

K_f = Fatigue notch factor

S_{max} = Maximum nominal stress

σ_{max} = Maximum notch stress

ε_{max} = Maximum notch strain

σ_r = Residual stress

The fatigue crack initiation life can then be obtained by substituting σ_r into Smith, Watson, and Topper's mean stress correction (Han et al., 2008)

Branco, Infante and Baptista (2004) found that hammer peening did improve fatigue performance of welded joints. They also found that fatigue performance of samples peened at cycles = 0 had similar performance to samples that were peened after a crack had begun to initiate.

The study by Bell, Militaru and Braid and the study by Han, Han, and Nam lead opposing conclusions regarding whether fatigue life improvement is better at high stress amplitude (low life) or low stress amplitude (long life). Bell et al. found that greater improvement was found at low stress ranges (1995). Han et al. found that fatigue performance improvements due to

hammer peening are greater at high stress and low life conditions than at low stress high cycle conditions (2008).

2.4 Rotary Flap Peening (Flail Peening)

2.4.1 Rotary Flap Peening Process

Rotary flap peening or flail peening is a peening process that is made possible by a tool developed by 3M corporation called a "Roto Peen" flap peening tool (Parkes, 1975). The UK's Ministry of Defense Standard 03-21 (2008) provides a clear description of the process: "The process entails the use of a thread woven multi-flap rotary brush on which are mounted hard shot, e.g. cast steel or tungsten carbide, (the type depending upon the individual operation), powered by a rotary power tool (Figure 2.4).

Figure 2.4 Rotary Flap Peening Tool (3M, 2003)

The shot impacts the surface of the work piece causing plastic deformation, thereby inducing a compressive stress (Figure 2.5). The surfaces requiring treatment are traversed at a

rate such as to give the required coverage. The process is usually applied manually to local areas of components or assemblies and is particularly useful for the peening of holes."

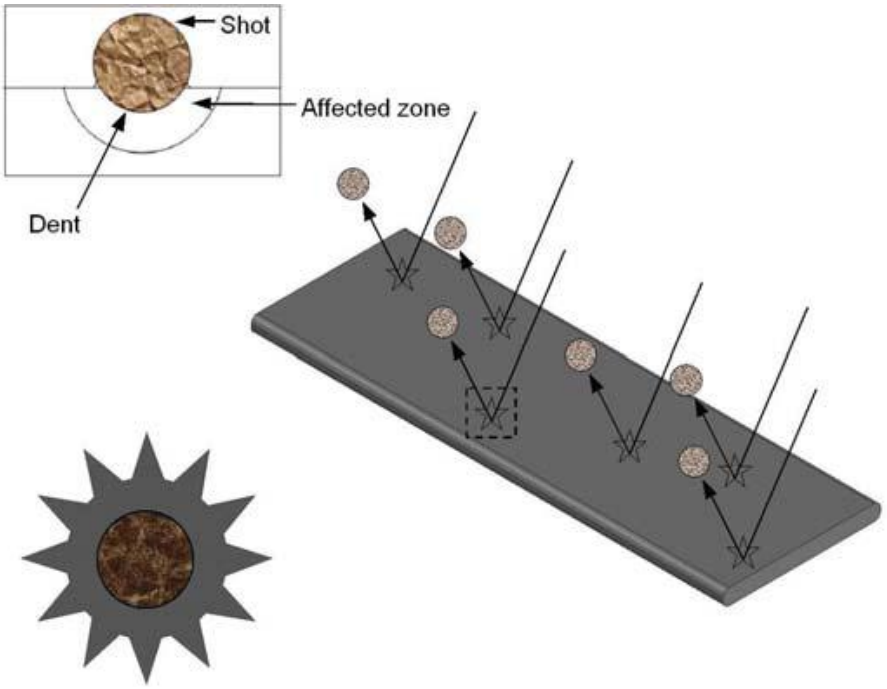

Figure 2.5 Schematic Diagram of Peening Process (Baskaran et al.2010)

The process of using a rotary flap tool for peening is described in detail in Military Specification MIL-R-81841 (1972) and AMS 2590. This procedure will be used as a guideline for preparing test samples for this project. Variables that will need to be controlled include distance from flap core to the surface being peened, tool revolution speed, the flap assembly itself, the speed of travel, type of joint, and the number of times the tool is moved across the part surface. Since the procedure is manual in nature it is highly operator-dependent. To increase the control over the process, peening intensity is measured by Almen strips, using the Almen scale of peen intensity (3M, 2003). These are test strips that are peened on one side. The Almen scale is a measurement of the curvature induced in the test strip after peening (Figure 2.6).

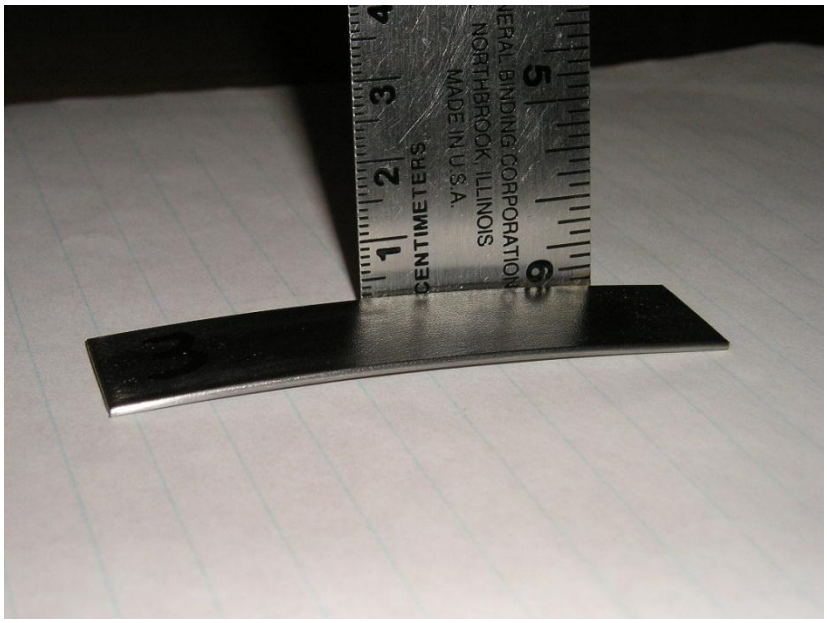

Figure 2.6 Curvature Induced in Almen A Test Strip due to Rotary Flap Peening

Bailey (1999) took an experimental approach to evaluate critical factors impacting the repeatability of the manual flap peening process. Bailey concluded that rotational speed of the peening tool used to spin the mandrel and standoff distance from the peened surface were the major variables of peening intensity control.

Typical applications for rotary flap peening include the peening of weld heat affected zones, landing gear assemblies, helicopter rotor hubs, and wing structures in the aerospace industry. Boeing, McDonnel Douglas, GE, and Lockheed have developed in-house specifications for use of rotary flap peening (3M, 2003).

2.4.2 Rotary Flap Peening Experimental Observations

There are not as many published studies quantifying the benefits of shot peening with a rotary flap tool as there are for hammer peening. Ofsthun (2003) conducted a fatigue experiment in which the inside surface of holes were peened with a rotary flap tool. He found that when the

bore of the hole being peened was smaller than the flap peen device there was no fatigue benefit. When the hole being treated was larger than the flap peening device there was a roughly 50% increase in fatigue performance (Ofsthum, 2003).

2.5 Fatigue Test Methods

A review of literature indicates that fatigue testing is very often performed through the use of a servo-hydraulic fatigue test machine. These machines can be controlled via electronic monitoring and control of measured stress, force, displacement, or strain. Infante, Branco, and Baptista (2004) used T-shaped fillet weld samples. These were cycled at constant amplitude at a frequency of 10-15 Hz and a stress ratio of R=0.1. Han, Han, and Nam (2008) used similar test samples and loading parameters. Bell, Militaru, and Braid (1995) used right angle fillet weld samples loaded in bending and subjected to constant-amplitude sinusoidal loading with an R value of 0.05. The equipment available for use in this project is a MTS 20,000 lb tensile load frame. Tension-tension fatigue testing ($R > 0$) will be used to eliminate issues associated with load control as test fixtures are unloaded from tension to compression.

ASTM standard E606 Standard Practice for Strain-Controlled Fatigue Testing describes a method for strain-controlled fatigue testing. Testing is typically done using constant-amplitude input under strain control. Load control is also discussed as an option for closed loop fatigue testing in this standard. ASTM E606 discusses several options for defining failure. Total fracture and separation is the most visible definition of failure, but other definitions include monitoring changes in the unloading modulus, the observance of microcracking, or the force (and associated stress) drop at a constant total strain value. For this effort, we will use T-shaped

fillet weld test samples cycled under load control. Failure will be defined as the increase in deflection by 150% under constant amplitude force-controlled loading.

2.6 Fatigue Life Prediction

2.6.1 Fatigue Prediction Using BS7608

British Standard BS7608 (1993) is commonly used in industry to predict fatigue life. This standard describes an approach to analysis of welded joints. Welded joints are assigned a classification based on weld geometry and loading direction. An S-N curve is defined for each different class of weld and type of loading. Stress amplitudes for use in conjunction with the given S-N curves are obtained either experimentally or through finite element methods. The standard form for S-N curves is an exponential curve fit known as Basquin's equation (Bannantine, 1990).

$$\Delta\sigma = SRI * N^{b}$$

Where:

$\Delta\sigma$ = Stress range (max stress – min stress)

SRI = Stress range intercept

N = Cycles to failure

b = Fatigue strength exponent

Values for SRI and b are defined for different weld assembly geometries and loading types according to Table 8 in British Standard BS7608 (1993). Figure 2.7 is an excerpt from this table.

Table 8. Classification of details: load carrying fillet and T-butt joints between plates in different planes

Product form	Location of potential crack initiation	Dimensional requirements	Manufacturing requirements	Special inspection requirements	Design stress area	Type number	Class	Notes	Sketch
Rolled steel structural plates, sections and built-up members	At toe of weld joining two members end to end with third member transverse through joint	Full penetration butt weld with longitudinal axes in line	Any undercut should be ground smooth particularly on the corners of member X Weld ends should be ground flush with edge of member X		Cross section of member X	8.1	F	Weld metal failure will not govern with full penetration welds. Member Y can be regarded as one with a non-load-carrying weld (see joint types 5.2 and 5.5). In this instance the edge distance limitation applies.	
		Partial penetration butt or fillet weld				8.2	F2	In this type of joint failure is likely to occur in the weld throat unless the weld is made sufficiently large. (See joint type 8.5.)	
	At toe of weld joining the end of one member to the surface of another	Full penetration butt weld				8.3	F	See joint type 8.1.	
		Partial penetration butt or fillet weld				8.4	F2	See joint type 8.2.	

NOTE. Butt welded joints should be made with an additional reinforcing fillet so as to provide a similar toe profile to that which would exist in a fillet welded joint (see **B.5.2.2**).

Figure 2.7 Table 8 - Classification of Weld Details from BS7608 (2003)

The use of additional modifying factors to account for stress concentration, loading, or surface finish are not necessary when using the BS7608 method of fatigue life estimation, as the S-N curves defined in this standard are based on curve fitting a large body of field fatigue data that already takes these factors into account. Mean stress correction is not considered in this method. Fricke stated (edited by Macdonald, 2011) that the mean stress effect can be very small in welded structured because of the very high residual tensile stresses present.

2.6.2 Fatigue Prediction Using Fatigue Notch Factor

Another method that has been explored for prediction of fatigue for welded joints is the use of a fatigue notch factor, $K_{f,}$ in combination with fatigue properties defined for the parent material. Bannantine et al. (1990) describe this process. First a theoretical stress concentration factor, K_t, is obtained based on the relevant component geometry and loading condition. Values for K_t are published and are included in Peterson's Stress Concentration Factors (Wiley, 2008). K_f is a function of the theoretical stress concentration factor, K_t, and a notch sensitivity factor, q. These three values are related in the following equation (Bannantine, 1990):

$$q = \frac{Kf - 1}{Kt - 1}$$

The value for q can be obtained from published tables (Bannantine, 1990). The resulting K_f value is then used to adjust the entire S-N curve. This approach is most applicable for high cycle fatigue. Bannantine et al. (1990) note that "A general trend is that the value of the fatigue notch factor decreases with increasing stress levels." This would need to be accounted for if variable-amplitude loading was considered.

2.6.3 Fatigue Prediction using Strain-Life Methods

Strain-life analysis considers both plastic and elastic strains in the fatigue calculation and relates these strains to life through a relationship defined by the Manson-Coffin or strain life curve (Bannantine, et al. 1990).

$$\Delta\varepsilon/2 = \sigma'f/E(2Nf)b + \varepsilon'f(2Nf)C$$

Where:

$2Nf$ = reversals to failure

$\sigma'f$= fatigue strength coefficient

b = fatigue strength exponent

$\varepsilon'f$= fatigue ductility coefficient

c = fatigue ductility exponent

Strain life analysis is not typically considered for welded joints, but Fricke (edited by Macdonald, 2011) suggests that it could be used along with fatigue properties of the parent materials and heat affected zone (HAZ).

2.6.4 Sources for Data to Conduct Predictive Analysis

For experimental analysis strains are measured through the use of foil strain gauges. Gauges are placed near the weld toe. Measured strains are converted to stresses using Hooke's law (assuming entirely elastic strain). The resulting stresses are used with the S-N curves for the appropriate weld classifications to predict fatigue life. This approach is used for both constant and variable amplitude loading. Results using this method have had strong correlation to physical test results for high cycle fatigue.

For finite element-based analysis stresses are obtained in a region close to the weld detail, but excluding stress concentrations due to the weld concentration itself (BS7608, 1993). These analytical stresses are used in the same manner as those obtained experimentally in combination with the S-N curves from the appropriate weld classification given in the standard.

2.7 Summary

Surface peening processes have been demonstrated to be beneficial to the fatigue life of welded structures. This is due to the introduction of surface compressive stresses in the weld and parent material that is a result of the peening impact. Two methods of peening that are applicable in the field without significant expense for equipment and facilities are hammer peening and rotary flap peening. Han et al. (2008), Bell et al. (1995), Maddox (1998), Kopov (1991), and Kirkhope et al. (1999) have all published studies attempting to quantify the benefits of hammer peening. These sources seem to agree that for high cycle fatigue hammer peening can increase fatigue life by a factor of two to ten. In some cases, low cycle fatigue life can be improved by a factor of up to 10 with hammer peening. The application of hammer peening seems to be somewhat variable, and is highly dependent upon the operator.

Rotary flap peening is a more clearly defined process than hammer peening. It is still variable, and dependent upon operator input. The body of published data quantifying the benefits obtained from rotary flap peening is not as large as for hammer peening. A direct comparison of the two methods quantifying the improvement in fatigue life for each was not available.

There exist several methods for fatigue life prediction in welded joints. British Standard BS7608 recommends analysis by the classification of welds into different types based on

geometry. S-N curves are defined for each weld type to facilitate fatigue prediction. Alternately, fatigue notch factors can be determined and applied to fatigue curves for parent materials for high cycle fatigue life estimation.

This project will focus on quantifying and comparing the benefits provided by hammer peening and rotary flap peening of welded assemblies. The analytical methods described above will be employed to determine predictive capabilities for fatigue evaluation of welded joints.

Chapter3 Experimental Setup and Procedures

3.1 Materials:

3.1.1 A36 Steel Material Properties

The test samples used in this project were made from ASTM A36 steel plate. A36 steel is a carbon steel that is commonly used for structural components. Previous test data has been obtained for both monotonic tensile tests and cyclic tensile tests for samples cut from similar A36 steel plates. Table 1.1 lists the monotonic and cyclic material properties for this material. Details regarding how this data was obtained can be found in Appendix 4.

Table 3.1 A36 Steel Material Properties

A36 monotonic properties	US customary units	SI units
Elastic Modulus *E*	32,440,000 psi	217,700 MPa
Ultimate strength, *Su*	83,400 psi	575 MPa
0.2% yield strength, *Sy*	56,500 psi	390 MPa
Strain at fracture ε	0.2223	
Monotonic strength coefficient, *K*	159,300	1,122
Monotonic strain hardening exponent, *n*	0.2538	
Tensile toughness	16700 psi	115 MPa
A36 cyclic properties		
*Cyclic strength coefficient *K'*	128,900 psi	890 MPa
*Cyclic strain hardening exponent *n'*	0.149	
Cyclic (0.2%) yield strength *Sy'*	50,900 psi	350 MPa
Fatigue ductility coefficient $\varepsilon'f$	0.6262	
Fatigue ductility exponent *c*	–0.544	
Fatigue strength coefficient $\sigma'f$	152,400 psi	1,050 MPa
Fatigue strength exponent *b*	–0.103	
Assumed elastic modulus *E*	29,500 ksi	203.4 GPa
*Values obtained from curve fit of data points, not power law approach		

3.1.2 Test Specimen Details

Test specimens were designed to transmit a uniform force to a 6.35 mm (¼ in) steel base plate through a load applied to a 19.05 mm (3/4 in) thick plate welded to the center. The two steel pieces were connected via fillet welds as shown in Figure 3.1. Figure 3.2 provides the overall sample dimensions. Units are in inches in this figure.

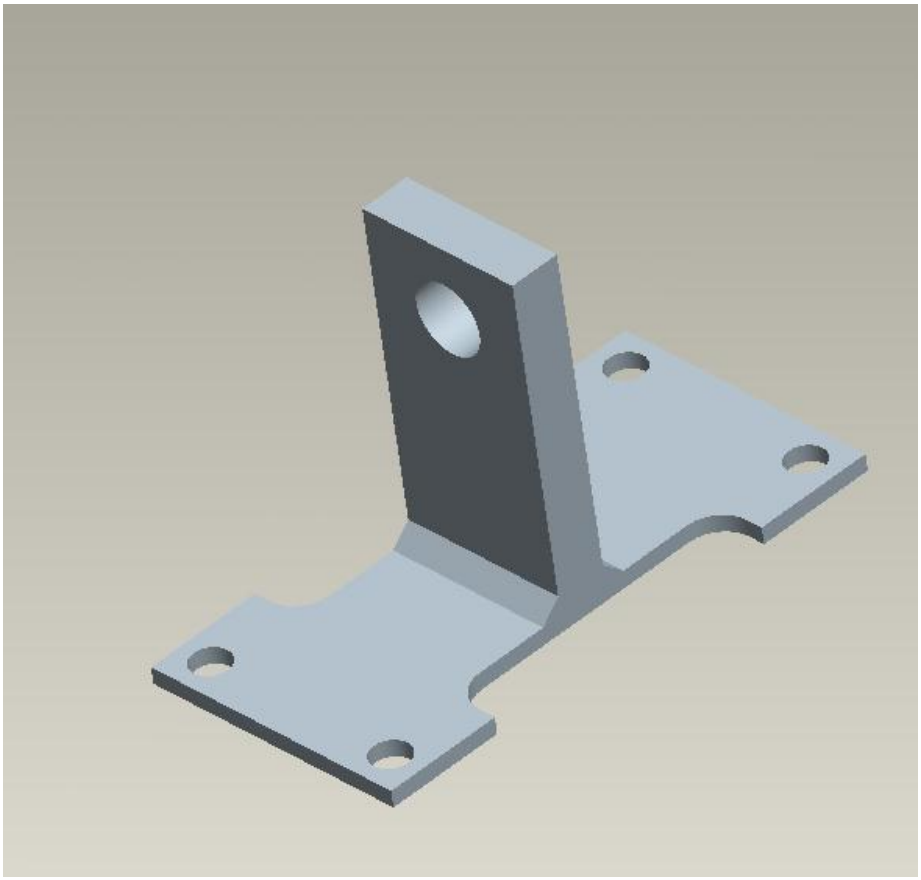

Figure 3.1 ISO View of Test Sample CAD Model

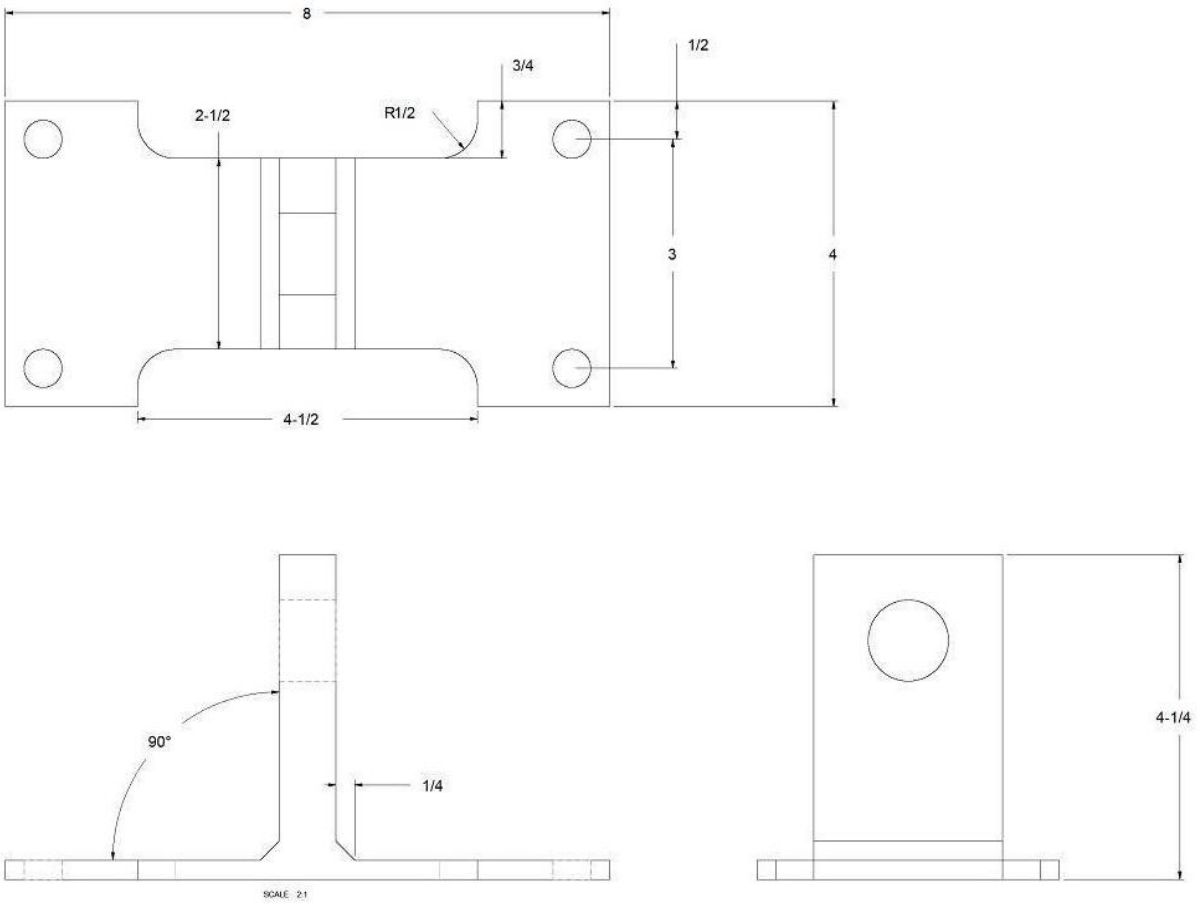

Figure 3.2 Test Sample Overall Dimensions (Dimensions in Inches)

Thirty test samples were used in this project. Table 1.2 lists each sample number, the intended peening treatment, and the expected use for the sample.

Table 3.2 Test Samples

Sample #	Peening	Sample Use
00	None	Strain Gage
0	None	Load Range Trial
1	None	Load Range Trial
2	None	High Cycle Fatigue
3	None	High Cycle Fatigue
4	None	High Cycle Fatigue
5	None	High Cycle Fatigue
6	None	Low Cycle Fatigue
7	None	Low Cycle Fatigue
8	None	Low Cycle Fatigue
9	None	Low Cycle Fatigue
10	Hammer	High Cycle Fatigue
11	Hammer	High Cycle Fatigue
12	Hammer	High Cycle Fatigue
13	Hammer	High Cycle Fatigue
14	Hammer	High Cycle Fatigue
15	Hammer	Low Cycle Fatigue
16	Hammer	Low Cycle Fatigue
17	Hammer	Low Cycle Fatigue
18	Hammer	Low Cycle Fatigue
19	Hammer	Low Cycle Fatigue
20	Rotary Flap	High Cycle Fatigue
21	Rotary Flap	High Cycle Fatigue
22	Rotary Flap	High Cycle Fatigue
23	Rotary Flap	High Cycle Fatigue
24	Rotary Flap	High Cycle Fatigue
25	Rotary Flap	Low Cycle Fatigue
26	Rotary Flap	Low Cycle Fatigue
27	Rotary Flap	Low Cycle Fatigue
28	Rotary Flap	Low Cycle Fatigue

3.2 Specimen Preparation

3.2.1 Specimen Fabrication

The experimental portion of this project was conducted on T-shaped steel welded test samples fabricated from stock A36 steel plate. The selected geometry for this test is shown in Figure 3.3. Descriptive drawings detailing the parts can be found in Appendix 1. Weld

consistency was an important factor for this project, so significant effort was made to ensure that a uniform, quality weld was made. Thirty weld samples were fabricated.

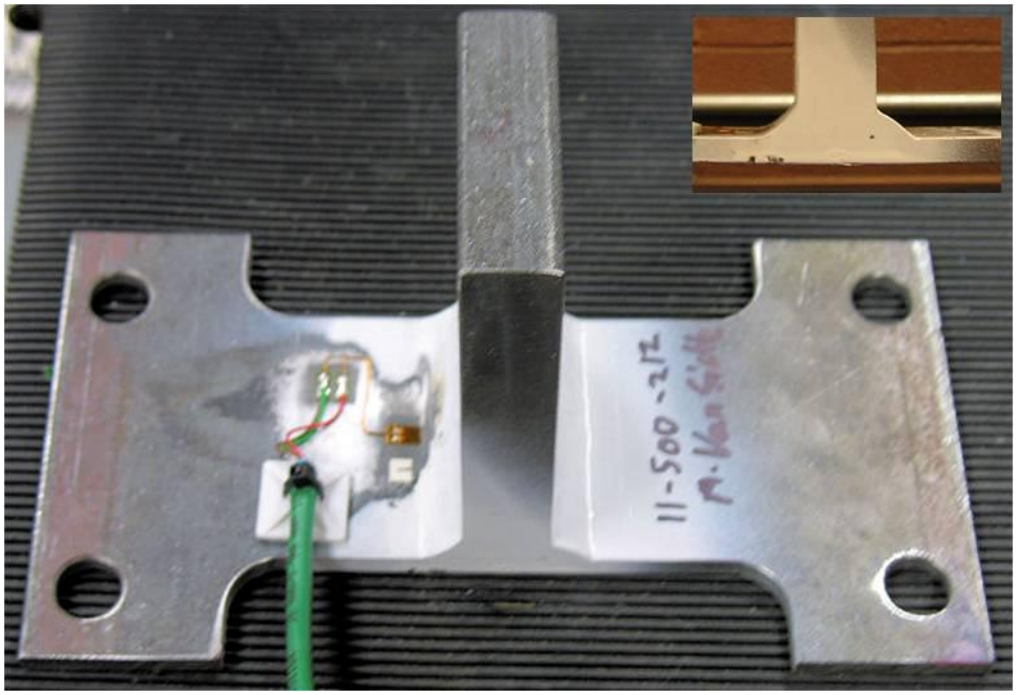

Figure 3.3 T-Fillet Weld Sample

Weld samples were machined out of three 1130 mm (44 ½ in) sections. A flat plate of 6.35 mm (¼ in) steel was welded to a 19.1 mm (3/4 in) plate. The two pieces were tack-welded together are regular intervals so that the tacks would be in between the test samples in scrap material (Figure 3.4). It was necessary to tack weld the assembly in this manner to prevent warpage of the assembly during final welding. A CNC plasma arc cutter was modified to hold a welding head so that uniform welding speed could be obtained. A constant-speed wire fed ARC welder was used to join the base to the T of the samples. Three of the full-length weld samples were made (Figure 3.5). From these 3 welded assemblies thirty test samples were machined. The test samples were shaped and spaced so that the tack welds described earlier in the process

were machined away in between the test samples, leaving only areas of continuous, non-overlapped weld for the test sections (Figure 3.6).

Figure 3.4 Tack Welded Test Samples

Figure 3.5 Fully Welded T-Samples (x3)

Figure 3.6 Machined T-Samples (x30)

The length of the welded section for each of the parts was 63.5 mm (2-1/2 inches). Fillet size was typically 8.1 mm (0.32 inches) on a leg (Figure 3.7 dimension A), with the diagonal of the weld typically measuring 11.4 mm (0.45 in) (Figure 3.7 dimension B). It is interesting to note that all parts warped upwards slightly after welding due to stresses input during the welding process (Figure 3.8).

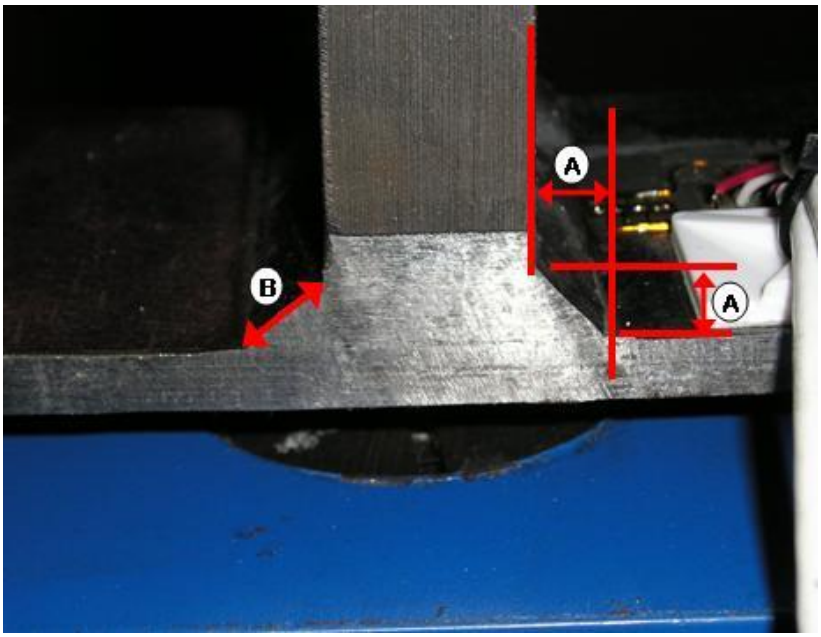

Figure 3.7 Fillet Dimensions

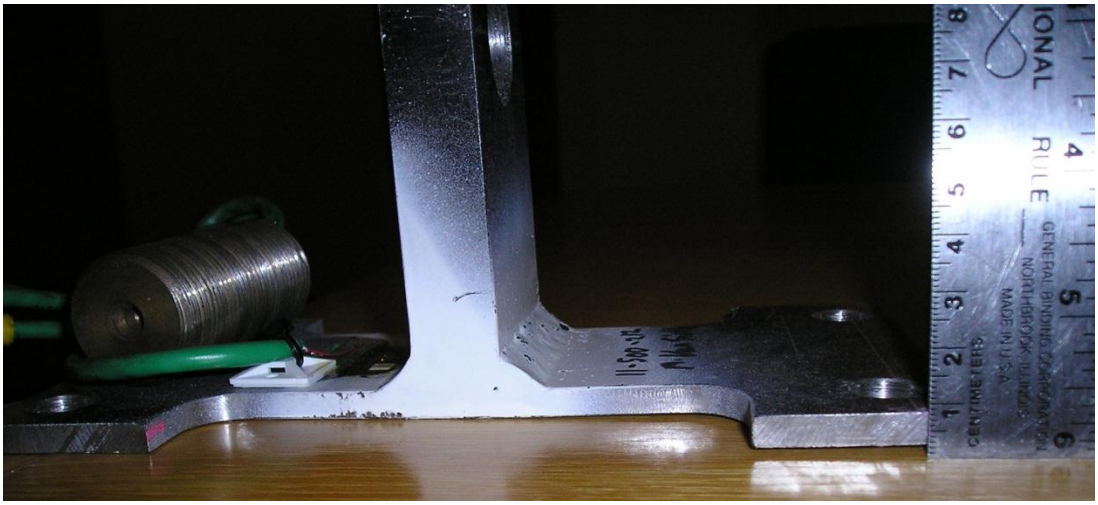

Figure 3.8 Base Plate Warpage – Baseline Welded Sample

Of the thirty total welded test samples eleven were not treated any further after fabrication. These samples comprised the baseline condition. Ten of the weld test samples were subjected to hammer peening surface impingement and nine were subjected to rotary flap peening of the fillet welds.

3.2.2 Baseline Welded Samples

After cycle testing was completed representative samples were selected for cross sectioning and metallographic inspection of the welds. Figure 3.9 shows an optical micrograph of a typical sectioned sample. Vickers micro-hardness measurements were taken with a Clemex ST-2000 Vickers Hardness Tester and Image Analyzer across the weld nugget and into the base material of the test sample. The load applied was 500 g, and the dwell at equilibrium was 10 seconds for each measurement. Figure 3.10 demonstrates that across the weld nugget hardness is approximately 210 HV, transitioning gradually to 180-190 HV through the HAZ into the base material.

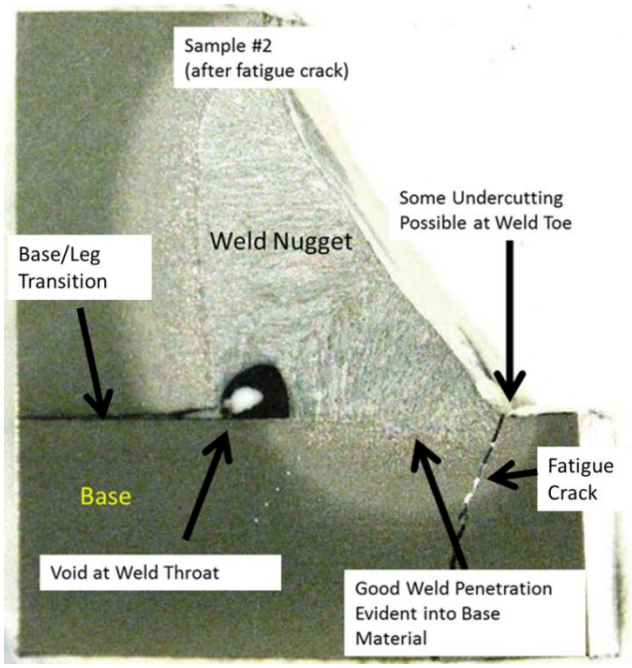

Figure 3.9 Weld Cross Section – Sample #2 (Un-Peened) 11x Magnification

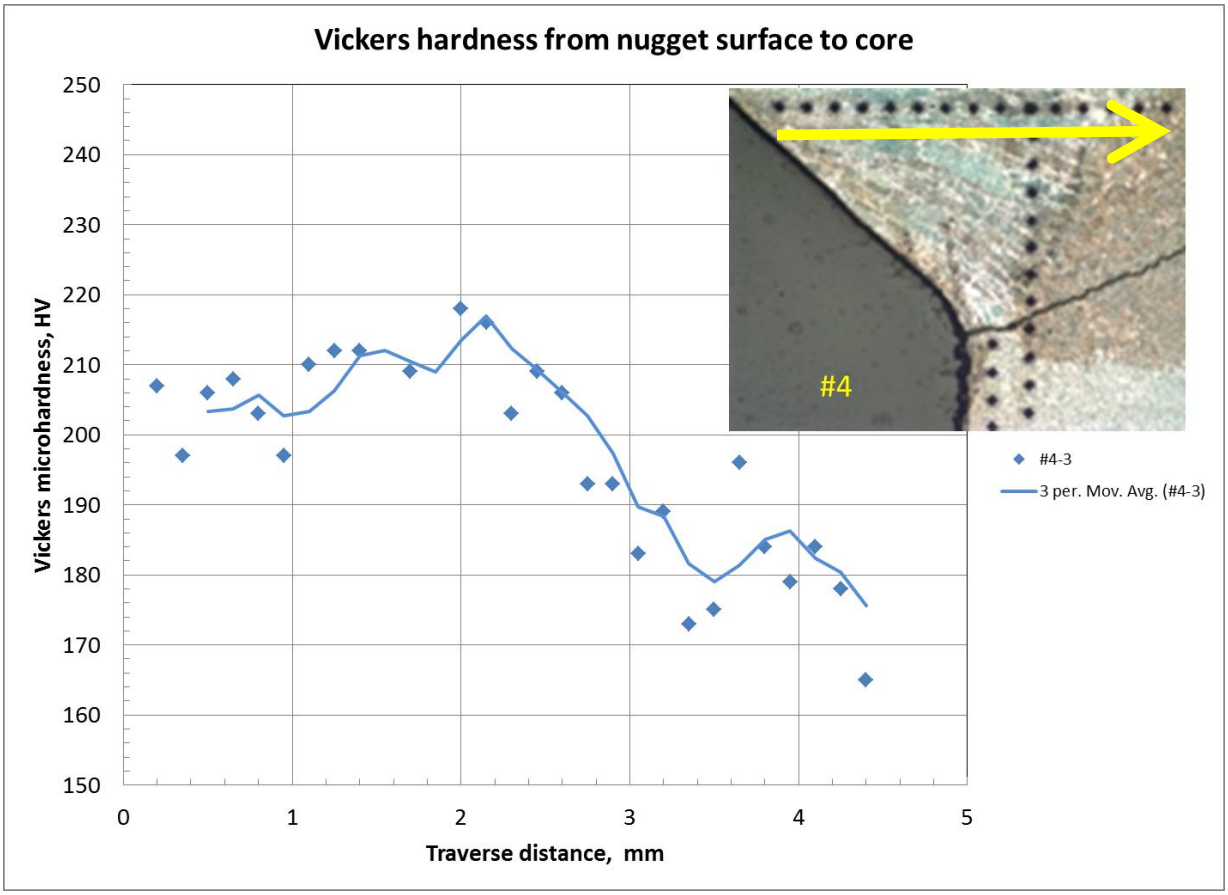

Figure 3.10 Vickers Hardness Measurements for Un-Peened Weld

Black Dots in Image are Hardness Measurement Locations Spaced 0.15 mm

Image is Taken at 20x Magnification After Fatigue Testing

3.2.3 Hammer Peened Samples:

3.2.3.1 Hammer Peen Process

Hammer peening was conducted manually through the use of a pneumatic hammer with a hardened steel tip of 4.8 mm (3/16-in) diameter (Figure 3.11, 3.12). In order to quantify the process settings the hammer was used on a load cell to record frequency and force of the hammer impact (Figure 3.11).

Figure 3.11 Pneumatic Hammer and Tip (Left) Hammer on Load Cell (Right)

Figure 3.12 Hammer Peen Tool and Test Sample

An in-line pressure regulator was used upstream of the hammer to adjust the provided pressure and to insulate the pneumatic hammer from variations in shop air pressure (Figure 3.13). Force data was collected at 50,000 Hz. The load cell was 45 KN (10,000 lb) capacity and was calibrated per standard practices. Test fixtures were machined to generate adapters on

which to impact the load cell. Data was collected at inlet supply pressures of 0.42, 0.55, and 0.62 MPa (60, 80, and 90 psi) (Table 1).

Table 3.3 Hammer force and supply pressure

Supply Pressure Mpa (psi)	Impact Frequency (Hz)	Impact Force N (lbf)
0.42 (60)	30.7	16,000 (3600)
0.55 (80)	34	20,500 (4600)
0.62 (90)	34.5	23,100 (5200)

A pressure regulator setting of 0.55 MPa (80 psi) was selected for hammer peening for this project. This pressure is readily available at most truck service shop facilities, even during peak usage hours. Ten samples were hammer peened with the following settings:

- Tool tip diameter: 4.8 mm (0.1875 in)
- Air pressure: 0.55 MPa (80 psi)
- Number of passes with tool: 1
- Hammer frequency: 34 Hz
- Force: 20,500 N (4600 lb)
- Travel speed: 3.8 mm/sec (0.15 in/sec)

The hammer peened samples flattened out after peening, losing the cupped shape that was introduced by the welding process (Figures 3.8, 3.16). Figure 3.14 shows a hammer peened surface in contrast to an un-peened surface. Figure 3.15 shows a typical hammer peened test sample.

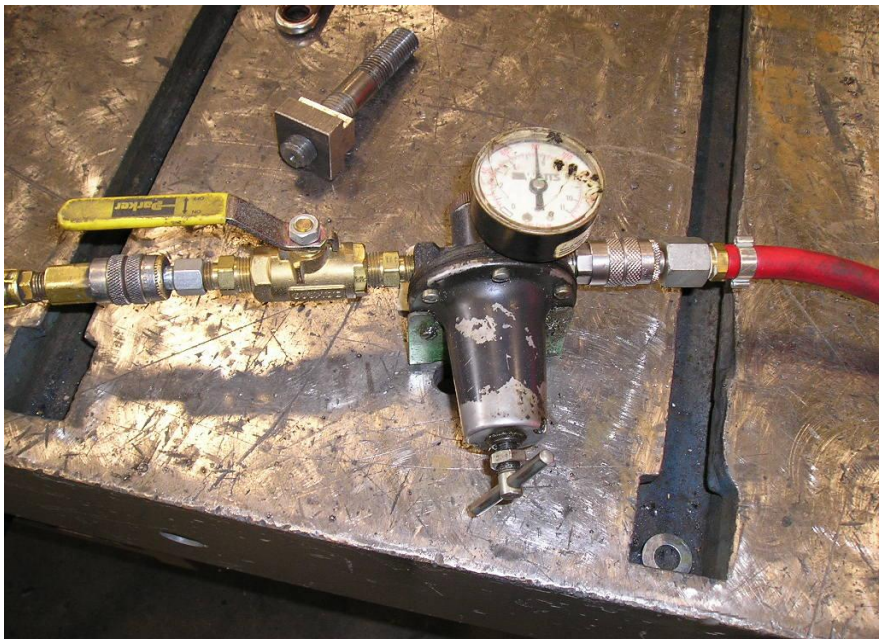

Figure 3.13 Air Pressure Regulator Upstream of Impact Hammer

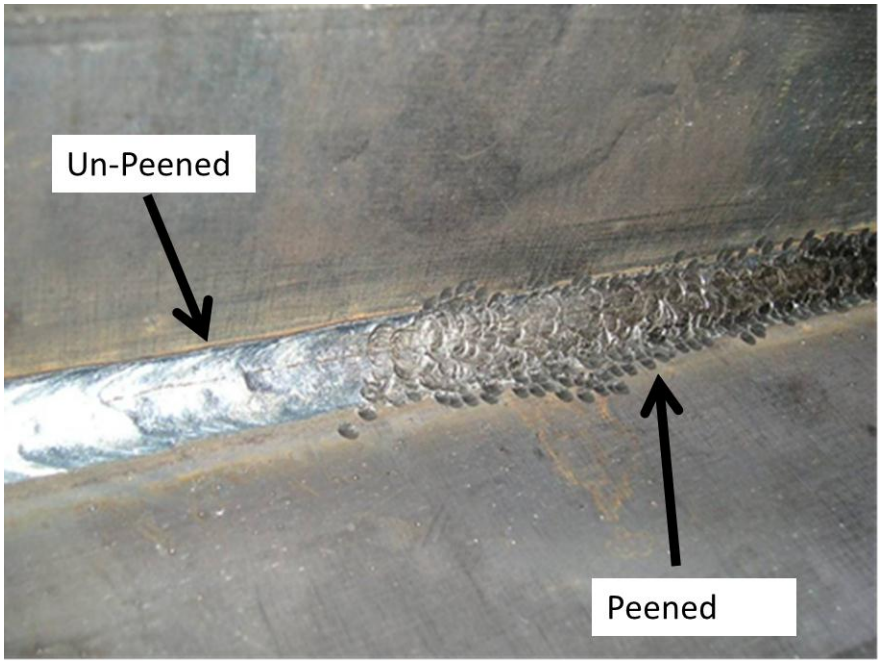

Figure 3.14 Hammer Peened Surface

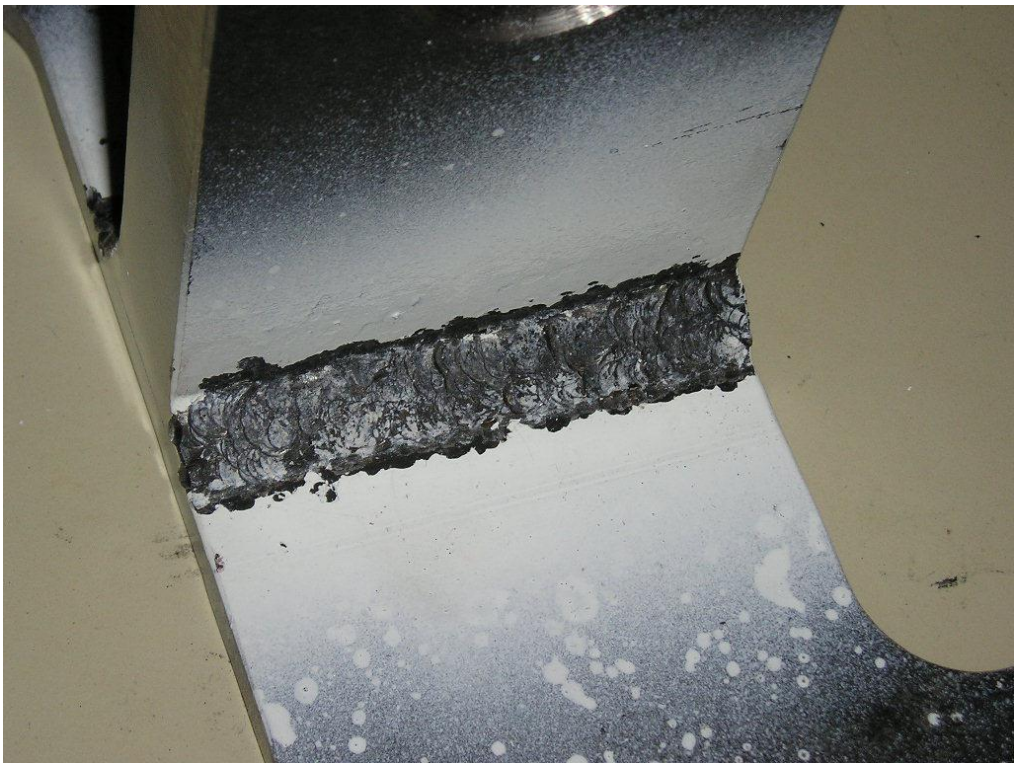

Figure 3.15 Typical Hammer Peened Test Sample

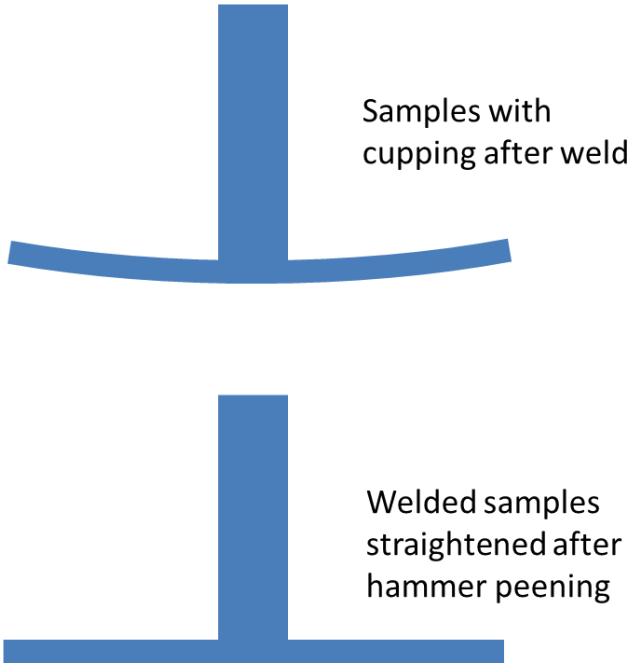

Figure 3.16 Base Cupped Shape Description

3.2.3.2 Micrograph Inspection and Hardness Profile

After fatigue testing was completed representative samples were selected for cross sectioning and micrograph inspection of the welds. Figure 3.17 shows one such sample. Hardness measurements were taken with a Vickers indenter across the weld nugget and into the base material of the test sample. Figure 3.18 demonstrates that across the weld nugget hardness is approximately 210 HV, transitioning gradually to 180-200 HV through the HAZ into the base material. These measurements were made after the sample had cracked due to fatigue loading.

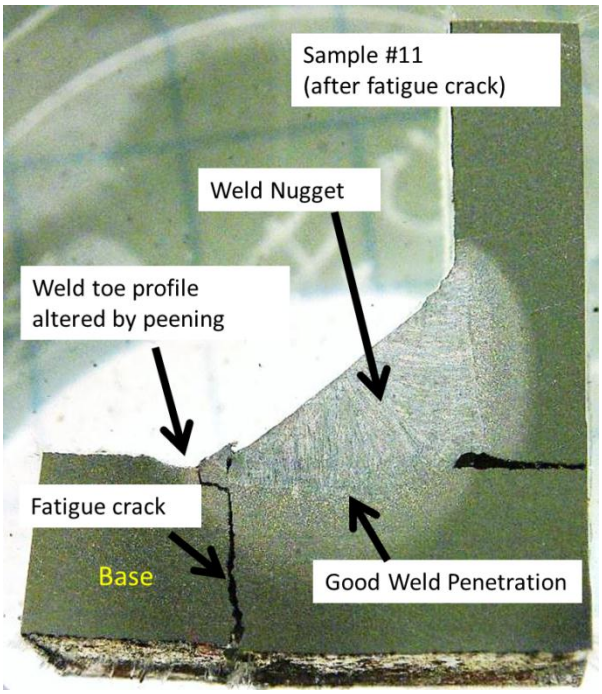

Figure 3.17 Weld Cross Section – Sample #11 (Hammer Peened) 11x Magnification

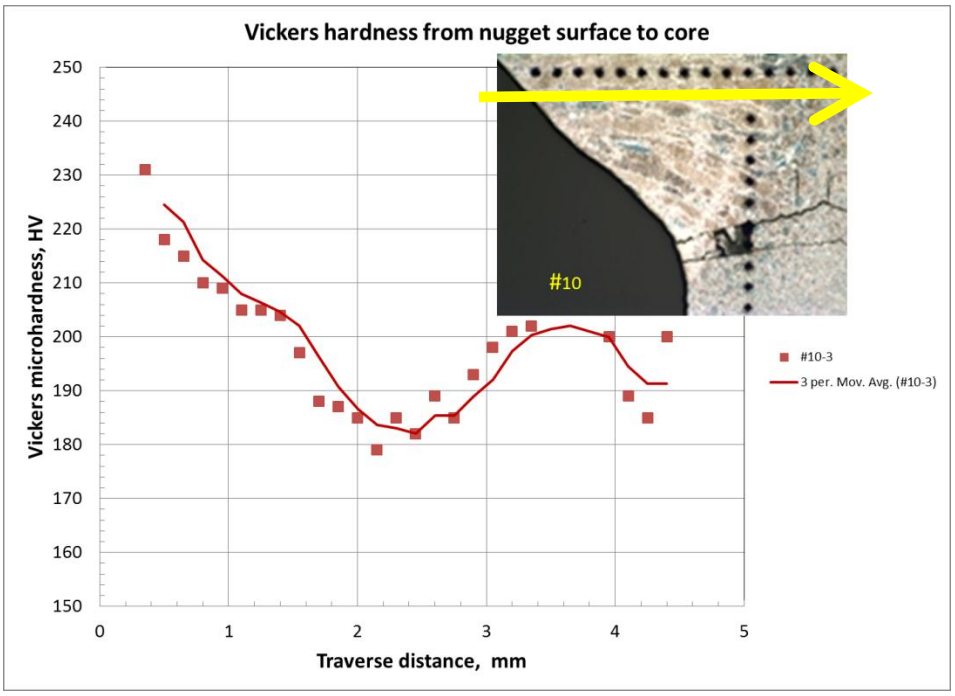

Figure 3:18 Vickers Hardness Measurements for Hammer Peened Weld

Black Dots in Image are Hardness Measurement Locations Spaced 0.15 mm

Image is Taken at 20x Magnification after Fatigue Testing

3.2.4 Rotary Flap Peened Samples

3.2.4.1 Rotary Flap Peen Process

Rotary flap peening was conducted manually using a 3M Roto Peen kit along with a right angle die grinder with pressure regulator (Figure 3.19). Peening intensity targets were set based on Military Specification MIL-R-81841 Rotary Flap Peening of Metal Parts (1972). According to this specification, Almen peening intensity for complete coverage for steel parts between 2.3 and 9.5 mm (0.09 and 0.375 inches) in thickness should be between 0.006A and 0.012A (arc-height inches). A rotary flap mandrel was used with a 14.3 mm x 31.8 mm (9/16 in x 1-1/4 in)

flap assembly (type TC330), which is constructed with a double row of 330 tungsten carbide shot.

To establish the settings for peening the test samples a rotary tachometer was used to measure the air tool rotational speed. The supply air pressure was reduced from shop supply air to provide a speed between 4200-5200 RPM. This variability in rotational speed was observed during several measurements and may be attributed to the rotary tool itself. Pressures this low are at the minimum end needed to operate the tool. The mandrel was held 6 mm (¼ in) above the peened sample.

Figure 3.19 Right Angle Grinding Tool with Peening Flap Installed and Rotary Tachometer

Peening settings were determined by peening several Almen test strips and measuring the deformation due to the imposed residual stresses. An Almen test strip holder was used to secure the test samples during peening (Figure 3.20). Several Almen A test strips were peened with various numbers of passes and peening time with the tool settings described above. It was found that total peening time on the sample was a more effective metric for controlling peening coverage than recording number of passes and speed of passes. The Almen test strips were

found to achieve full saturation at between 2-3 minutes of peening (Table 3.4). Almen test strip deformation was measured with a digital Almen gage (Figure 3.22). Almen intensity was converted from 3M peening intensity, which is achieved on the 3M magnetic Almen strip holder, to Almen "A" intensity through the use of tables provided in the application notes for 3M's Roto Peen Flap Assemblies TC330 User Guide (2003).

Figure 3.21 shows a comparison of one of the saturated Almen A test strips (top) versus an un-peened test strip (bottom). The image is magnified eight times.

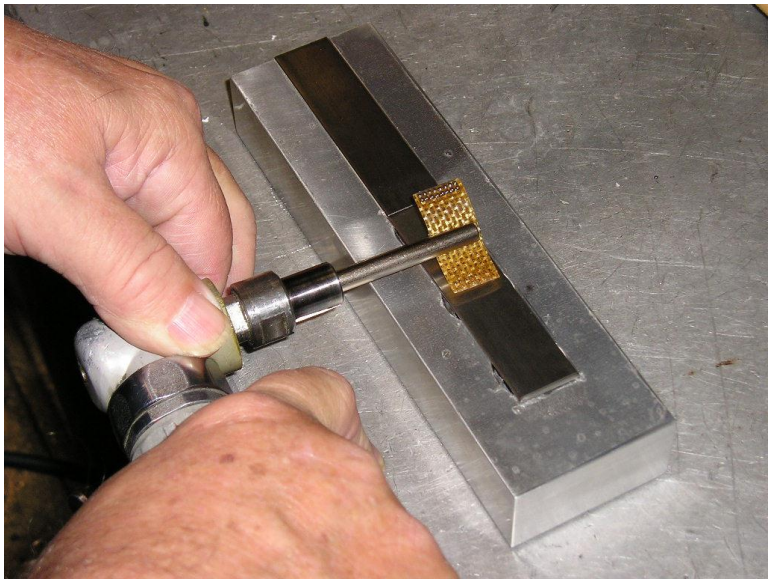

Figure 3.20 Peening Almen Test Strips

Table 3.4 Peening Time and Intensity

Sample	Peening Time	3M Peening Intensity	Almen Intensity	Operator
1	2 min	14	10	A
2	3 min	18	13	A
3	3 min	17.7	12	A
4	3 min	16.6	11.5	B

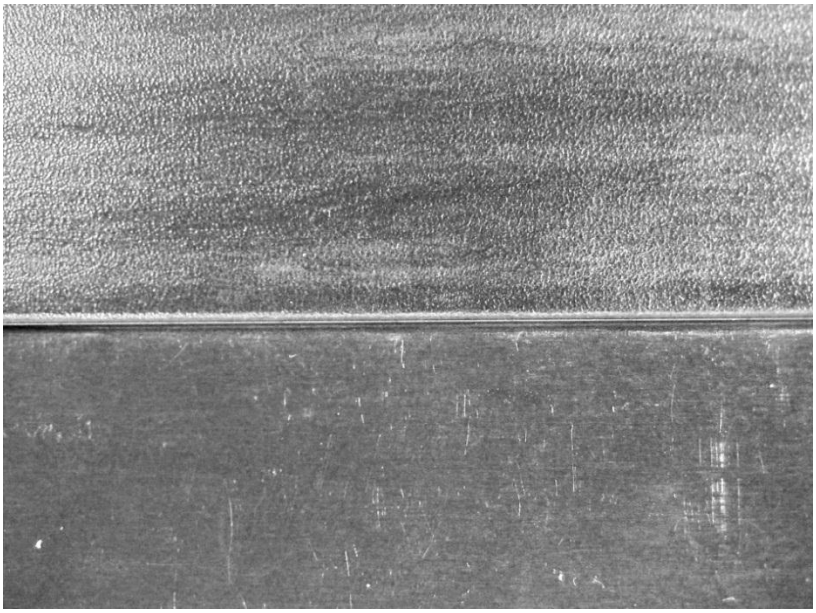

Figure 3.21 Peened Almen Test Strip (Top) vs. Un-Peened (Bottom) 8X Magnification

Figure 3.22 Digital Almen Gage with Test Strip in Measurement

Nine of the T-shaped fillet weld samples were peened using the same settings that were established for the Almen test strips. Fatigue test specimens were peened for five minutes on each side of the welded joint to ensure saturation (Figure 3.23). Unlike the hammer peened test samples, the flap peened samples did not flatten out during peening. These samples retained the upward bow that was introduced during welding (Figure 3.8).

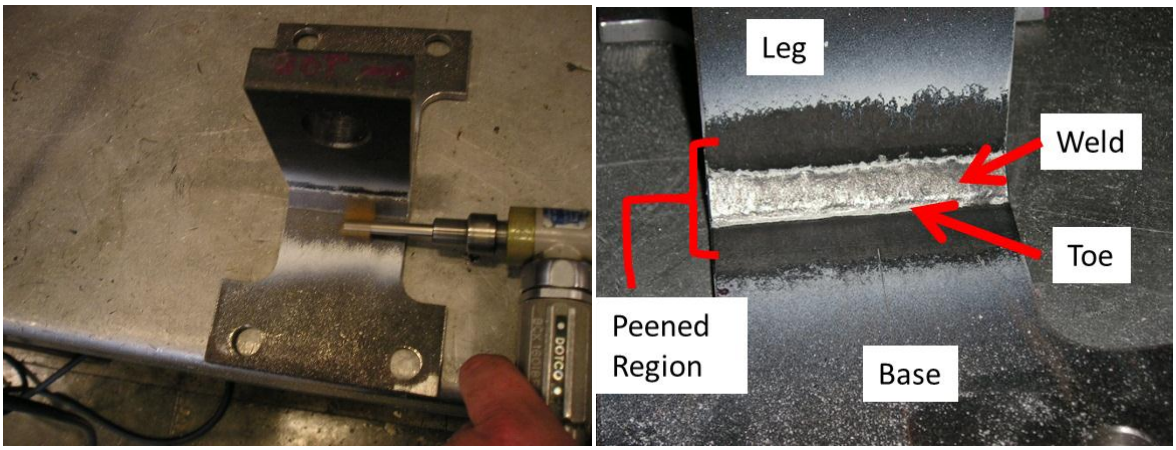

Figure 3.23 Flap Peening of Test Samples

3.2.4.2 Micrograph Inspection and Hardness Profile

After cycle testing was completed representative samples were selected for cross sectioning and micrograph inspection of the welds. Figure 3.24 shows one such sample. Hardness measurements were taken with a Vickers indenter across the weld nugget and into the base material of the test sample. Figure 3.25 demonstrates that across the weld nugget hardness is approximately 190-200 HV, transitioning sharply to 220 HV at the weld nugget transition to parent material and then falling gradually to 180 HV into the base material.

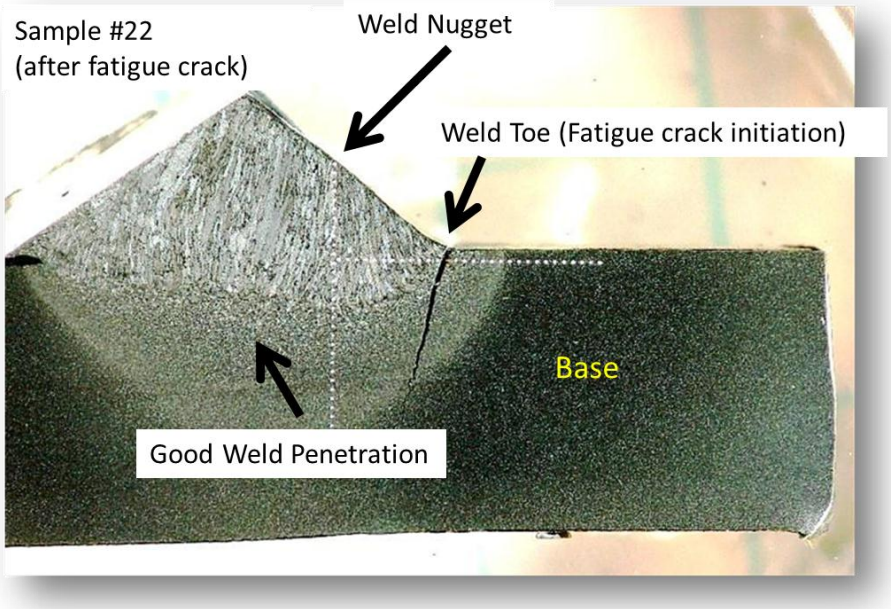

Figure 3.24 Weld Cross Section – Sample #22 (Flap Peened) 20x Magnification

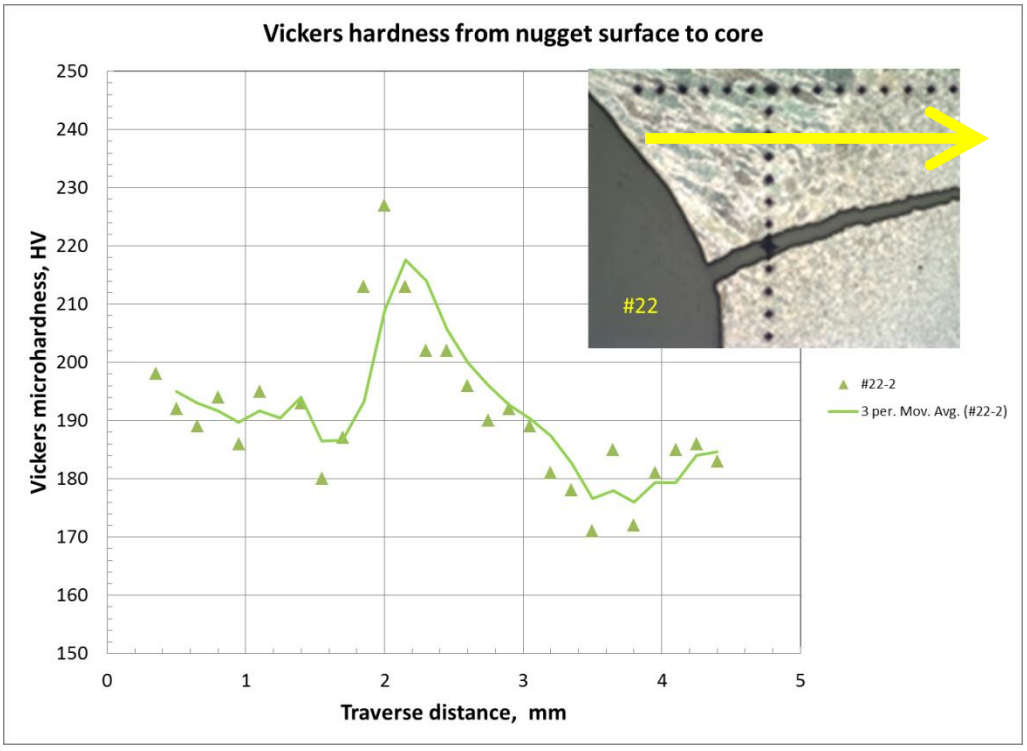

Figure 3:25 Vickers Hardness Measurements for Flap Peened Weld. Black Dots in Image are Hardness Measurement Locations Spaced 0.15 mm. Image is Taken at 20x Magnification

3.3 Fatigue Test System

3.3.1 Test Setup and Description

Test fixtures were designed and fabricated to provide the desired boundary conditions for the test samples. These boundary conditions will be discussed further in Chapter 5. The tensile test samples were installed into a MTS Model 810 22-kip hydraulic load frame as seen in Figure 3.26 and 3.27. Specimens were loaded and cycled according to Table 3.5.

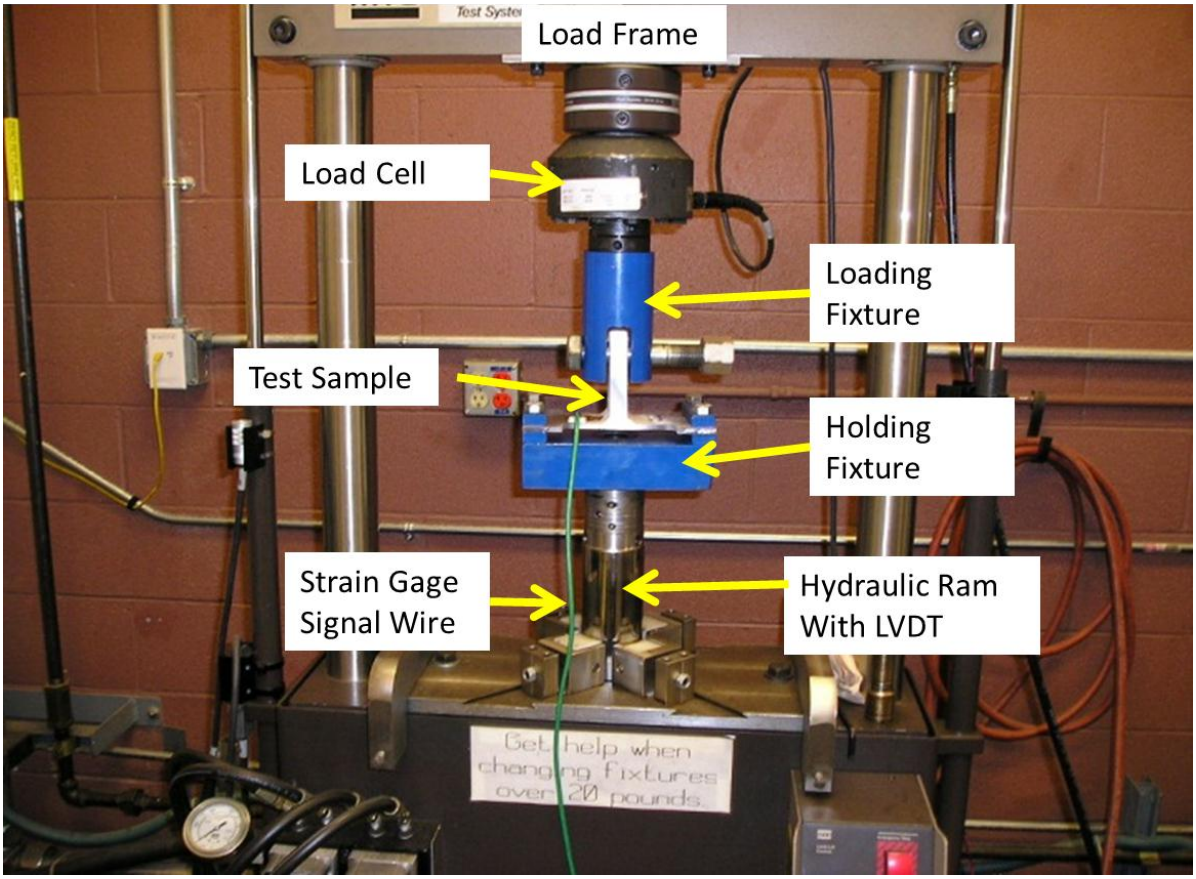

Figure 3.26 Test Specimen Installed in MTS Load Frame

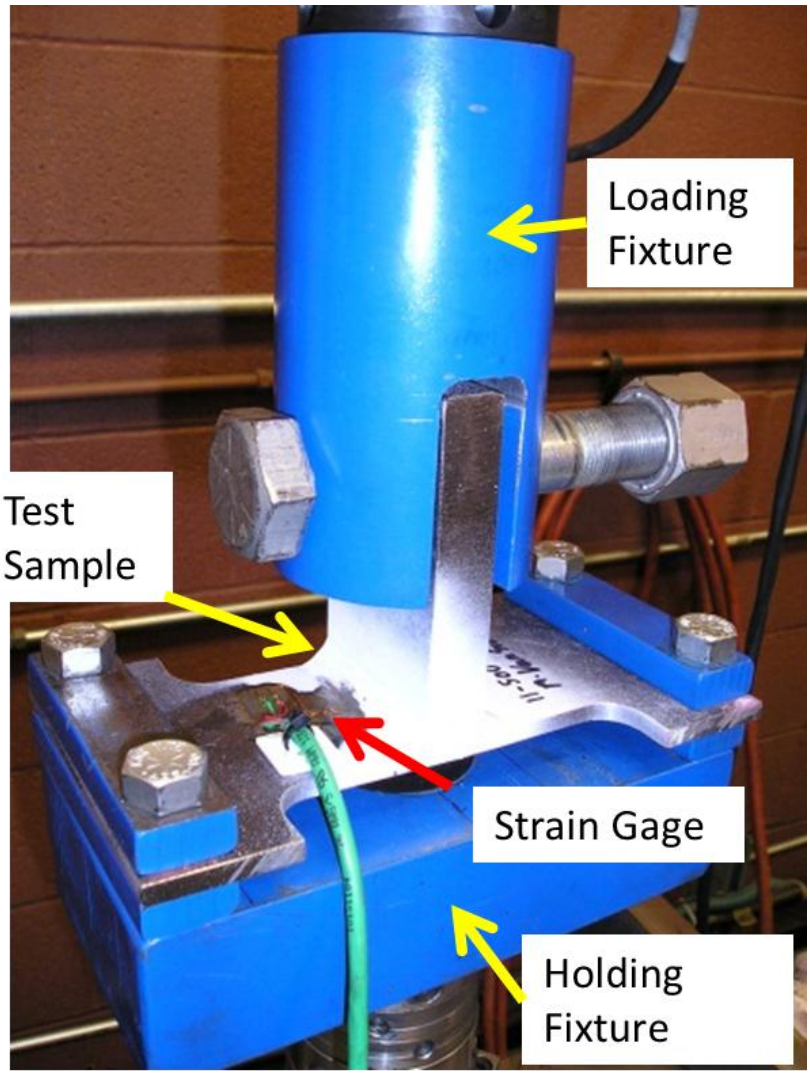

Figure 3.27 Strain Gage Test Sample Installed in MTS Load Frame

Table 3.5 Sample Cycle Description

Sample #	Peening	Sample Use	Max Force N (lbf)	Min Force N (lbf)
00	None	Strain Gage	4448 (1000)	0
0	None	Load Range Trial	4448 (1000)	445 (100)
1	None	Load Range Trial	8896 (2000)	445 (100)
2	None	High Cycle Fatigue	7562 (1700)	445 (100)
3	None	High Cycle Fatigue	7562 (1700)	445 (100)
4	None	High Cycle Fatigue	7562 (1700)	445 (100)
5	None	High Cycle Fatigue	7562 (1700)	445 (100)
6	None	Low Cycle Fatigue	22,240 (5000)	445 (100)
7	None	Low Cycle Fatigue	22,240 (5000)	445 (100)
8	None	Low Cycle Fatigue	22,240 (5000)	445 (100)
9	None	Low Cycle Fatigue	22,240 (5000)	445 (100)
10	Hammer	High Cycle Fatigue	7562 (1700)	445 (100)
11	Hammer	High Cycle Fatigue	7562 (1700)	445 (100)
12	Hammer	High Cycle Fatigue	7562 (1700)	445 (100)
13	Hammer	High Cycle Fatigue	7562 (1700)	445 (100)
14	Hammer	High Cycle Fatigue	7562 (1700)	445 (100)
15	Hammer	Low Cycle Fatigue	22,240 (5000)	445 (100)
16	Hammer	Low Cycle Fatigue	22,240 (5000)	445 (100)
17	Hammer	Low Cycle Fatigue	22,240 (5000)	445 (100)
18	Hammer	Low Cycle Fatigue	22,240 (5000)	445 (100)
19	Hammer	Low Cycle Fatigue	22,240 (5000)	445 (100)
20	Rotary Flap	High Cycle Fatigue	7562 (1700)	445 (100)
21	Rotary Flap	High Cycle Fatigue	7562 (1700)	445 (100)
22	Rotary Flap	High Cycle Fatigue	7562 (1700)	445 (100)
23	Rotary Flap	High Cycle Fatigue	7562 (1700)	445 (100)
24	Rotary Flap	High Cycle Fatigue	7562 (1700)	445 (100)
25	Rotary Flap	Low Cycle Fatigue	22,240 (5000)	445 (100)
26	Rotary Flap	Low Cycle Fatigue	22,240 (5000)	445 (100)
27	Rotary Flap	Low Cycle Fatigue	22,240 (5000)	445 (100)
28	Rotary Flap	Low Cycle Fatigue	22,240 (5000)	445 (100)

3.3.2 Strain Data Collection

One un-peened T-sample was instrumented with a uni-axial strain gage (Vishay part number CEA-06-062UW-350). This gage was placed so that the foil sensing grid was centered approximately 1 mm away from the toe of the fillet weld. The foil element was oriented 90 degrees from the weld. Additional gage details are included in Appendix 2. The gaged sample was installed in the hydraulic load frame as shown in Figures 3.26 and 3.27. Thy hydraulic ram was actuated in load control up to 4448 N (1000 lb) and back down to 0 N while recording strain, force, and ram displacement. Figure 3.28 is a plot of measured strain vs. hydraulic ram force. Figure 3.29 is a plot of measured strain vs. hydraulic ram displacement. Figure 3.30 is a plot of hydraulic ram force versus hydraulic ram displacement. These three plots include data collected during both loading and unloading of the specimen.

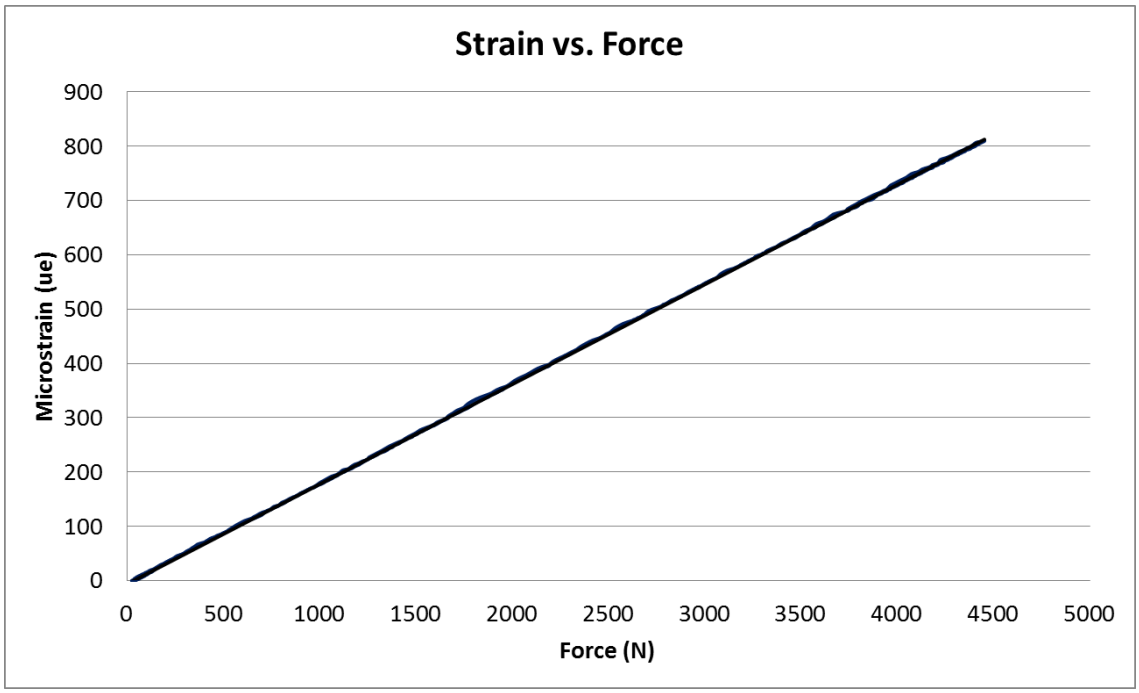

Figure 3.28 Strain vs. Force Plots

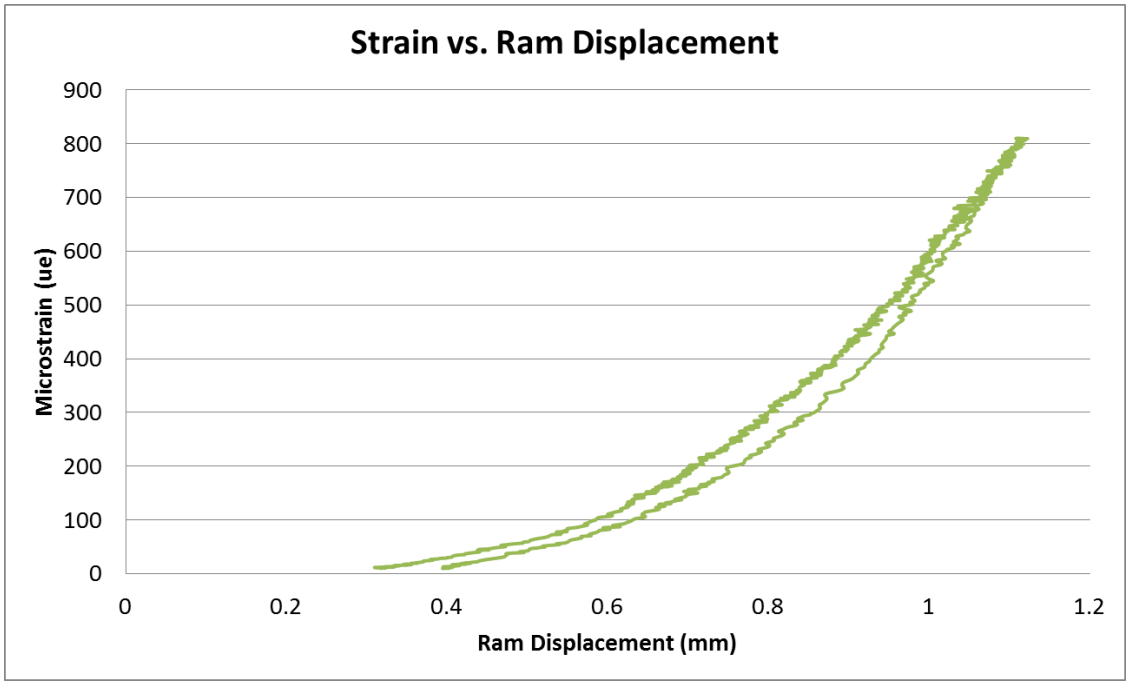

Figure 3.29 Strain vs. Hydraulic Ram Displacement

.

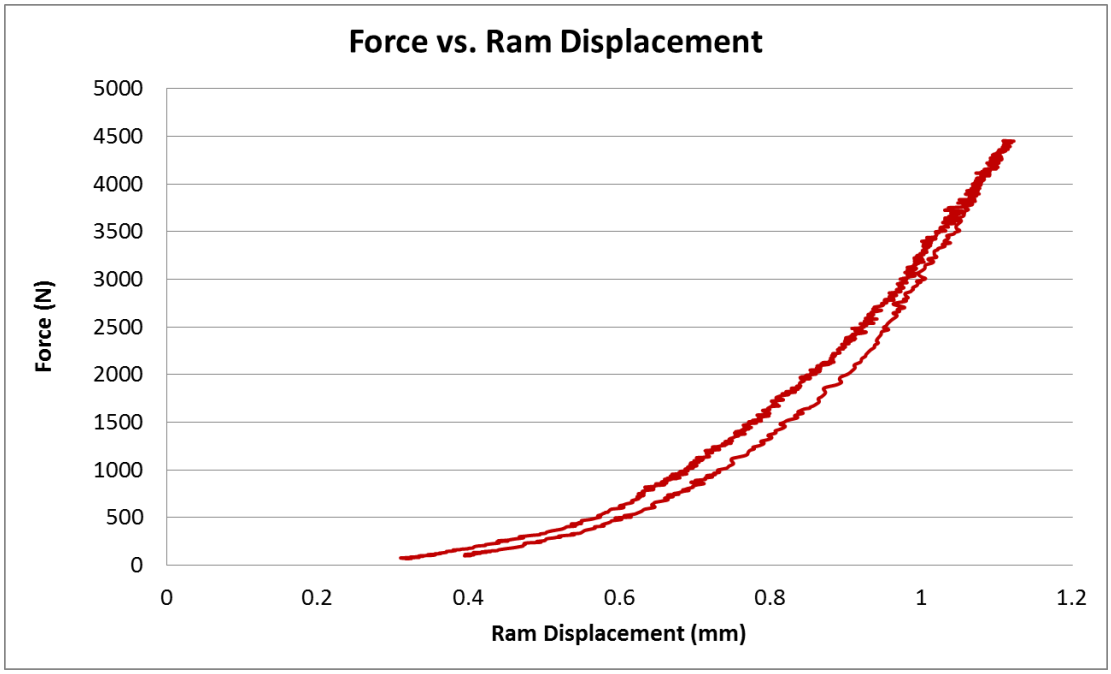

Figure 3.30 Applied Force vs. Hydraulic Ram Displacement

The force versus strain curve was very linear in nature, indicating that load control should produce good results. The non-linear nature of the plots in Figure 3.29 and 3.30 may be attributed to the nature of the connection between the upper head on the hydraulic load frame and the loose attachment to the test sample. It can be noted that after 0.76 mm (0.03 inches) of displacement both the strain and force vs. ram displacement curves are linear. This observation will be used in Chapter 4 to correlate numerical models. Some hysteresis is also evident in Figures 3.29 and 3.30. This is also believed to be due to the nature of the upper ram head connection to the test sample. This connection was achieved by the use of a pin through an over-sized hole in the test sample (Figure 3.27). During fatigue cycling some relative motion between the test sample and loading fixture was evident, indicating that the holes in the loading fixture and test samples may have not been perfectly concentric.

3.3.3 Tension-Tension Cycle Test Parameters

The measured strains from the first sample were used to select forces to cycle the test specimens to achieve either low cycle or high cycle fatigue life. The S-N curve for Class F welds from British Standard BS7608 Practice for Fatigue Design and Assessment of Steel Structures (1993) was used to select approximate loading amplitudes (Figure 3.31). The measured strains were converted to stress values by using Hooke's Law for uni-axial stress, $\sigma = \varepsilon E$ (Bannantine et al., 1990). This is relevant for the case of pure bending stress in the elastic region of stress.

Load amplitudes were further refined by cycling test samples at 4448 N (1000 lb), 8896 N (2000 lb), and 22,240 N (5000 lb) maximum loads. Target life for the baseline samples was 2000 to 5000 cycles for the low cycle fatigue samples and 200,000 to 500,000 cycles for the high cycle fatigue samples. The low cycle fatigue values were chosen because most S-N curves are

defined beginning at 1000 cycles (Bannantine et al. 1990). It was desired that samples reach at least 1000 cycles to enable use of available material fatigue properties. The high cycle targets were selected because the samples were experiencing high cycle fatigue behavior at 200,000 cycles, but the test duration was not excessively long.

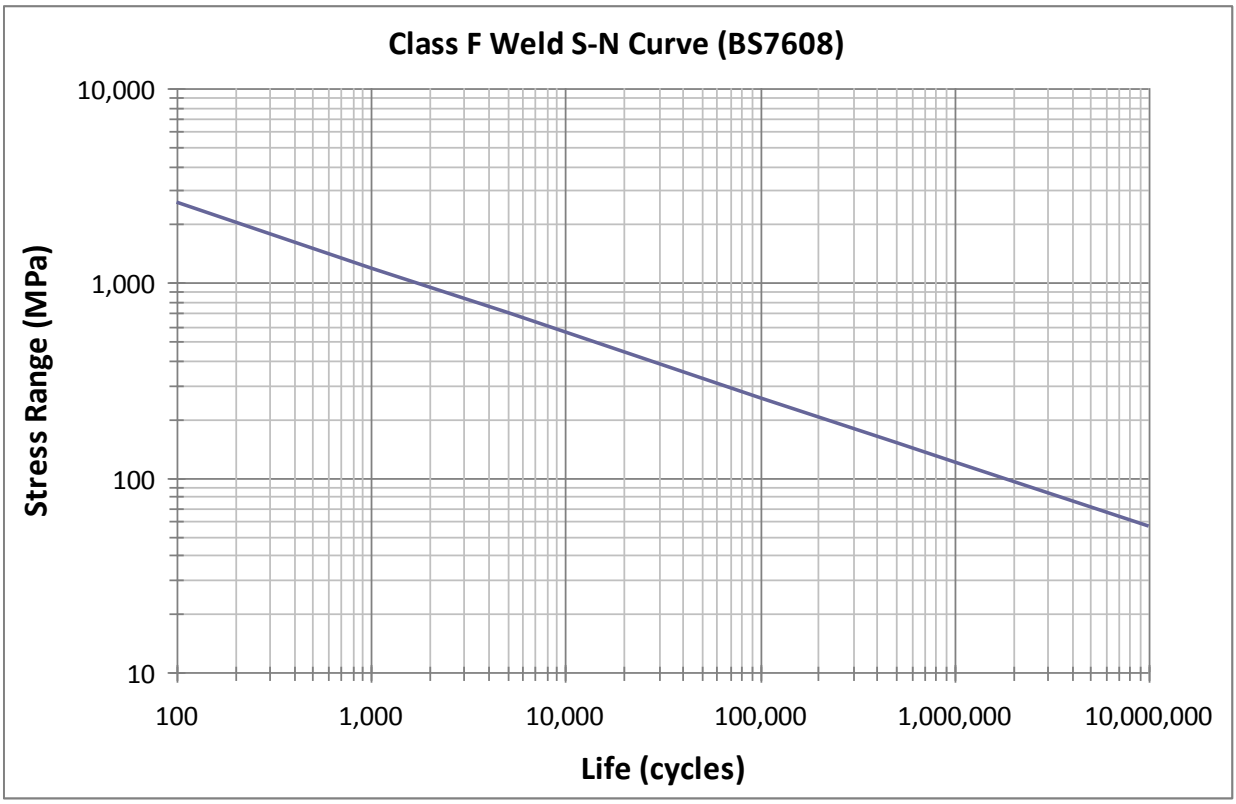

Figure 3.31 S-N Curve for Class F Weld from BS7608

Test samples were loaded into the tensile test machine and cycled under load control with deflection limits set to suspend testing when a crack occurs. The test controller was set to cycle the specimens using a sine wave force input. Low cycle fatigue samples were cycled from 445 N (100 lb) tension to 22,240 N (5000 lb) tension. High cycle fatigue samples were cycled from 445 N (100 lb) tension to 7616 N (1700 lb) tension. All samples were subjected to tension-tension loading due to the assembly tolerances in the test fixtures. Previous experience has shown that the test controller used for this project experiences control issues when the loading

cycle includes a transition with no resistance, as passing from tension to compression through the gap designed into the fixture to allow for easy assembly. In order to avoid these control issues it was decided that this test would not be fully reversed. The 445-7616N (100-1700 lb) samples were cycled at 4 Hz. The 445 – 22,240 N (100-5000 lb) samples were cycled at 2 Hz. These loading frequencies were selected based on previous experience with the MTS load frame and controller system. These frequencies allow accurate control of the hydraulic ram for tests with deflections of the amplitude needed for this effort. The 445 N (100 lb) minimum load was selected for both loading levels to keep a minimum load close to zero on the load fixture at all times in order to prevent issues with non-linear control due to slop in the specimen loading fixture (Figure 3.27).

The test controller was set to shut off after the resulting deflection from the specified load increased by 0.4 mm (0.015 in) deflection under the high cycle test load and by 6.4 mm (0.25 in) deflection under the low cycle test load. It was found that these limits stopped the test after a crack had progressed along the entire top surface of the weld, but before the crack propagated through the test sample and resulted in full fracture. The test was visually monitored every few hours. Cycle count to failure was recorded for each test specimen. Test samples were split into the following groups:

a. Baseline untreated weld, high stress (low cycle fatigue): qty = 4
b. Baseline untreated weld, low stress (high cycle fatigue): qty = 4
c. Hammer peened weld, high stress (low cycle fatigue): qty = 5
d. Hammer peened weld, low stress (high cycle fatigue): qty = 5
e. Rotary flap peened weld, high stress (low cycle fatigue): qty = 4
f. Rotary flap peened weld, low stress (high cycle fatigue): qty = 5

Budgetary and schedule constraints prevented more than 2 load levels for each sample configuration.

3.3.4 Predictive Analysis procedures

3.3.4.1 Fatigue Analysis Based on S-N Approach per BS7608

In addition to quantifying and comparing the benefits of surface impingement through the use of hammer and rotary flap peening it was desired that some investigation occur related to predicting fatigue life using standard industry methods. The first method used was stress life analysis using guidelines set forth in British Standard BS7608. This method is sometimes called the nominal stress approach.

This analysis was conducted in nCode GlyphWorks release 8.0. For this analysis the stress range was synthesized based on the applied force vs. stress range calculation described in Chapter 3.3.2. Strain was cycled from 81 to 1379 microstrain for the high cycle fatigue sample. Life was calculated by translating strain to stress via simple multiplication by the elastic modulus, assumed to be 207 GPa for Steel. For the low cycle fatigue strain cycle the predicted stress range was 822 MPa. For the high cycle fatigue strain cycle the predicted stress range was 268 MPa. The S-N curve was selected based on Class F welds, as defined in Table 8 of BS7608 (1993). The standard form for S-N curves is an exponential curve fit previously described in Chapter 2.

Basquin's Equation: $\Delta\sigma = SRI * N^b$

Where:

$\Delta\sigma$ = Stress range (max stress – min stress)

SRI = Stress range intercept

N = Cycles to failure

b = Fatigue strength exponent

For F2 Welds, SRI and b are defined as follows: SRI = 1.2x10^4, b = -0.3333 (nCode material database and BS7608, 1993).

Based on the above calculation, a fatigue life of 89,300 cycles was predicted for a stress range of 268 MPa (high cycle fatigue value). When the low cycle stress range (822 MPa) was used as input, static failure was predicted. Reference Figure 5.4 for a comparison of this to observed test values.

3.3.4.2 Fatigue Analysis Based on e-N approach and Fatigue Notch Factor

A similar approach to fatigue life estimation based on the parent material fatigue properties and an assumed fatigue notch concentration factor, Kf, is sometimes used for fatigue analysis of welded joints. For this project, strain-life material data for A36 steel was available from previous work by the author (Appendix 3). Strain-life analysis considers both plastic and elastic strains in the fatigue calculation and relates these strains to life through a relationship defined by the Manson-Coffin or strain life curve as previously defined in Chapter 2.

Strain-life equation: $\Delta\varepsilon/2 = \sigma'_f/E(2N_f)b + \varepsilon'_f(2N_f)C$

Where:

$2N_f$ = reversals to failure

σ'_f= fatigue strength coefficient

b = fatigue strength exponent (Basquin's exponent)

ε'_f= fatigue ductility coefficient

c = fatigue ductility exponent

This analysis was also conducted in nCodeGlyphWorks release 8.0. For this analysis the strain range was synthesized based on the applied force vs. stress range calculation described in Chapter 5. Strain was cycled from 81 to 1379 microstrain for the high cycle fatigue sample. The strain life curve used for this calculation is found in Attachment 3.

Based on the above calculation, a fatigue life of 156,000 cycles was predicted for a strain range of 1298 microstrain (high cycle fatigue value) and K_f of 2.0. When the low cycle strain range (3974 microstrain) was used as input, static failure was predicted. Reference Figure 5.4 for a comparison to the observed test values.

The K_f value is one variable that is commonly tuned based on experimental data to achieve a good life prediction. The value of 2.0 has been commonly used for fatigue analysis of welded joints. Other values may be better suited. As stated in Chapter 2, a fatigue notch factor, K_f, can be used that is a function of the theoretical stress concentration factor, K_t) and a notch sensitivity factor, q

$$q = \frac{Kf - 1}{Kt - 1}$$

The value for q was obtained from published tables (Bannantine et al. 1990). For A36 steel with tensile strength of 550 MPa (80 ksi) q is approximately 0.7 for a notch radius of 1 mm (0.04 in). A 1 mm notch radius was recommended by Macdonald (2011) for determining notch concentration factors for fillet welds.

Chart 2.30a of Peterson's Stress Concentration Factors (Pilkey, 2008) indicates that for a 6.35 mm (1/4-in) thick plate with a 1mm radius notch that the stress concentration factor, K_t, should be 1.9. Substituting this into the equation above, along with q=0.7 we obtain a fatigue

notch factor, K_f, = 1.63. As shown in Figure 5.4, this K_f value provides excellent correlation to experimental data when used with the stress-life or strain life approach.

Chapter 4 Numerical Modeling

4.1 Finite Element Model Construction

A secondary goal of this project was to investigate methods of fatigue life prediction using finite element methods and to see how these compared to experimental observations for the welded structures. The tools available for this exercise were Altair HyperWorks Version 11, used for model construction and analysis setup and post-processing , ABAQUS Standard Version 6.12, used as the finite element solver, and nCode DesignLife Version 9.0, used as the fatigue analysis engine.

The first step of the analysis was to construct a model of sufficient detail to well represent the geometry of interest. The model was constructed entirely of solid hex elements, or bricks, with three elements through the minimum thickness component. Average element size was 2 mm. C3D20R (quadratic solid) elements were selected. Welds were modeled using solid elements to approximate the weld geometry. The completed model had a total of 30,468 elements and 143,881 nodes (Figure 4.1). All materials were assigned material properties consistent with A36 steel, with density = 7.8 x 10^-9 Mg/mm^3, elastic modulus = 207 GPa, and Poisson's ratio = 0.3. The model was constrained at the base. A vertical load of 4,448 N was distributed over 77 nodes in the top hole. Analysis outputs were nodal displacement and elemental stress and strain.

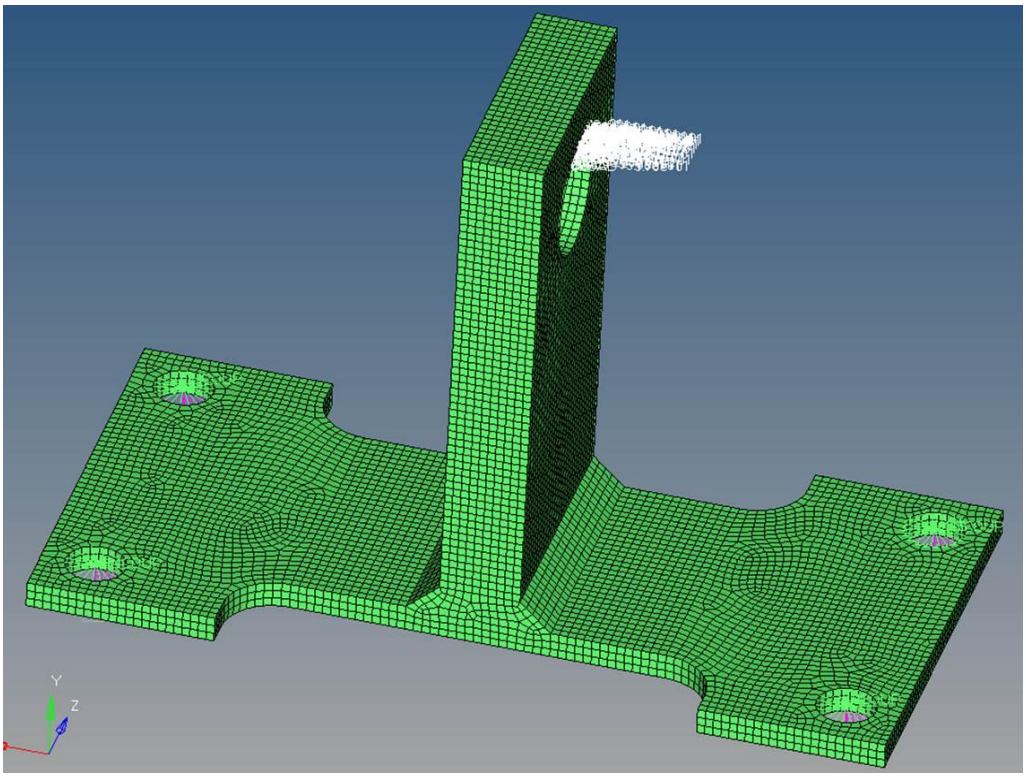

Figure 4.1 FE Model

4.2 Boundary Condition Selection and Correlation to Experimental Data

Correlation to test data was the initial step for finite element analysis. The strain gage application and loading discussed in section 3.3.2 was used to establish correlation. Strain amplitude at 4,448 N (1000 lb) was recorded experimentally to be 810 microstrain. Although the plots that included cylinder ram displacement were highly nonlinear due to the region of motion where slack was removed in the loading system, the portion of the plot from 400 to 800 microstrain is very linear (Figure 3.29). This section of data was fit to a line using the least squares method. The resulting line indicates that if the entire range were idealized to be linear then deflection at 4448 N would be 0.45 mm. These strain and displacement values were used for correlation targets.

Four different boundary conditions were modeled. *The first constraint* attempted (A) was to rigidly constrain in XYZ translation the nodes around the perimeter of the mounting holes and

along the perimeter of the steel bar used to clamp the test samples. Refer to Figure 4.2A and 4.3. This boundary condition produced a result that was too stiff. Refer to Table 4.1 below for a comparison of stiffness and strain to experimental values. *The second constraint* attempted was to rigidly constrain in XYZ the nodes around the perimeter of the mounting holes (Figure 4.2B). This constraint also proved to be too stiff, as can be seen in Table 4.1. *The third constraint* attempted was to constrain in XYZ only two nodes along the perimeter of each mounting hole, allowing the part to pivot at the hole centers (Figure 4.2C). This constraint was too compliant, as can be seen in Table 4.1. *The final constraint* attempted was to apply a rigid kinematic constraint to the perimeter nodes of each mounting hole (Figure 4.2D). These kinematic constraints were connected to ground via the use of bar (B31) elements that were given a cross sectional area equivalent to the 1/2-inch (12.5 mm) bolts used in the test fixture. The end of these bolts was held in all 6 degrees of freedom. This constraint matched test observations for both displacement and strain to within 10% of experimental observations. Displacement plots for all four conditions can be found in Figure 4.4. Strain plots for all four conditions can be found in Figure 4.5. Figure 4.6 shows the strain gage location relative to the weld toe. For correlation purposes strains were taken at a point approximately at the center of the second element away from the weld toe. This closely corresponds to the center of the gage section of the 1.6 mm (0.0625-inch) strain gage used in this project.

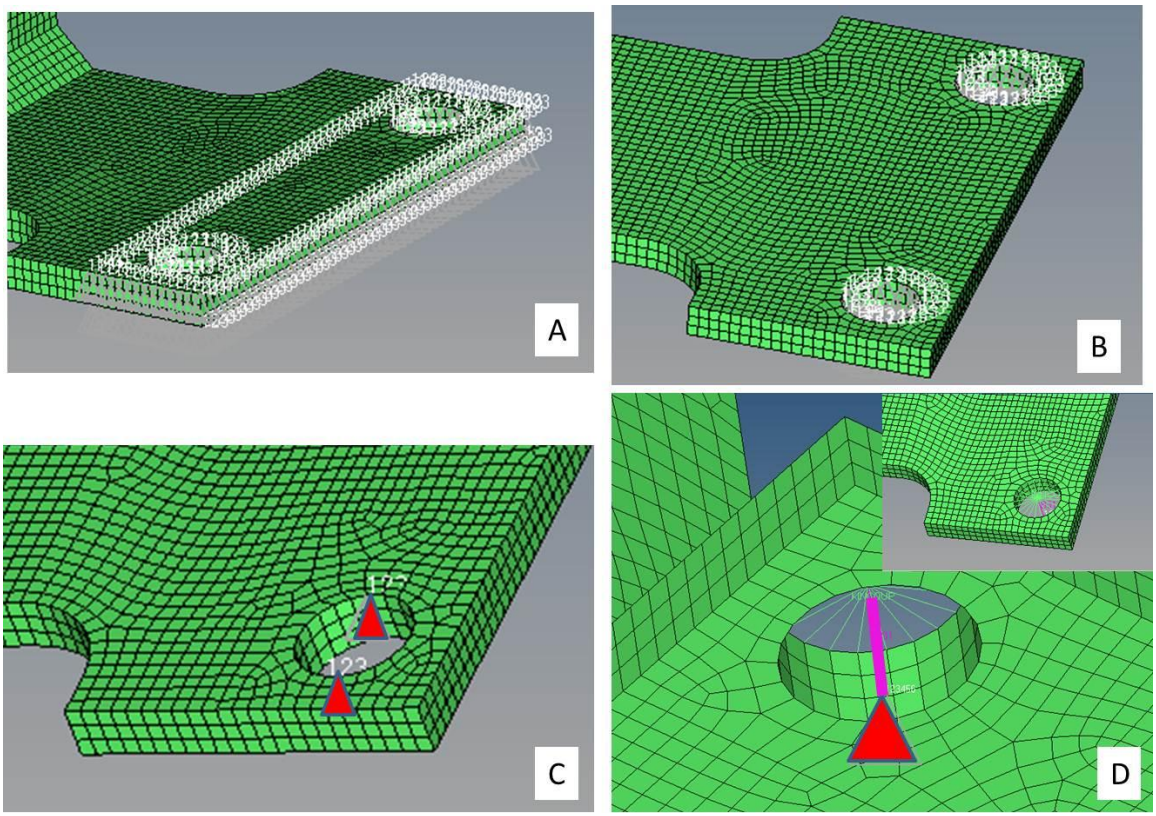

Figure 4.2 Boundary Condition Study

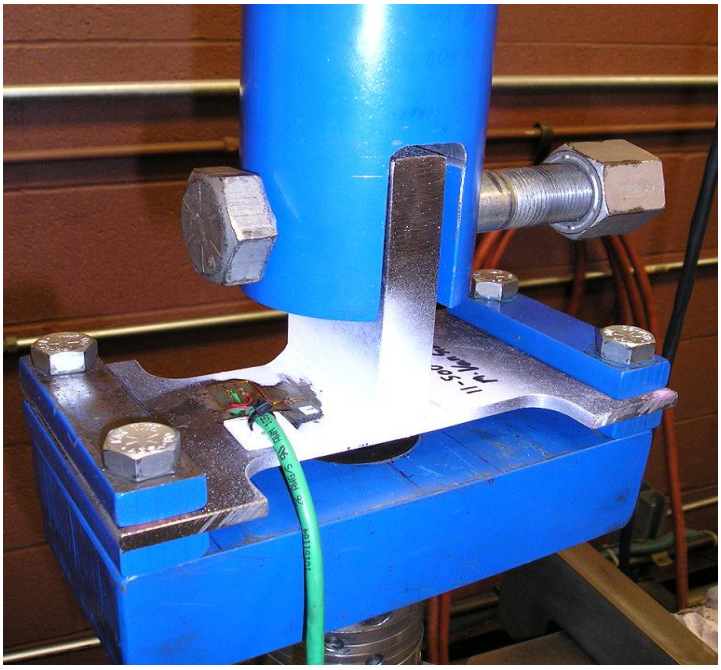

Figure 4.3 Test Sample Boundary Conditions

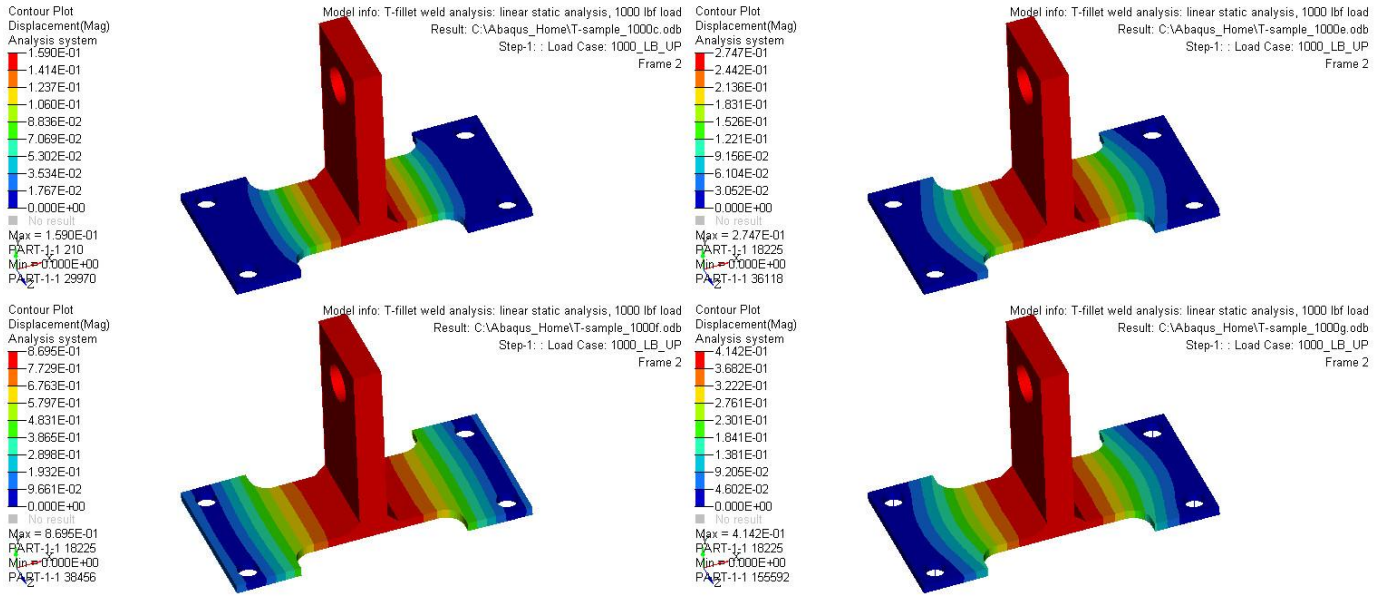

Figure 4.4 Displacement Results for Boundary Conditions A-D

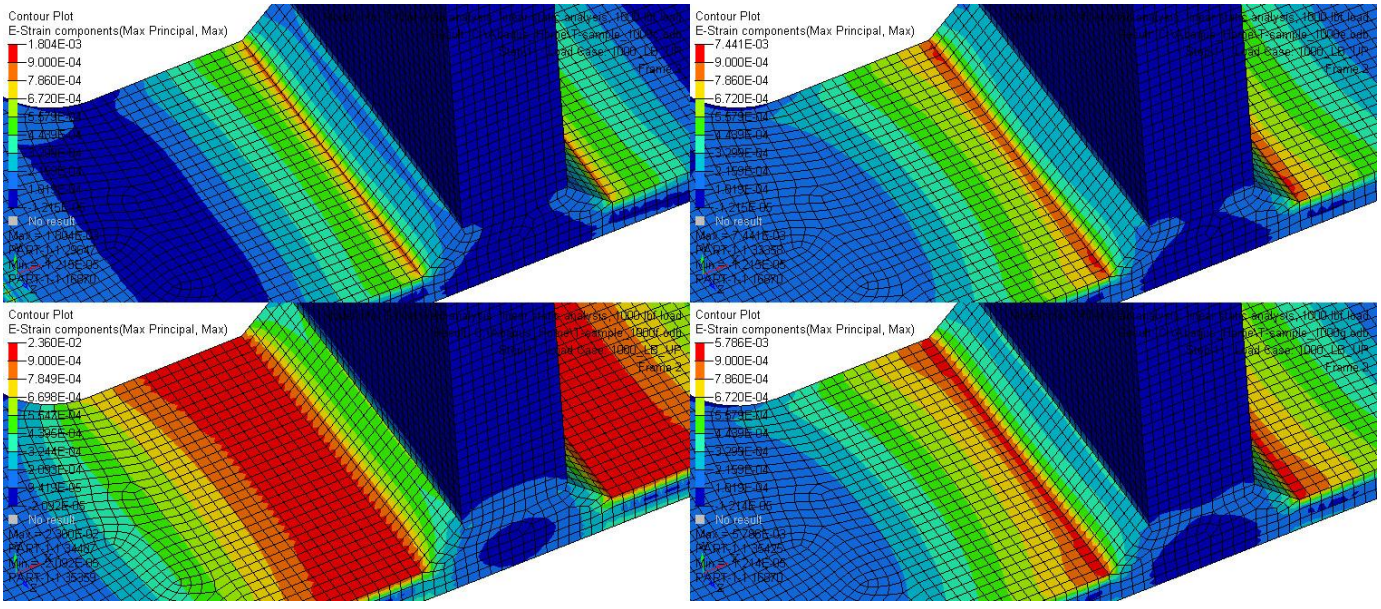

Figure 4.5 Max Principal Strain Results for Boundary Conditions A-D

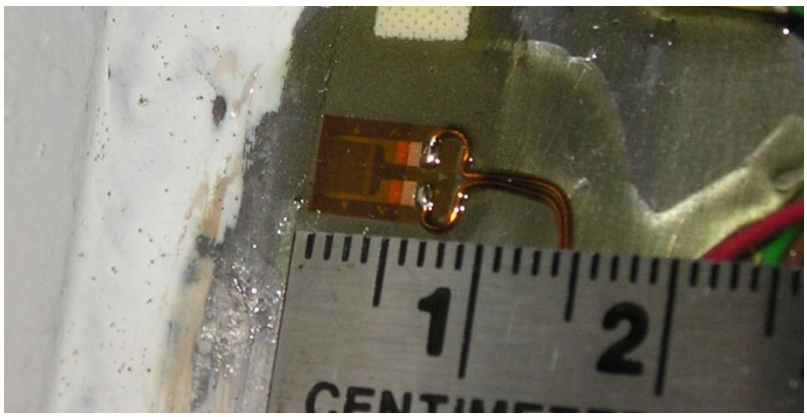

Figure 4.6 Strain Gage Location Relative to Weld Toe

Table 4.1 Boundary Condition Sensitivity Results

Boundary Condition		microstrain (ue)	deflection (mm)	% difference (ue)	% difference displacement
A	Perimeter of bar and perimeter of holes held 1,2,3	558	0.16	-31%	-64%
B	Perimeter of holes held 1,2,3	672	0.27	-17%	-40%
C	Two Points on each hole held 1,2,3,	1240	0.87	53%	93%
D	Perimeter of hole held with kinematic constraint, connected to a beam element whose end was fixed in 1-6	786	0.41	-3%	-9%
	Test Data	810	0.45	0%	0%

4.3 Fatigue Analysis Results using Numerical Methods

Both stress life and strain life analyses were conducted using the finite element results. These analyses were conducted using nCode's DesignLife Version 9.0 fatigue analysis tool. The FEA results from boundary condition set D from the previous section were used as an input to

the analysis. This result was from a 4448 N (1000-lb) vertical load. A test cycle was defined as alternating from 0.1 times 4448 N value to 1.7 times 4448 N. Both stress and strain results were available from the FE output.

Stress life analysis was conducted with material property assumptions of Class F weld per British Standard BS7608. Other relevant settings selected included 50% chance of survival and the use of max principal stress in the fatigue calculation. Life predictions indicated the minimum life in element 41833, located at the toe of the weld approximately 10 mm inboard of the part edge (Figure 4.7). Minimum life predicted was 182,000 cycles, which compares well, if conservatively, to the value of 287,000 cycles observed in the baseline test specimens for a 50% survival rate. Figure 4.8 shows the minimum life predictions for high cycle fatigue.

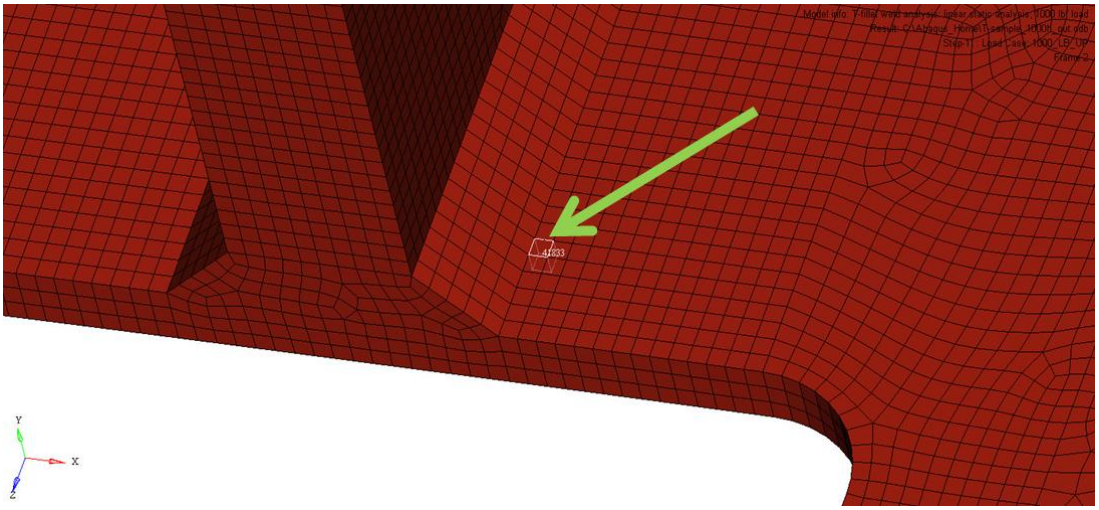

Figure 4.7 Minimum Life Element 41833

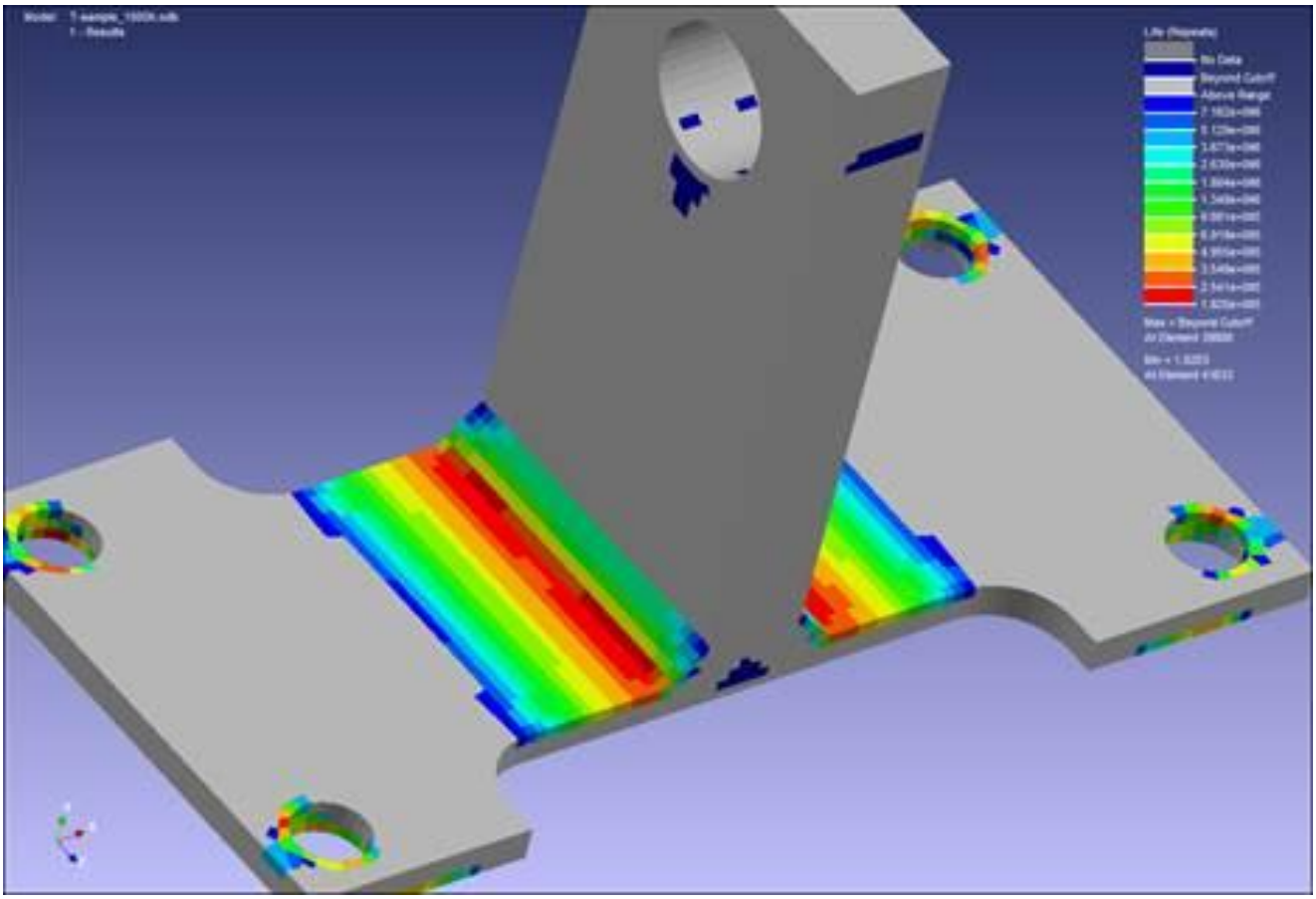

Figure 4.8 Image of S-N Analysis with class F welds per BS7608

Strain life analysis was conducted using A-36 steel material strain-life properties. These have been determined by the author in a prior test effort, and can be found in Attachment 3. Other relevant settings include the use of max principal strain, the selection of a 50% certainty of survival, the use of Neuber's rule for elastic-plastic correction, the use of Smith Watson Topper mean stress correction, and use of a K_f value of 1.63. This value was determined in section 3.3.4.2. The value 1.6 was suggested as a minimum by Fricke in the works edited by MacDonald (2011).

Life predictions indicated the minimum life in element 41833, located at the toe of the weld approximately 10 mm inboard of the part edge (Figure 4.7). Minimum life predicted was

210,000 cycles, which compares well to the value of 287,000 cycles observed in the baseline test specimens for a 50% survival rate. Figure 4.9 shows the minimum life predictions for high cycle fatigue.

Low cycle fatigue predictions for both stress life and strain life methods predicted static failure, a conservative assumption that was not supported by test data.

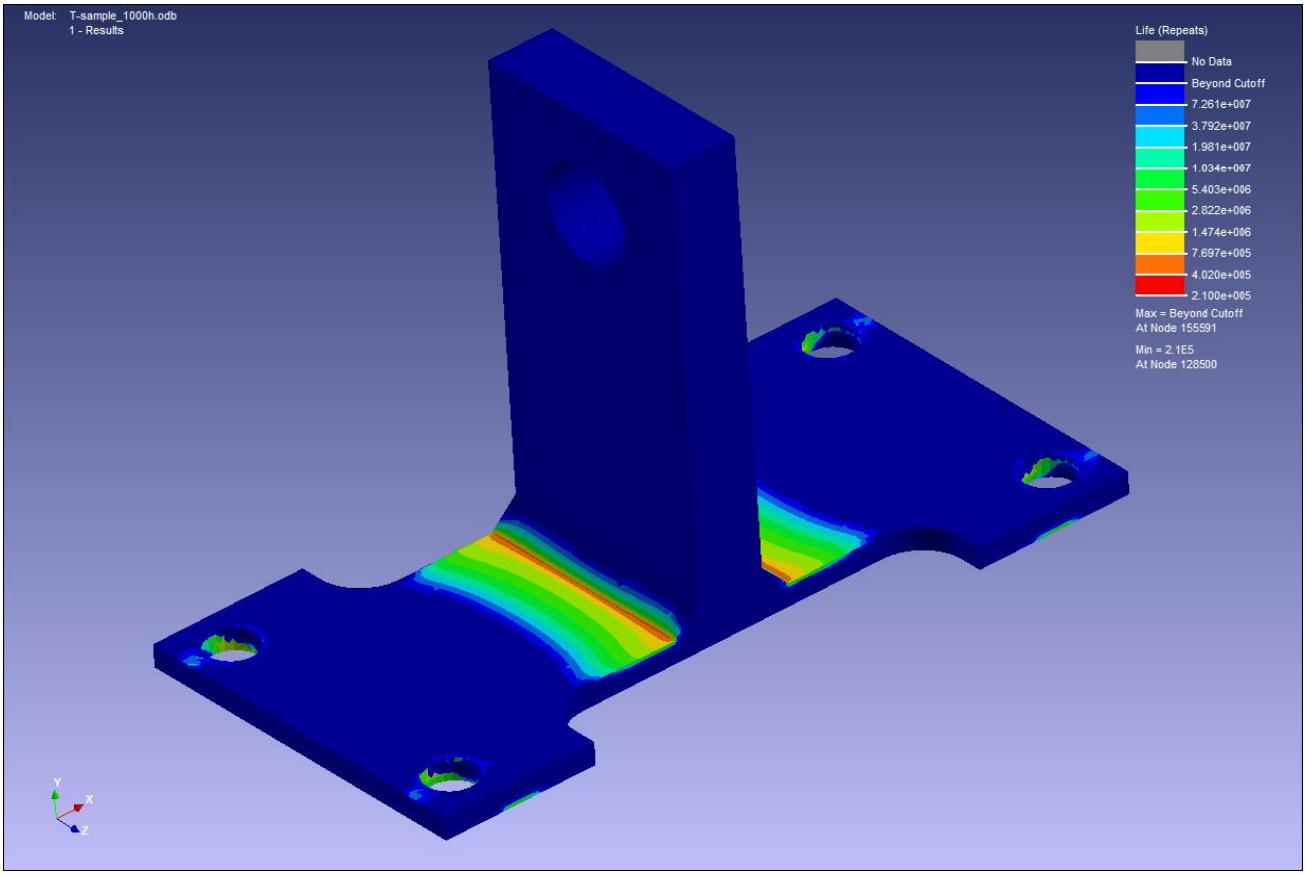

Figure 4.9 Image of e-N analysis with A36 Steel Material Properties

Chapter 5 Experimental Fatigue Results

5.1 Life Curves

Figure 5.1 shows the force-life curve for the baseline, hammer peened, and rotary flap peened test samples. Figure 5.2 is a plot of strain amplitude versus cycles to failure. Force was converted to strain based on the load versus experimental strain plot from Figure 3.27. Force was multiplied by the slope of this plot, which was found to be 0.182 microstrain per Newton (0.811 microstrain per pound). Figure 5.3 is a plot of stress amplitude versus cycles to failure. This plot was also calculated from the strain gage data in combination with the relationship for stress and strain under uniaxial loading mentioned earlier, $\sigma = \varepsilon E$. Where E is the elastic modulus of the parent material and is equal to 207GPa. All plots use engineering stress and engineering strain.

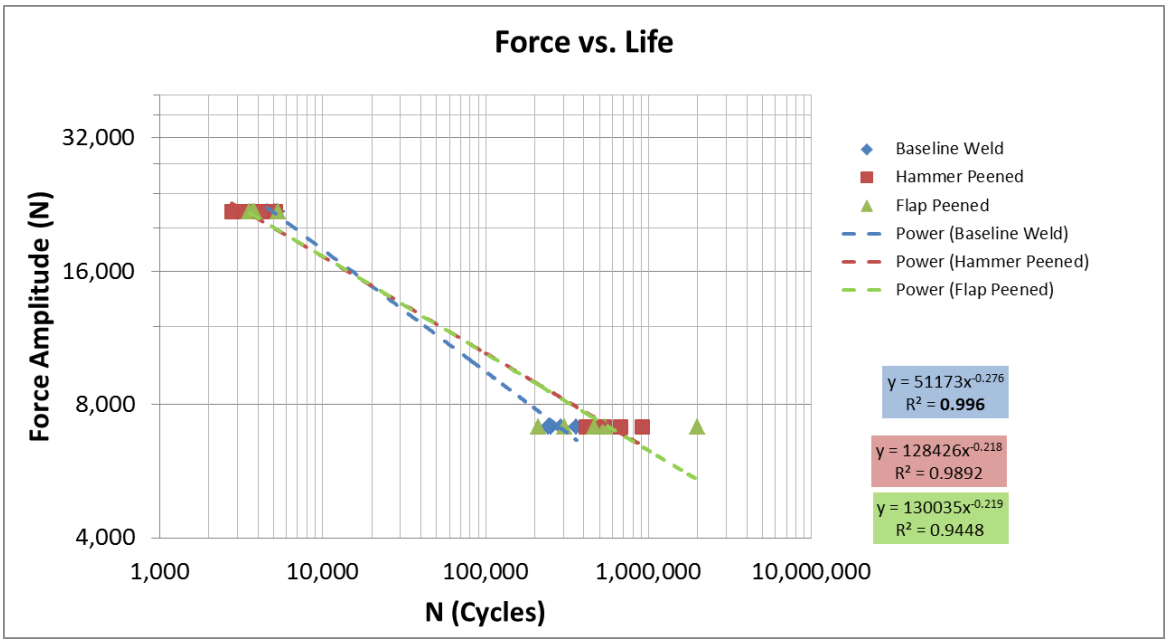

Figure 5.1 Force vs. Life Plot

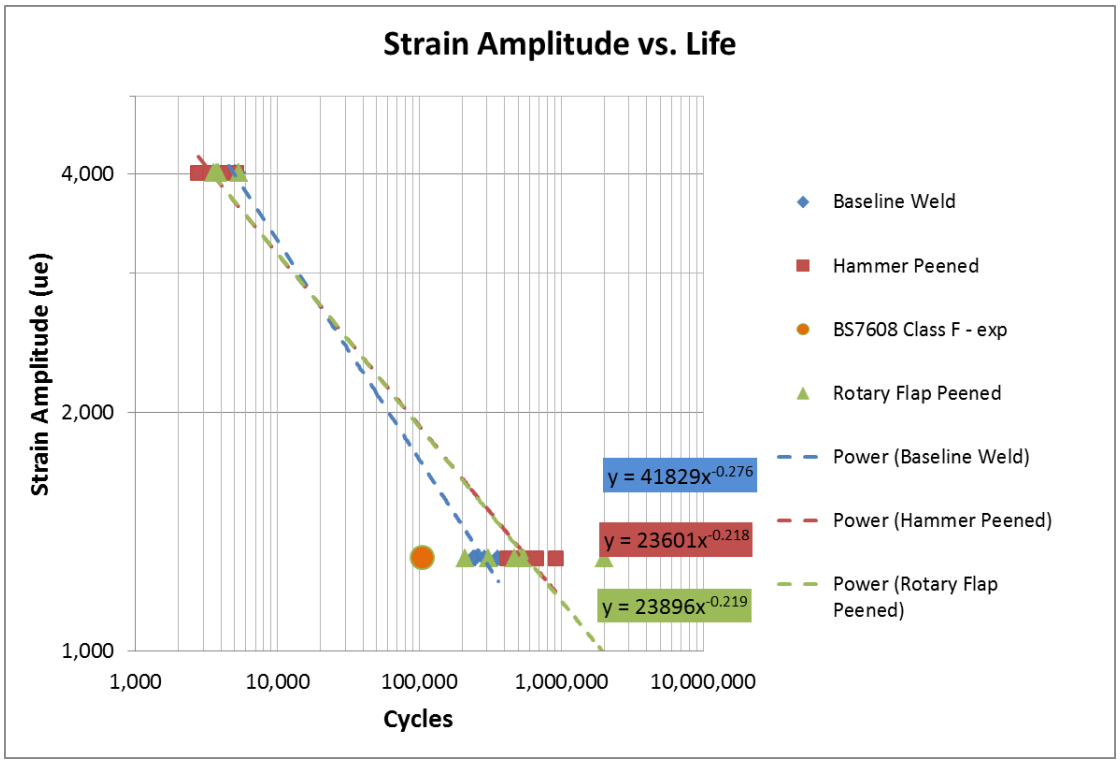

Figure 5.2 Engineering Strain vs. Life Plot

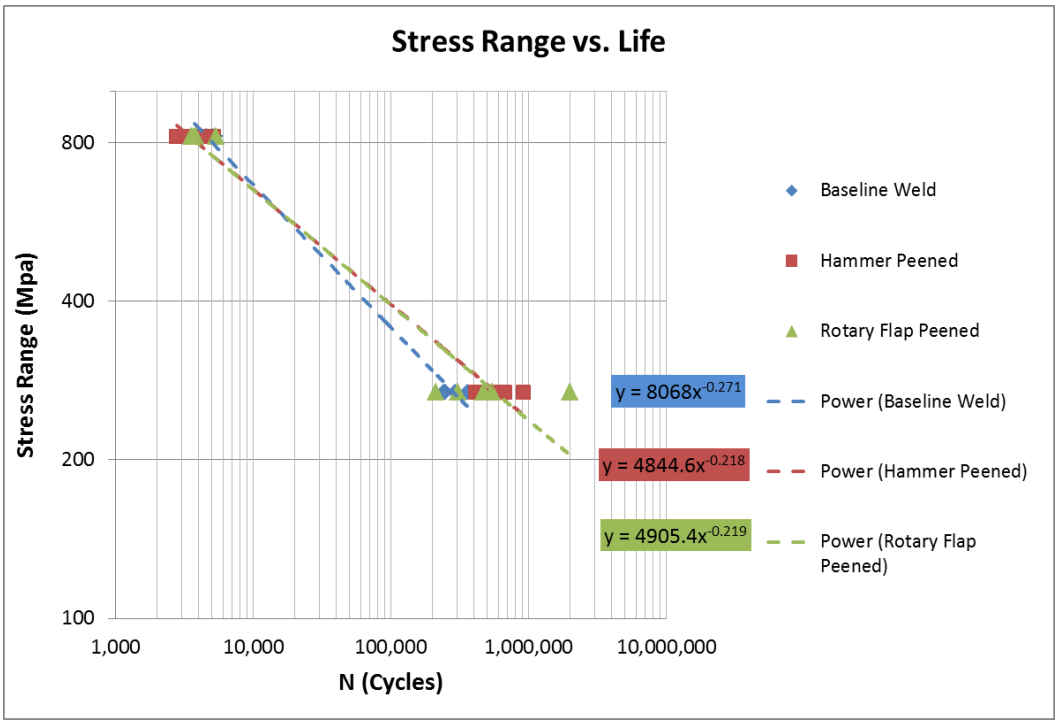

Figure 5.3 Engineering Stress vs. Life Plot

Figure 5.4 is a plot that includes the experimental fatigue life and predicted fatigue life for the following approaches.

- Experimental values
    - Baseline (un-peened) fatigue samples
    - Hammer peened fatigue samples
    - Rotary flap peened fatigue samples
- Predictive values based on measured strains
    - Stress life analysis using Class F weld properties per BS7608
    - Strain life analysis with A36 steel material properties and $K_f = 2.0$
    - Strain life analysis with A36 steel material properties and $K_f = 2.2$
    - Strain life analysis with A36 steel material properties and $K_f = 1.63$
    - Stress life analysis with A36 steel material properties and $K_f = 1.63$

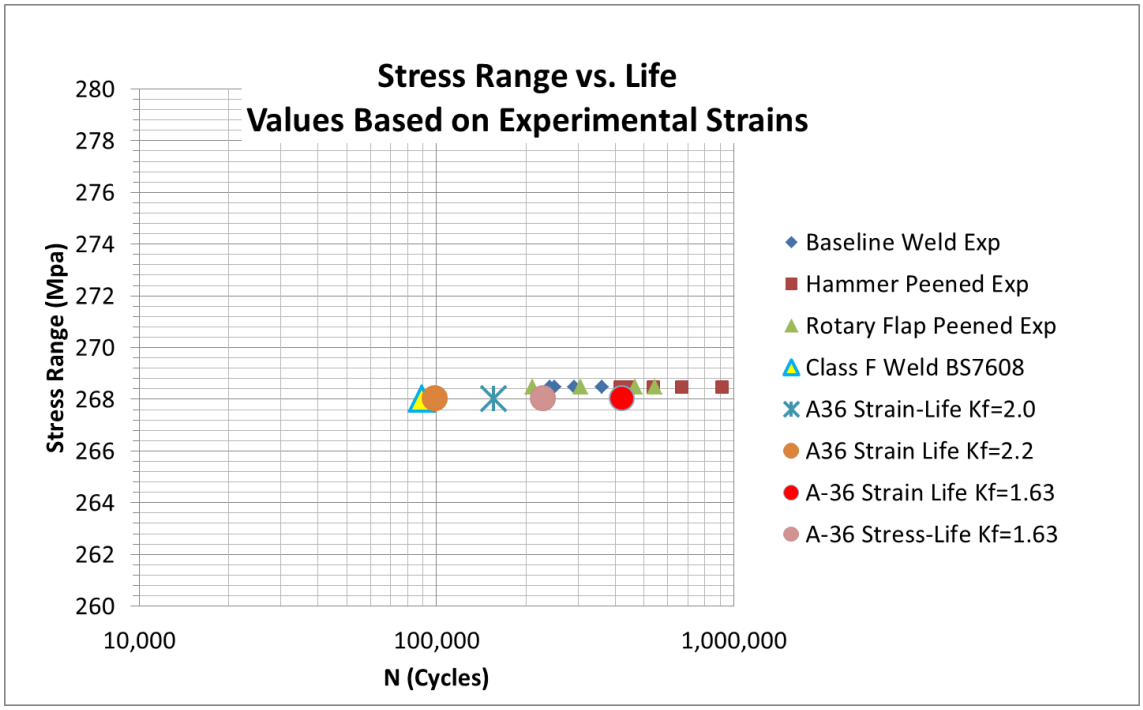

Figure 5.4 Life Predictions Based on Experimental Measurements and S-N or e-N Curves

5.2 Table of Raw and Calculated Data

Table 5.1 summarizes the fatigue life for each of the cycled test specimens.

Table 5.1 Cycle Test Data

Sample	Peening	Life (cycles)	Max Force (lbf)	Min Force (lbf)	Frequency (Hz)	Strain (max, ue)	Strain (min, ue)	Stress (max, MPa)	Stress (min, MPa)	Stress Range (MPa)
2	None	250,000	1700	100	4	1379	81	285	17	268
3	None	360,000	1700	100	4	1379	81	285	17	268
4	None	240,787	1700	100	4	1379	81	285	17	268
5	None	291,000	1700	100	4	1379	81	285	17	268
6	None	5,276	5000	100	2	4055	81	839	17	822
7	None	5,079	5000	100	2	4055	81	839	17	822
8	None	4,560	5000	100	2	4055	81	839	17	822
9	None	3,741	5000	100	2	4055	81	839	17	822
10	Hammer	414,000	1700	100	4	1379	81	285	17	268
11	Hammer	441,000	1700	100	4	1379	81	285	17	268
12	Hammer	536,000	1700	100	4	1379	81	285	17	268
13	Hammer	913,000	1700	100	4	1379	81	285	17	268
14	Hammer	669,000	1700	100	4	1379	81	285	17	268
15	Hammer	4,178	5000	100	2	4055	81	839	17	822
16	Hammer	5,137	5000	100	2	4055	81	839	17	822
17	Hammer	2,768	5000	100	2	4055	81	839	17	822
18	Hammer	2,781	5000	100	2	4055	81	839	17	822
19	Hammer	3,332	5000	100	2	4055	81	839	17	822
20	Rotary Flap	467,000	1700	100	4	1379	81	285	17	268
21	Rotary Flap	210,800	1700	100	4	1379	81	285	17	268
22	Rotary Flap	544,000	1700	100	4	1379	81	285	17	268
23	Rotary Flap	2,000,000	1700	100	4	1379	81	285	17	268
24	Rotary Flap	306,220	1700	100	4	1379	81	285	17	268
25	Rotary Flap	5,344	5000	100	2	4055	81	839	17	822
26	Rotary Flap	3,833	5000	100	2	4055	81	839	17	822
27	Rotary Flap	3,709	5000	100	2	4055	81	839	17	822
28	Rotary Flap	3,548	5000	100	2	4055	81	839	17	822
The following samples were used for test set-up										
00	None	Strain gauged sample, was not cycled								
0	None	2,500,000	1000	100	4	811	81	168	17	151
1	None	109,082	2000	100	4	1622	81	336	17	319

5.3 Applied Statistics

As can be observed from the data presented in Table 5.1, there is considerable spread observed in the experimental failure data. For example, Samples 21 and 23 were fabricated and

peened using the same methods and loaded at the same amplitude, but observe an order of magnitude difference in fatigue life. This variation, and that of all other fatigue samples, was examined using statistical methods. Using the software statistics tool Minitab 16 the high cycle fatigue data was examined for distribution type. Weibull, lognormal, and normal distributions all had excellent correlations to experimental test data (Figure 5.5). The experimental data was fitted to a Weibull distribution, as this is an established best practice for reliability evaluation (Figure 5.6).

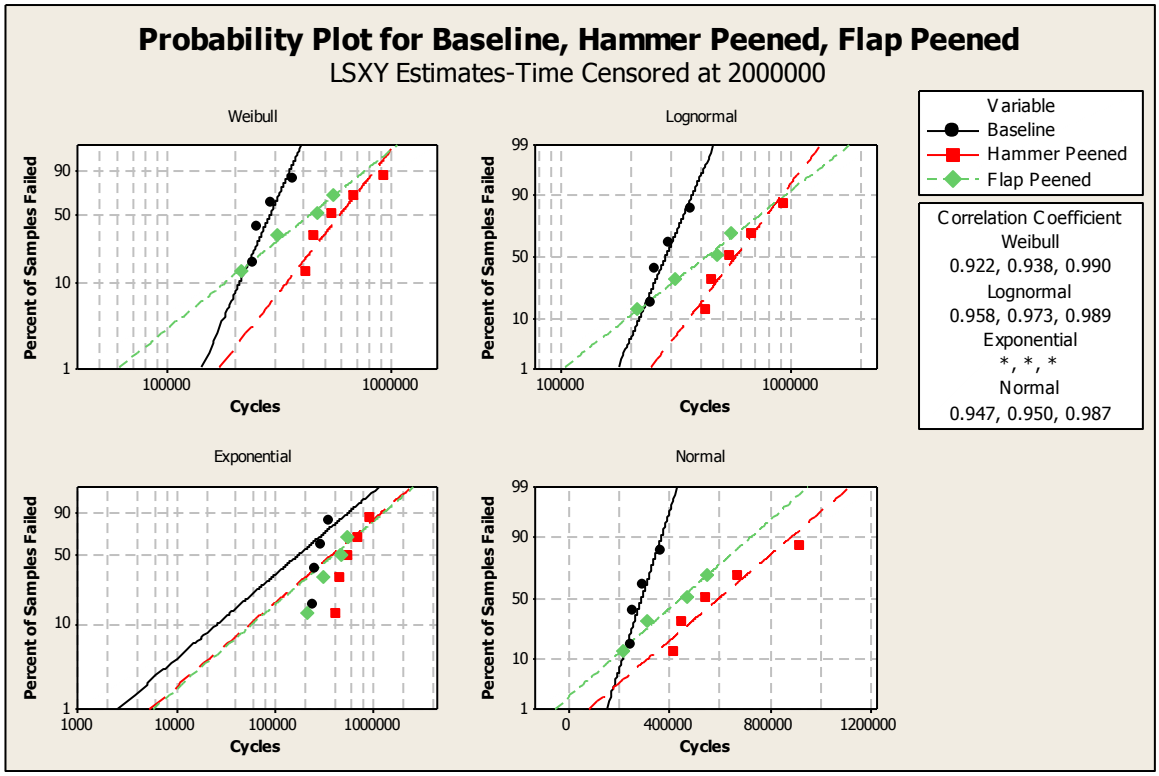

Figure 5.5 Distribution Correlation

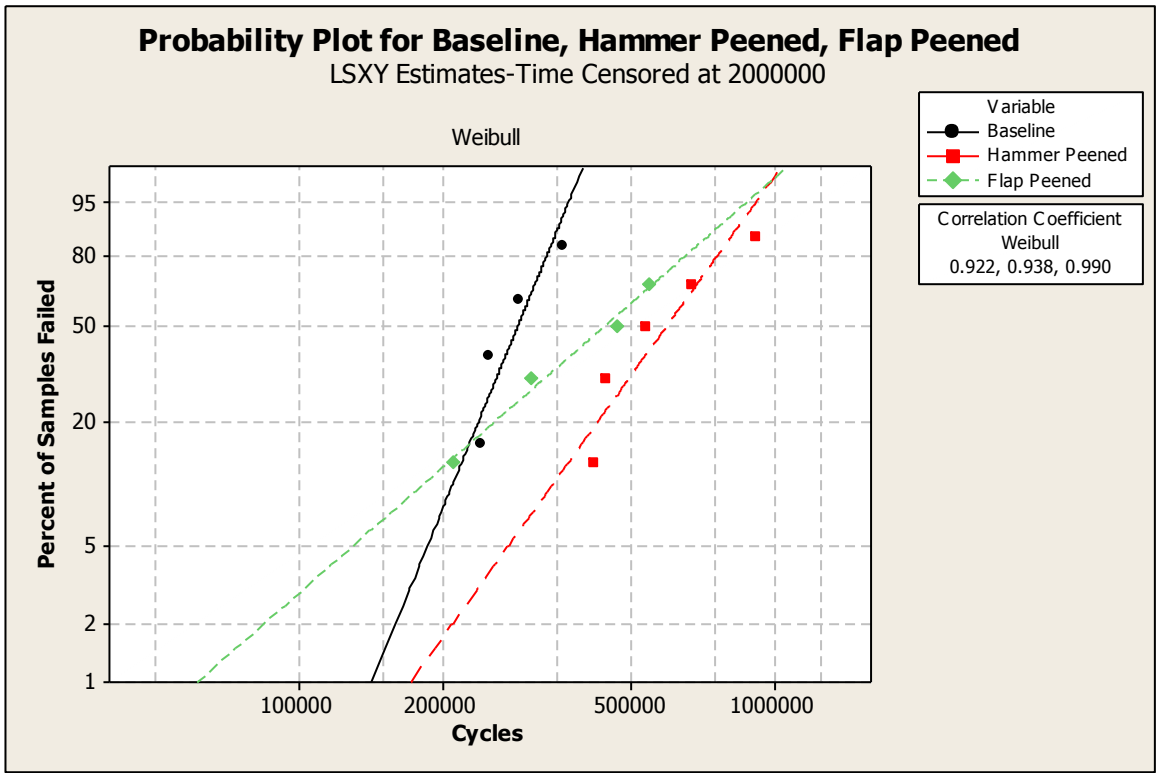

Figure 5.6 Weibull Distribution for High Cycle Fatigue

It is evident from examining the failure probability distribution that the peening methods used in this research introduced large variability in the samples. The 50% and 90% confidence values for cycles to failure, along with percent change from the baseline, are included in Table 5.2 below. When seen graphically, as in Figure 5.5, it is evident that one would come to a different conclusion based on the confidence value selected.

Table 5.2 Life Probability for Low and High Cycle Fatigue

High Cycle Fatigue Distribution						
	Baseline	% of Baseline	Hammer Peened	% of Baseline	Flap Peened	% of Baseline
50% confidence	287,088	100%	590,348	206%	436,336	152%
90% confidence	209,564	100%	340,153	162%	181,443	87%
Low Cycle Fatigue Distribution						
	Baseline	% of Baseline	Hammer Peened	% of Baseline	Flap Peened	% of Baseline
50% confidence	4,701	100%	3,640	77%	4,121	88%
90% confidence	3,544	100%	2,321	65%	3,086	87%

The low cycle fatigue data was also evaluated for distribution type, with similar results. Figure 5.6 shows the Weibull distribution plot for the low cycle fatigue samples. There is not as much scatter in this data, and trends are easier to identify.

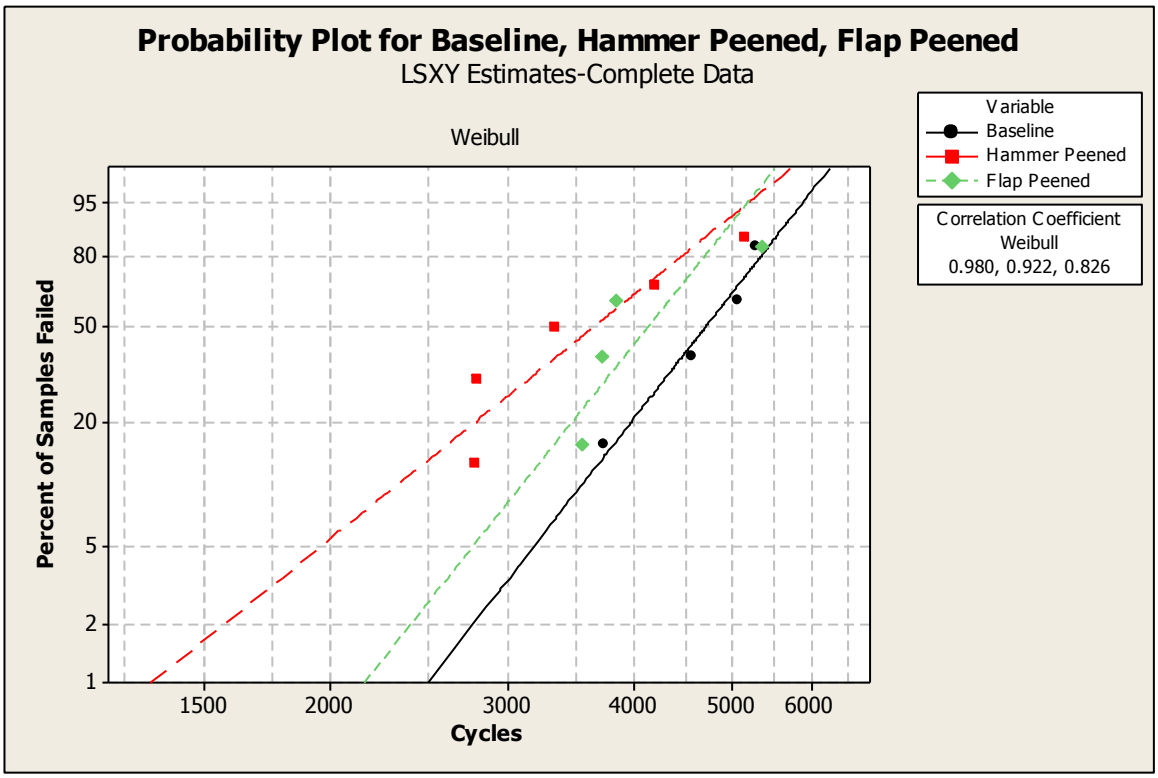

Figure 5.7 Weibull Distribution for Low Cycle Fatigue

Chapter 6 Microscopy failure analysis

Several of the cracked test samples were inspected after testing using microscopy failure analysis techniques. The four methods of evaluation used were visual examination of surface integrity, fractography, microstructure evaluation, and microhardness measurement. Figure 6.1 shows three of the samples that were examined. The part on the left in the image, sample 4, was an un-peened sample that was used to establish the baseline sample life. The center image, sample 10, was hammer peened. The right hand image, sample 22, was rotary flap peened to an Almen intensity of 12A.

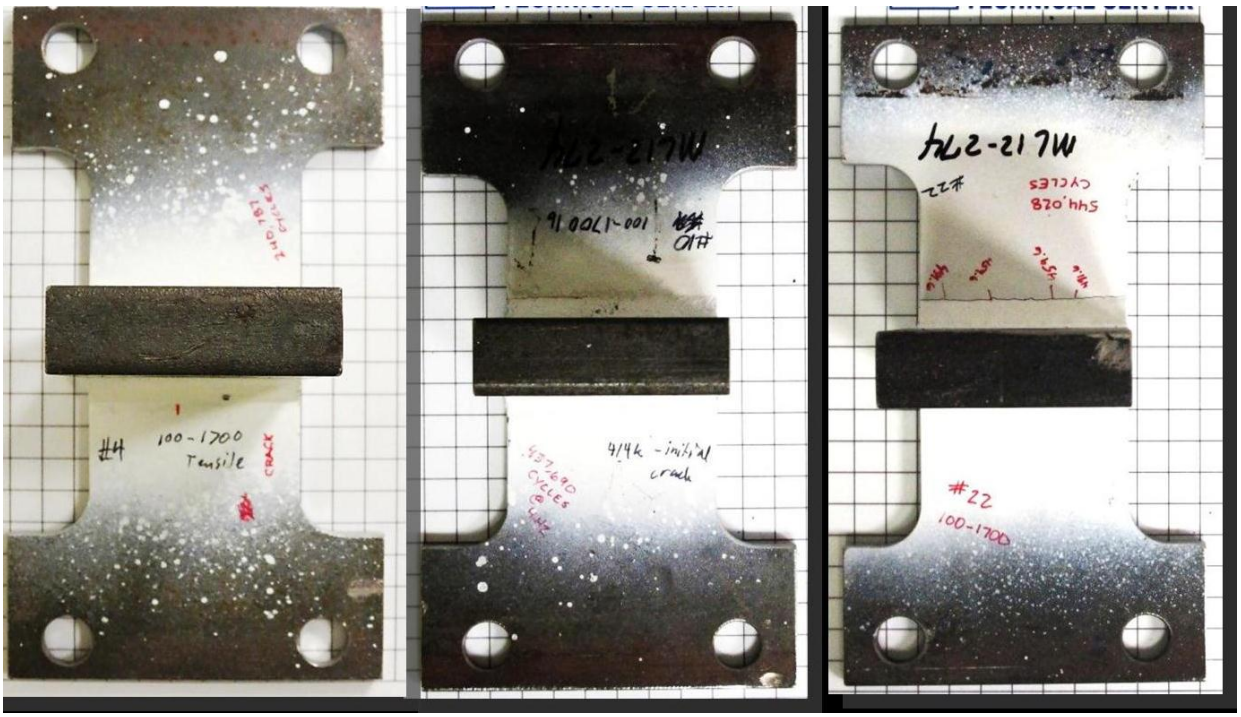

Figure 6.1 Test Samples Inspected

Un-peened Sample #4, Hammer Peened Sample # 10, Flap Peened Sample #22.

6.1 Peened Surface Inspection

Figures 6.3, 6.4, and 6.5 highlight the variability of surface integrity both before and after the two different peening operations. Each of these three figures shows the weld nugget at the left, the weld toe at center, and the base leg at the right.

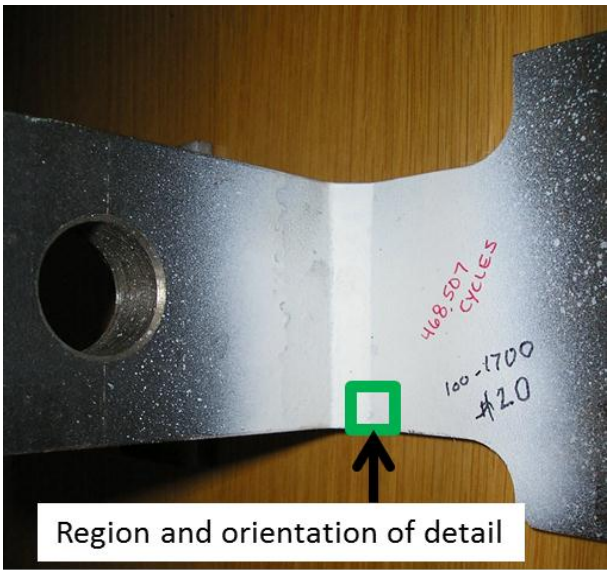

Figure 6.2 Location of Detail Images (Typical Part) Figures 6.3-6.5

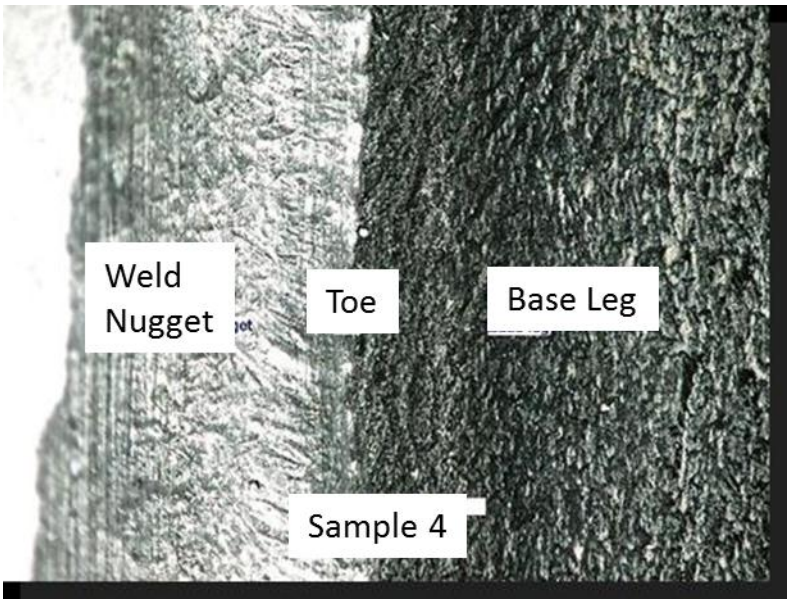

Figure 6.3 Surface Detail – Baseline (Un-Peened) Sample (20x Magnification)

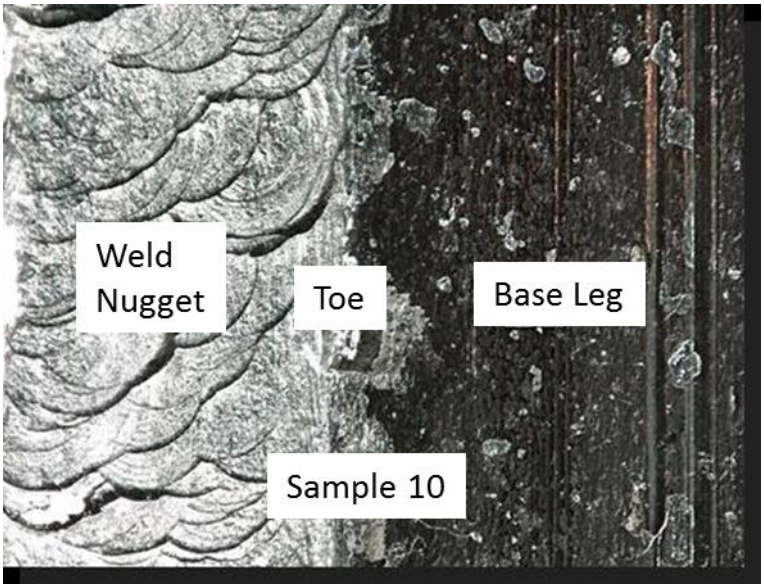

Figure 6.4 Peened Surface Detail – Hammer Peened Part (20x Magnification)

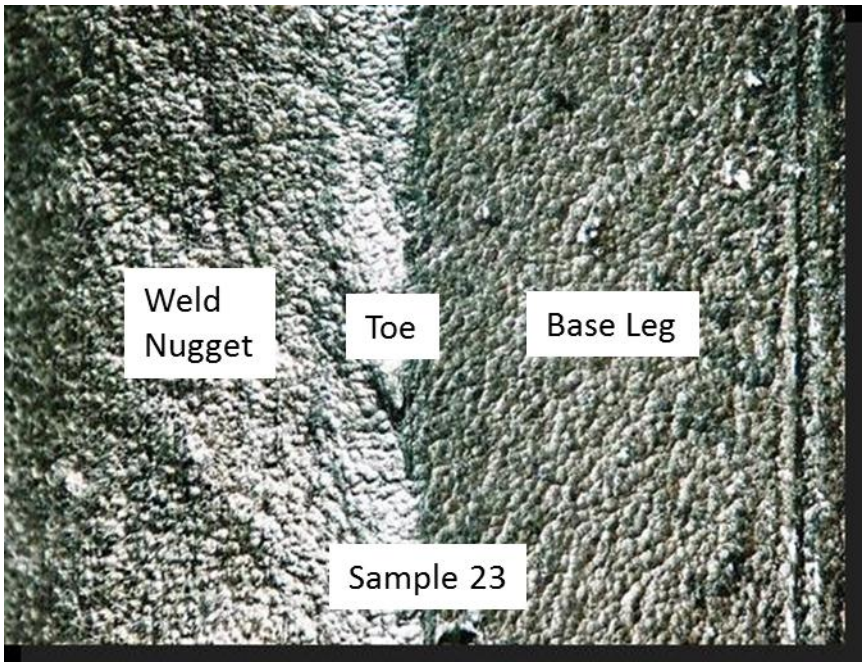

Figure 6.5 Peened Surface Detail – Flap Peened Part (20x Magnification)

It can be seen from these images that the un-peened sample has variation in surface integrity between the weld and the base material. The hammer peened surface seen in Figure 6.4

shows the significant modification in the peened surface, including the creation of ridges and valleys in the weld surface. The flap peened surface has the greatest uniformity of the three samples examined.

The rotary flap peened samples displayed the largest variation in fatigue life. The extremes of this performance occurred in sample 23, which was suspended without failure at 2 million cycles, and sample 21, which failed at approximately 211,000 cycles. In order to gain understanding of this variability the weld toe was examined under 20X magnification. Figure 6.6 below shows sample 21. Figure 6.7 shows the weld toe of sample 23. It is observed from these two images that the transition from the weld to the base material across the toe of the weld is very smooth for sample 23, while for sample 21 there is a groove in the part at this location. It is reasonable to conclude that the shot used in the flap peening process was too large to effectively peen this groove, resulting in a region without the beneficial surface compressive residual stresses. The smooth transition sample allowed good peen coverage, with overlapping dimples evident upon inspection, greatly prolonging the sample life.

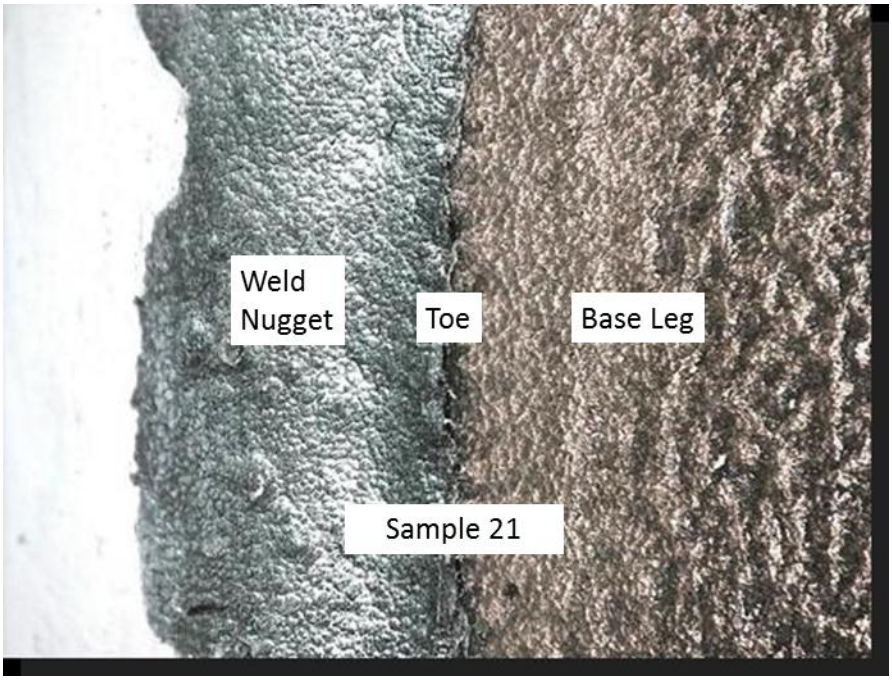

Figure 6.6 Weld Toe for Sample 21 (211,000 cycle failure)

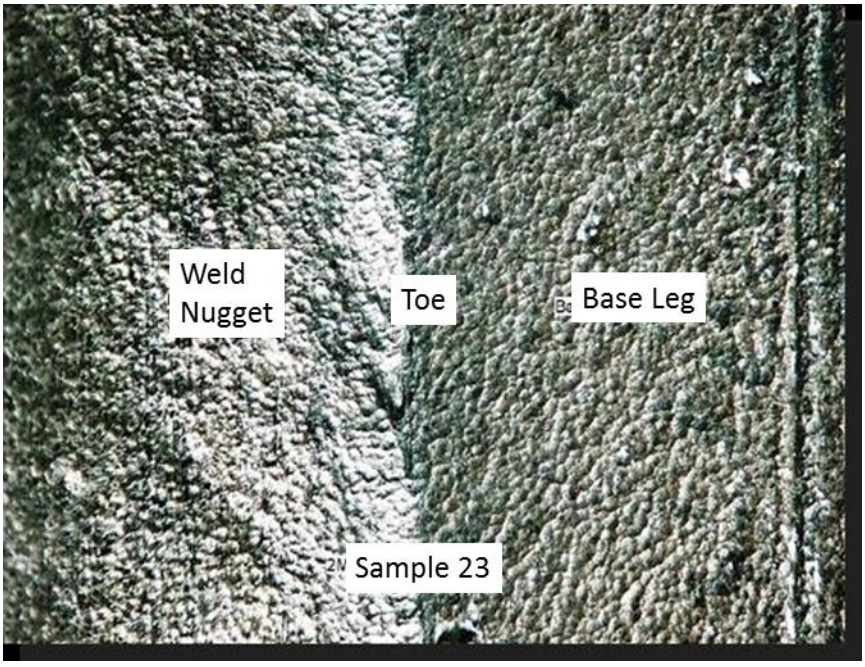

Figure 6.7 Weld Toe for Sample 23 (Suspended without Failure at 2,000,000 cycles)

6.2 Fracture Surface Examination

For three different test samples the crack was opened up completely to examine the fracture surface. Figure 6.8 shows where these inspections occurred on the test samples. Figures 6.9 – 6.11 show these fracture surfaces with fracture faces across the top and base leg at the bottom of the image. All images were originally obtained at 50x magnification in a scanning electron microscope (SEM) using the backscattered electron mode. Sample 4 was not peened. It is evident on this sample (Figure 6.9) that there were numerous crack origins at the weld toe across the fracture surface. Sample 10 was hammer peened. The crack origins for this sample are discrete, originating at un-peened areas (Figure 6.10). Sample 22 is similar, with crack origins evident in areas of no peening (Figure 6.11). These images show the effects of poor surface integrity on continuous or discrete crack origination.

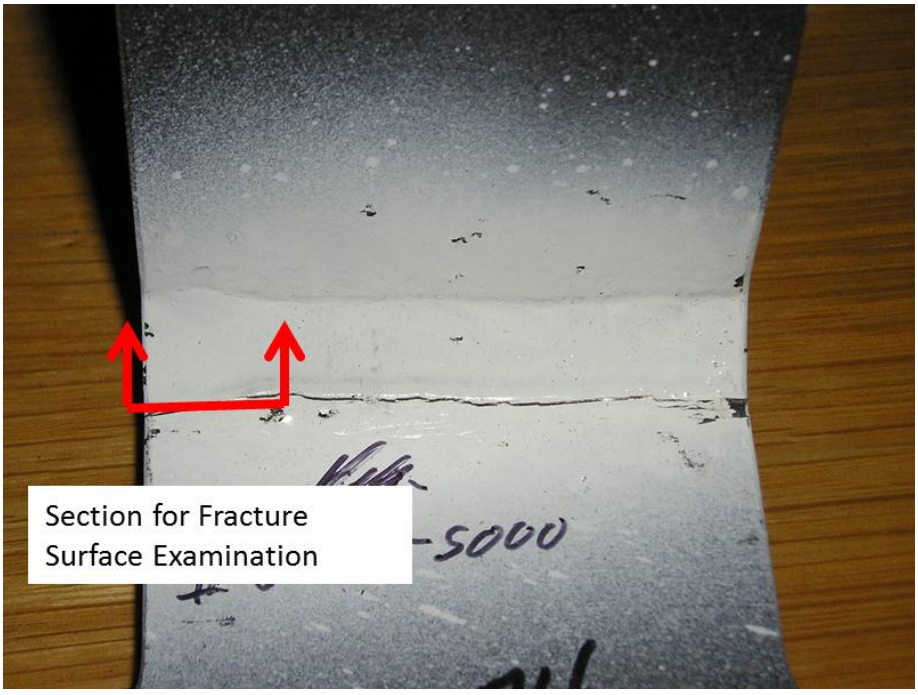

Figure 6.8 Location of Fracture Surface Inspection

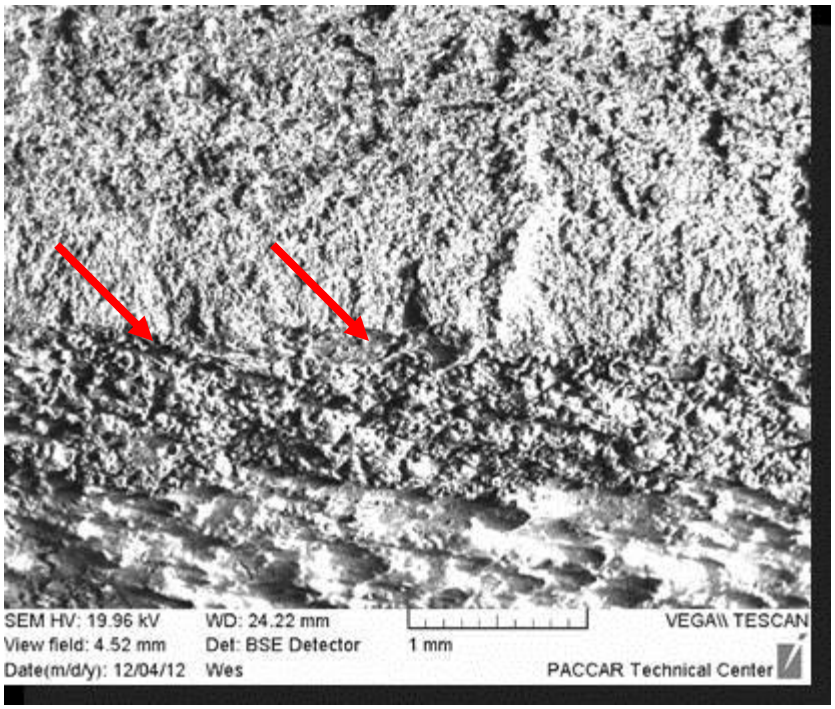

Figure 6.9 Fracture Surface for Sample 4 – Un-Peened

Arrows Point to Crack Initiation Sites

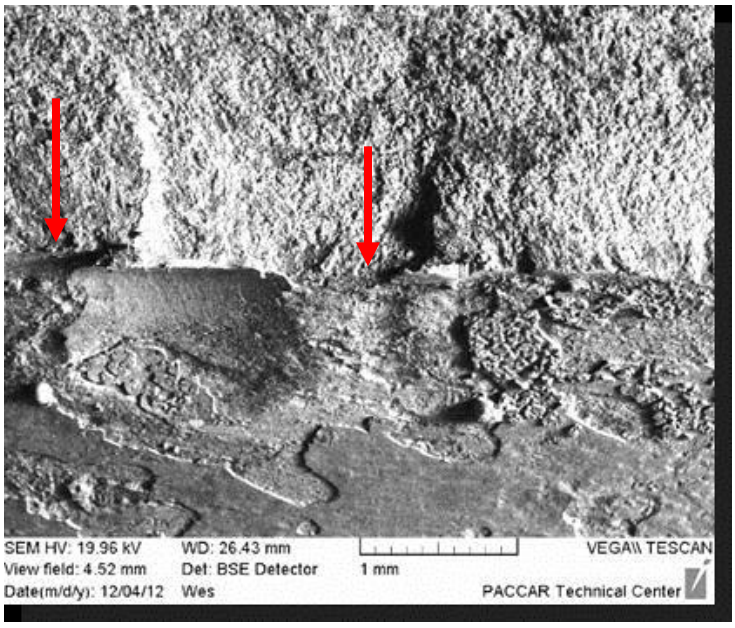

Figure 6.10 Fracture Surface for Sample 10 – Hammer Peened

Arrows Point to Crack Initiation Sites

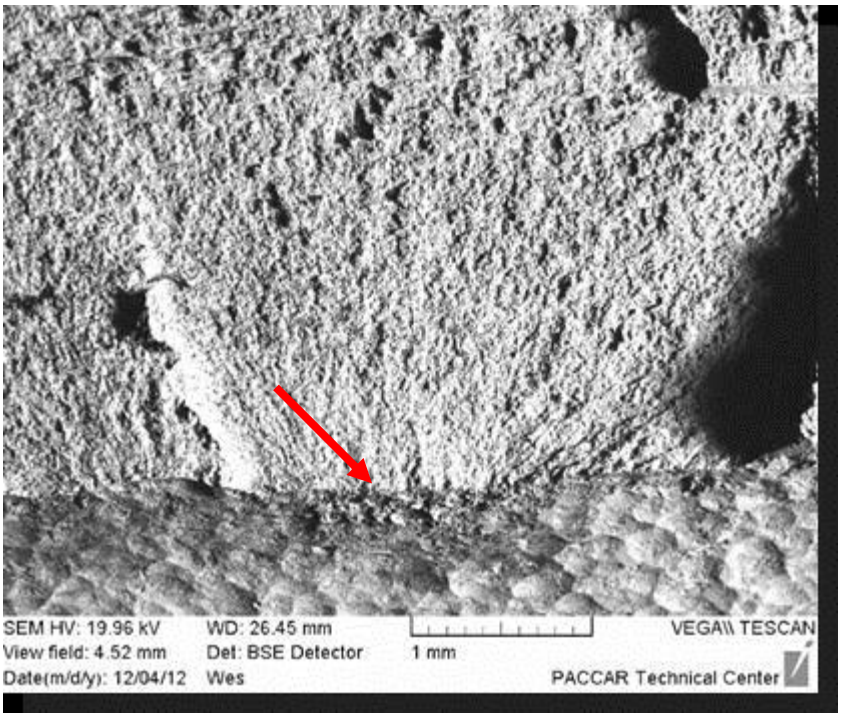

Figure 6.11 Fracture Surface for Sample 22 – Flap Peened

Arrow Points to Crack Initiation Sites

6.3 Cross Section Examination

Test samples 4, 10, and 22 were sectioned perpendicular to the crack direction in order to examine the crack profile and weld section. Figure 6.12 shows the approximate location of the sections on a representative fatigue sample. Figures 6.13-6.15 were obtained at 50x magnification with a light microscope after the samples had been polished and etched with a 2% or 4% Nital solution. Figure 6.13 shows that the un-peened sample crack initiated in multiple locations near or at the weld toe. Figure 6.14 shows that for the hammer peened samples cracks originated in the weld nugget and at the weld toe in discrete locations. There is also some evidence of micro cracking internally in this sample (shown by the yellow

arrows in the image). Figure 6.15 shows that for the flap peened sample crack origins were at discrete locations in areas of the weld toe with little or no peening. The large void seen in Figure 6.15 is due to a measurement point for the Vickers hardness test described in the next section. For all samples cracking originates at or near the weld toe.

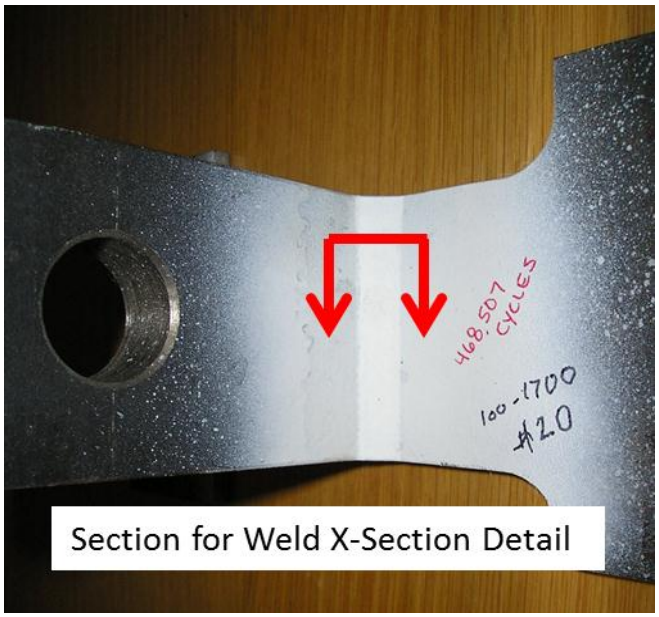

Figure 6.12 Location of Section Cut

Figure 6.13 Un-Peened Test Sample 4 Crack Site

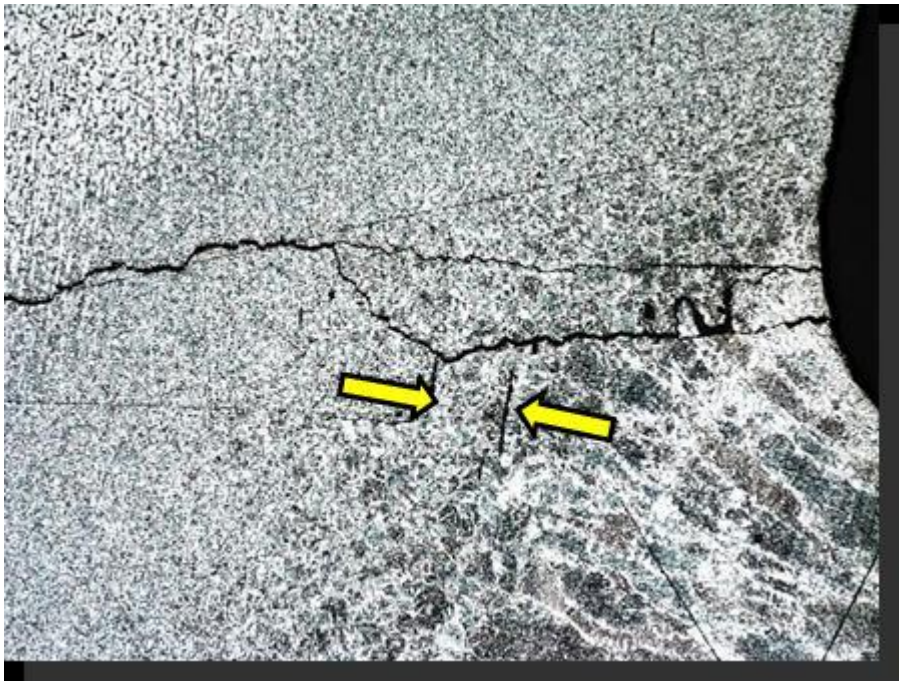

Figure 6.14 Hammer Peened Test Sample 10 Crack Site

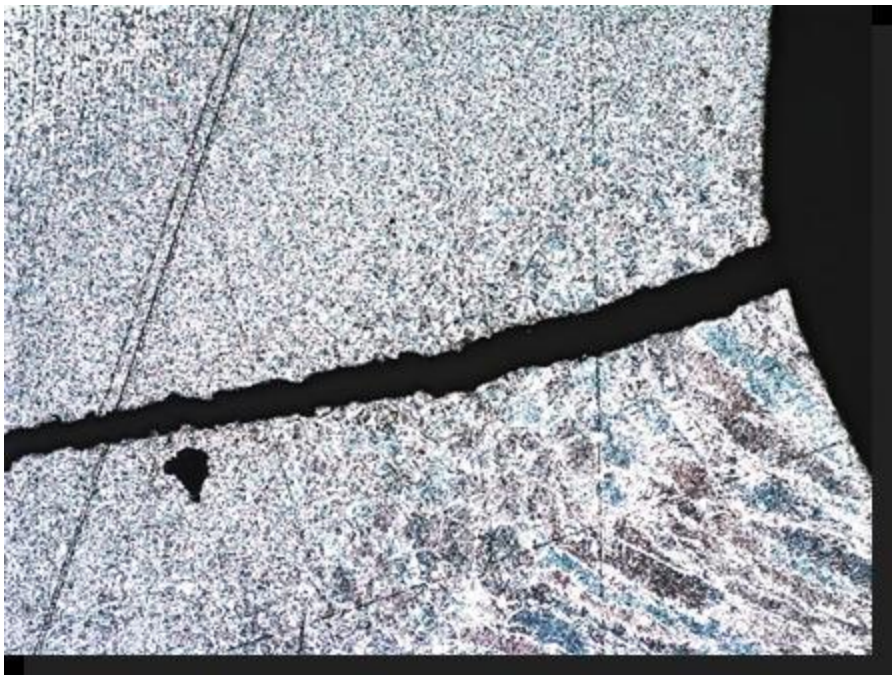

Figure 6.15 Flap Peened Sample 22 Crack Site

4.4 Microhardness Comparisons

Microhardness was measured on the same sections identified in Figures 6.12-6.15. Measurements were taken every 0.15 mm traversing two linear paths. The first path began in the weld nugget away from the crack origin and traveled through the weld nugget and into the parent material. This is the vertical line of indentations shown in Figures 6.16 through 6.18. The second path began at the weld nugget and traveled across the weld toe and into the base leg of the parent material, remaining close to the surface of the material. This is the horizontal line of indentations evident in Figures 6.16 through 6.18. Note that this horizontal line of hardness measurements spans across the fatigue crack in the test samples. All images were captured at 20x magnification after sample polishing and etching with 2% or 4% Nital solution.

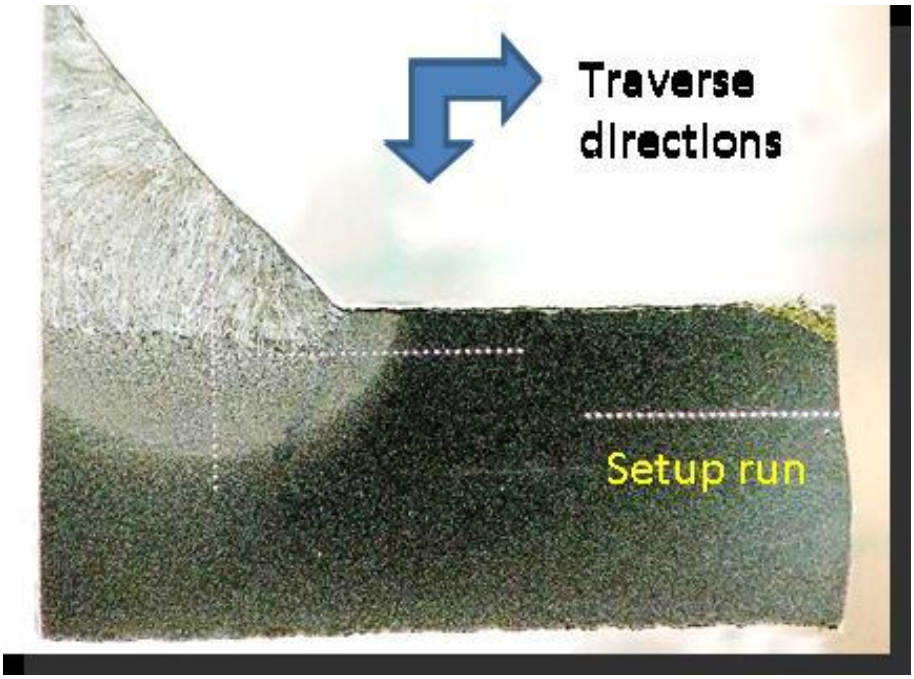

Figure 6.16 Microhardness Measurements – Un-Peened Sample 4

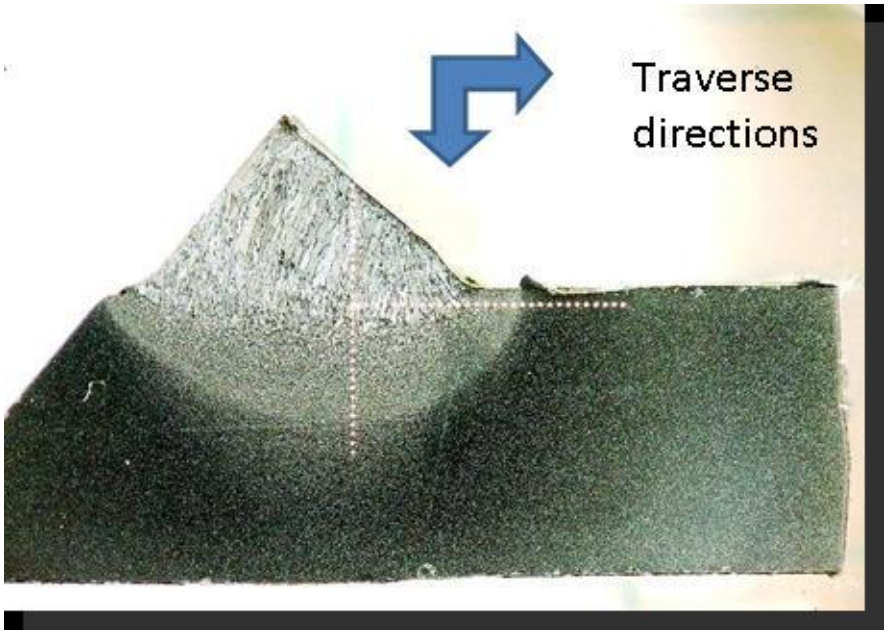

Figure 6.17 Hammer Peened Sample 10

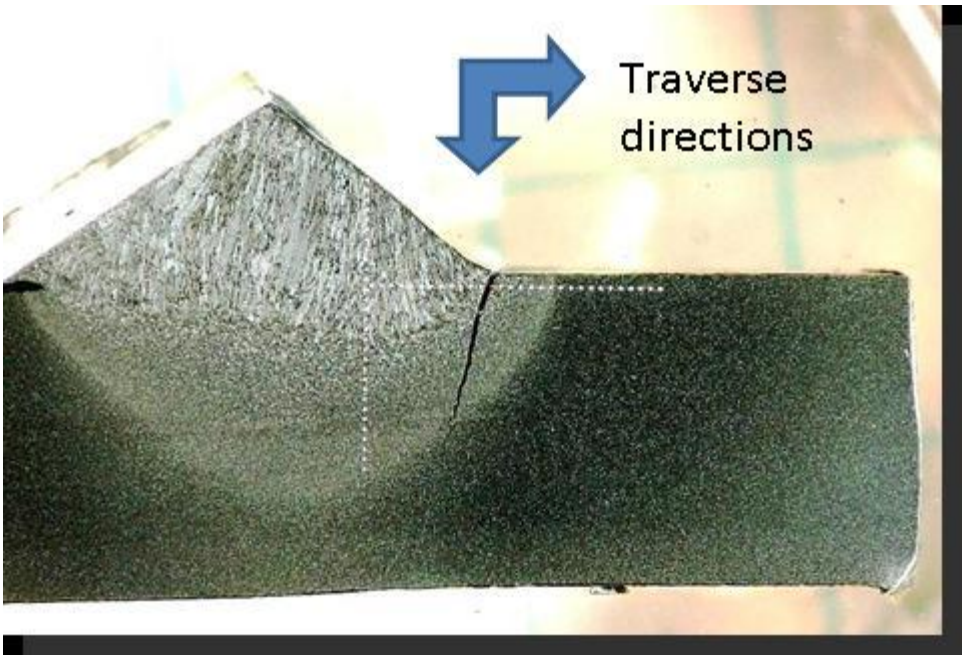

Figure 6.18 Flap Peened Sample 22

Plots of microhardness versus position across the weld are included in Figures 6.19 and 6.20. In both of these plots sample 4 (blue) is the un-peened test case. Sample 10 (red) is the hammer peened test sample and sample 22 (green) is the rotary flap peened test sample. It can be noted that the hammer peening produced more work hardening of the weld nugget than the baseline or flap peened samples. It is possible that this observation could cause embrittlement and multiple fatigue cracks in the nugget, in the HAZ toe, and microcracking internal to the nugget as seen in Figure 6.14. From Figure 6.19 it also appears that the hardened surface extended further away from the weld toe in the parent material. Earlier it was noted that the hammer peened test samples un-cupped during peening, recovering their original flatness that was lost during welding. This observation of greater surface hardness in the weld and the base leg near the toe of the weld provides some additional explanation for this behavior. The baseline and rotary flap peened samples did not demonstrate similar behavior. As can be seen from Figures 6.19 and 6.20, samples 4 and 22 were similar in surface hardness

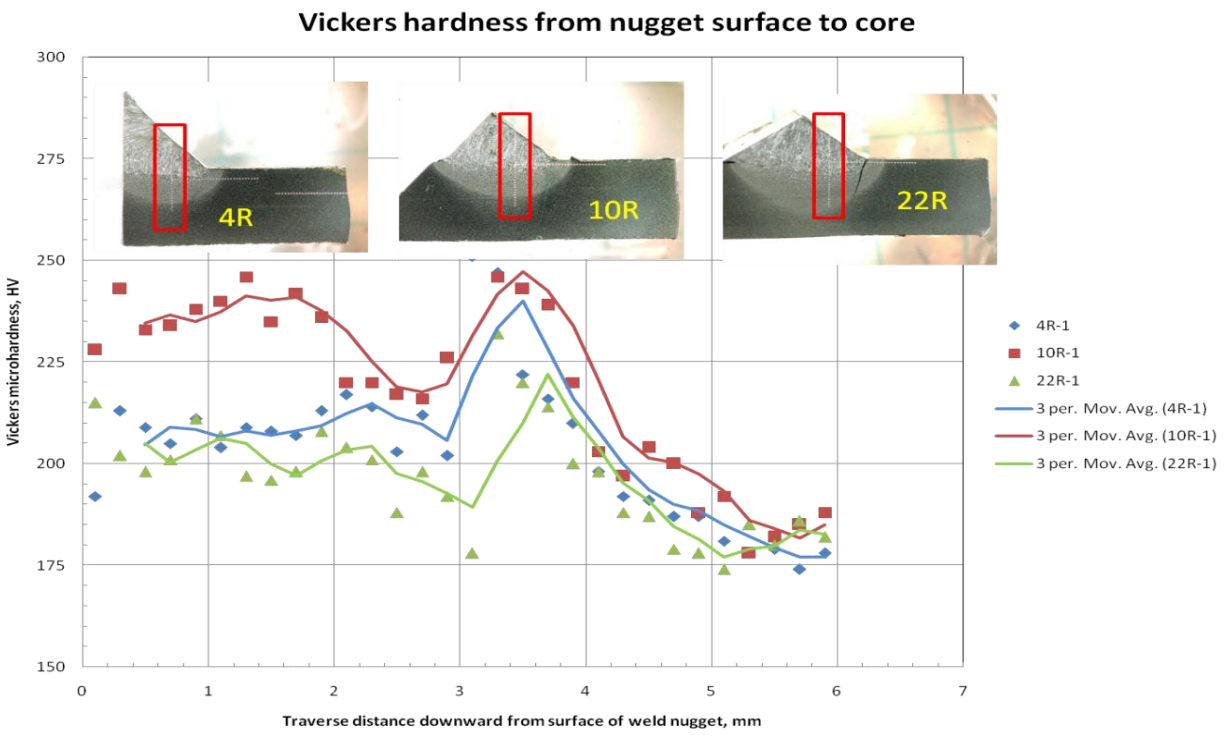

Figure 6.19 Plot of Microhardness vs. Distance Inward from Surface of Weld Nugget

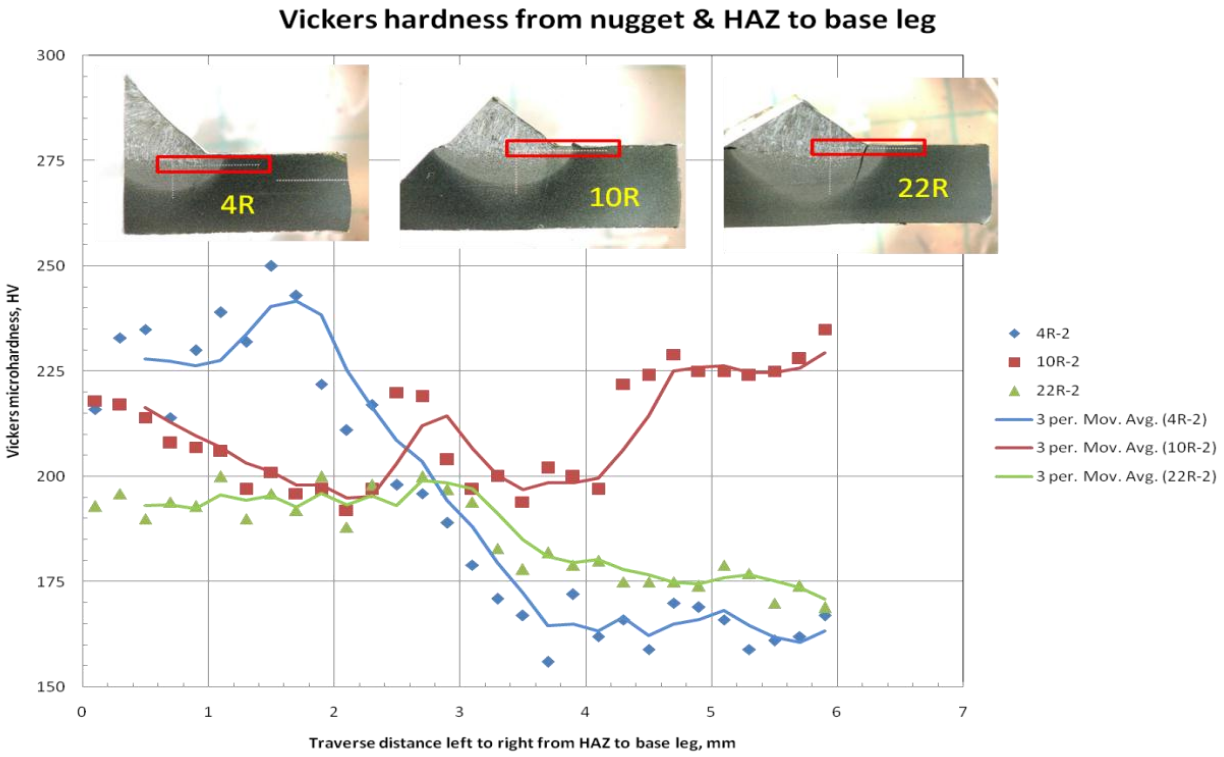

Figure 6.20 Plot of Microhardness vs. Position Across Weld and Toe

Chapter 7 Discussion

7.1 Fatigue Life Estimation

The results presented in Section 5.3 identified significant improvement in high cycle (low stress) loading and a decrease in performance in low cycle (high stress) loading, in general agreeing with Bell et al.'s observations (1995). However, Han et al. found that fatigue performance improvements due to hammer peening are greater at high stress and low life conditions than at low stress high cycle conditions (2008). Results for high cycle fatigue life improvement for hammer peening were generally in agreement with published literature (Table 7.1). The observed result from this investigation is at the low end of the published data, but followed the trends of published literature.

Published results for fatigue tests on flap peened parts were not abundant. Kirkhope et al (1999) observed a 30% improvement for shot peened samples (not flap peened) over un-peened samples. This is comparable to the 52% improvement in life (at 50% confidence) that was observed in this project for rotary flap peened samples.

Table 7.1 Comparison of Hammer Peen Results to Published Values

Hammer Peening Improvement Observations - High Cycle Fatigue		
Source	Factor Change	Life Direction
Reported results (50% confidence)	106%	Improvement
Kirkhope et al (1999)	50% to 200%	Improvement
Maddox (1998)	100%	Improvement
Bell et al. (1995)	1000%	Improvement
Han et al. (2008)	1000%	Improvement
Hammer Peening Improvement Observations - Low Cycle Fatigue		
Source	Change	Life Direction
Reported results (50% confidence)	33%	Reduction
Kopsov (1991)	40% to 70%	Reduction
Bell et al. (1995)	200%	Improvement

Published results for low cycle fatigue life for hammer peened welds include observations that time to crack initiation can either be increased or decreased (Table 7.1). Test observations from this research matched observations by Kopsov, but disagreed with experiments by Bell et al. (Table 7.1). It was noted that the low life fatigue samples did not see much benefit due to hammer or flap peening. Based on the Weibull plot in Figure 5.6 it may be concluded that peening reduces the low cycle fatigue life as compared to the baseline samples. This could be in part due to the surface irregularities introduced by the peening process, as observed in Figures 6.4 and 6.6. Figure 7.1 is a Weibull plot for the low cycle fatigue samples that includes 90% confidence intervals for the sample failure data. It can be readily seen from this plot that at a point where 50% of test samples have failed the confidence bands overlap between the baseline, hammer peened, or rotary flap peened life. Based on this observation in cannot be said with great confidence that these three sample populations have different lives.

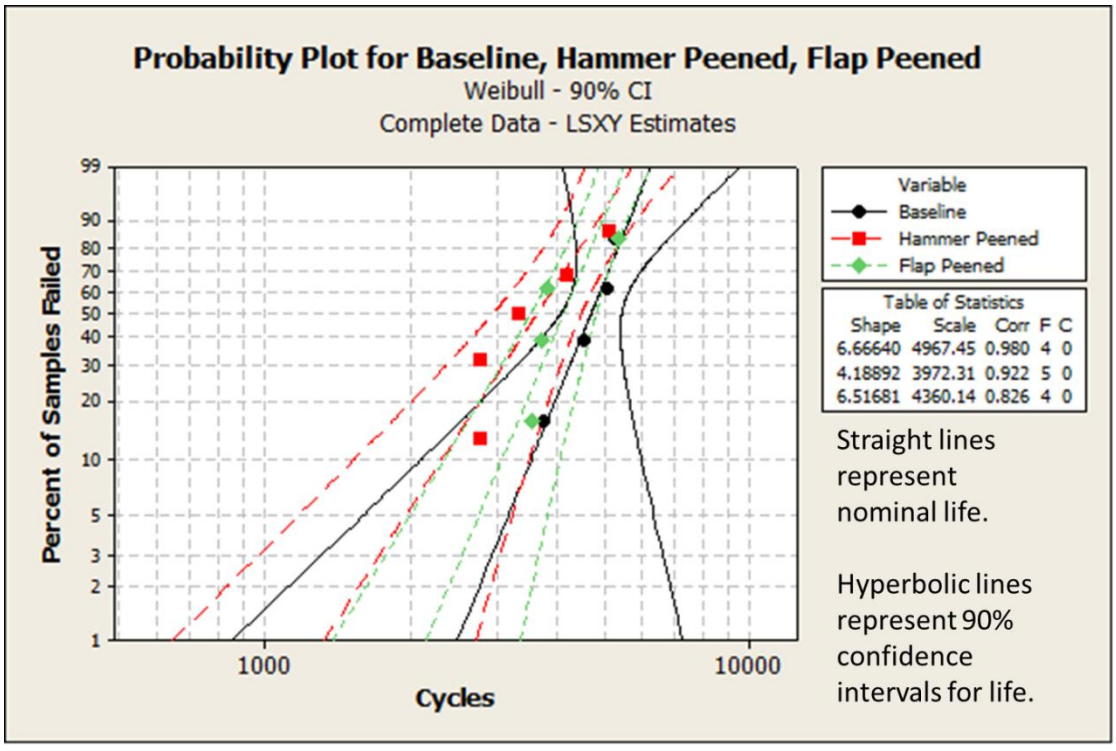

Figure 7.1 Weibull Plot with 90% Confidence Intervals for Low Cycle Fatigue Samples

Figure 7.2 is a Weibull plot for the high cycle fatigue samples that includes 90% confidence intervals for the sample failure data. It can be readily seen from this plot that at a point where 50% of test samples have failed the confidence bands do not overlap between the baseline and hammer peened samples, indicating that there is greater than 90% confidence that the hammer peened samples do have improved life. The confidence intervals for the flap peened samples do overlap both the hammer peened samples and the baseline samples at 50% failure rate. Based on this observation it cannot be said with 90% confidence that the rotary flap peened samples have improved life at a 50% failure rate, even though sample 23, a flap peened sample, had the greatest fatigue life of all samples tested and was suspended without failure at 2 million cycles.

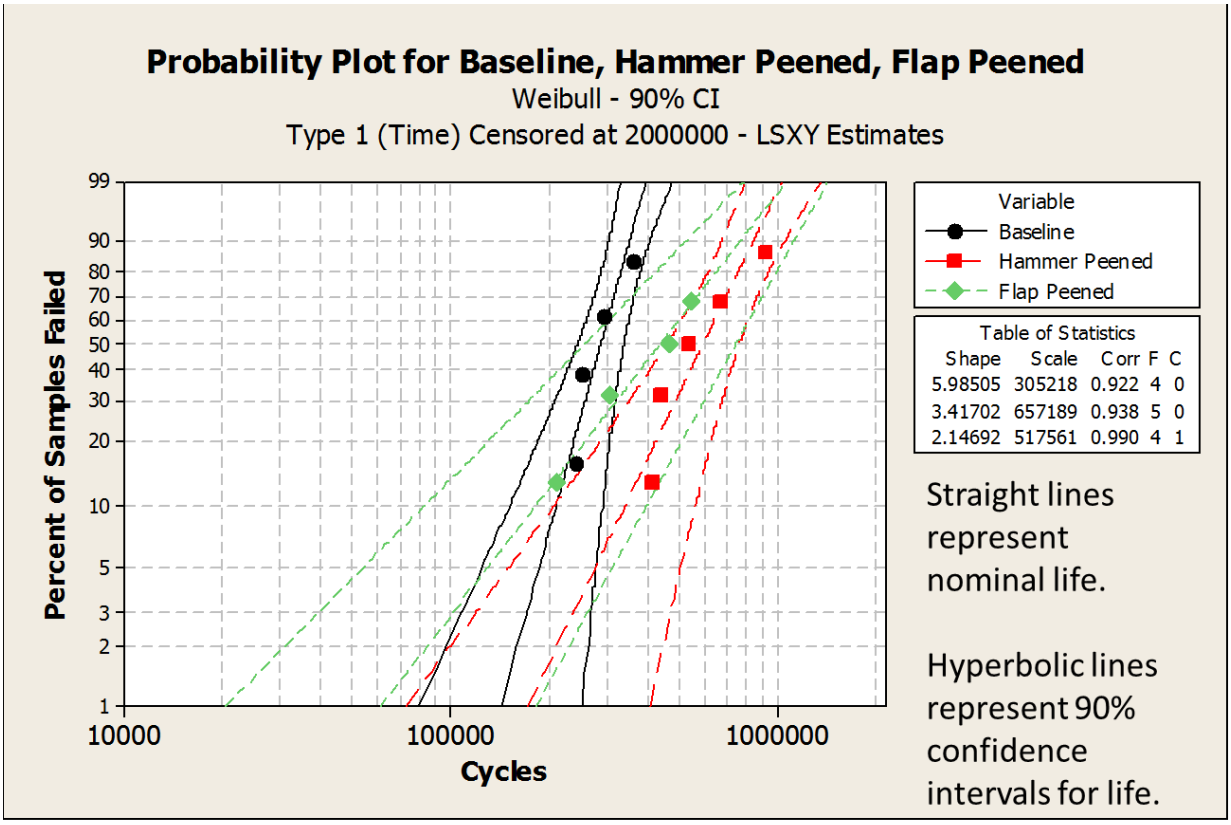

Figure 7.2 Weibull Plot with 90% Confidence Intervals for High Cycle Fatigue Samples

7.2 A36 Steel Material Properties

It is noted that the A36 steel material properties used for this project (Table 3.1 and Appendix 4) are higher than published minimums from ASTM A36 (2008). A comparison of strength values for A36 steel follows:

- Yield strength = 390 MPa measured, 250 MPa ASTM minimum requirement
- Tensile strength 575 MPa measured, 400-550 MPa ASTM defined range

Based upon Vickers Hardness measurements away from the HAZ of the weld, the test specimens used in this project had a hardness of 160-170 HV away from the weld, corresponding to a tensile strength of 550-570 MPa (ASTM E140, 2007), which is comparable to the data set used for fatigue life prediction in this project.

7.3 Sample Variation

The welding and peening processes used in this project were highly manual in nature. This introduced the potential for variation in weld quality and peening coverage between samples. The difference in weld toe geometry between samples 21 and 23, as seen in Figures 6.6 and 6.7, is an example of how this variation impacted test results. Sample 21 experienced failure at 211,000 cycles, while sample 23, which was welded and peened in the same manner, was suspended at 2 million cycles without cracking. This is probably due to the undercut present in the weld toe evident in sample 21 (Figure 6.6). This undercut is smaller than the diameter of the shot used in the rotary flap peening process. This prevented this region for receiving uniform peening coverage. The more gradual weld toe transition evident in sample 23 allowed for full peening coverage and greatly improved life.

Inspection of the hammer peened weld specimens indicates that peening did not consistently cover the entire weld toe region (Figure 6.4). It is possible that improved results

could have been achieved if peening had extended further across the weld toe into the base material.

It is likely that more repeatable samples could be produced through the use of automated welding and peening processes. However, the purpose of this project was to evaluate these manual processes that can be accomplished in the field away from sophisticated manufacturing facilities. The variation seen in this test is likely typical, if not better than, what would be seen in the field.

7.4 Additional Process Considerations

Early failures typically originated where peening was unable to achieve coverage of the sample geometry. In samples where full coverage was achieved fatigue life was significantly improved. It is possible that grinding the toe of the weld into a smooth concave radius prior to peening the weld would dramatically reduce variability in performance and improve overall performance. Grinding the toe of the weld removes any undercut or potential sharp notch in this region. This would be beneficial for two reasons. It would reduce the notch stress concentration and it would allow for more uniform peening coverage by exposing an unobstructed surface for peening.

7.5 Test Variability

Although every effort was made to conduct a repeatable fatigue cycle test, there are potential variations in the sample installation that could influence fatigue life results. The test samples were installed in a similar manner each time, but variation in mounting holes and loading hole placement between samples and variations in the curvature of the sample base due

to heat from the welding process could slightly alter the alignment of the sample in the hydraulic load frame and alter the resulting stress distribution in the test specimens.

7.6 Hammer Peened Samples Observations

Hammer peening did introduce significant compressive stresses into the peened area of the test samples. This is evident from Figure 6.19, in which the hammer peened test sample has increased hardness near the surface of the weld as compared to the baseline or flap peened samples. This is also evident in Figure 6.20, which shows increased hardness in the hammer peened sample as the hardness measurements near the surface of the sample. The hammer peened samples also experienced different weld initiation site than the baseline or flap peened samples. Figure 7.3 shows crack initiation occurring in the weld nugget near the toe of the weld. All baseline or flap peened samples examined showed crack initiation only at the weld toe in the base material (Figure 6.13 and 6.15). This observation is consistent with results reported by Bell et al. (1995) who found crack initiation in the weld root, propagating through the weld throat, then through the base material.

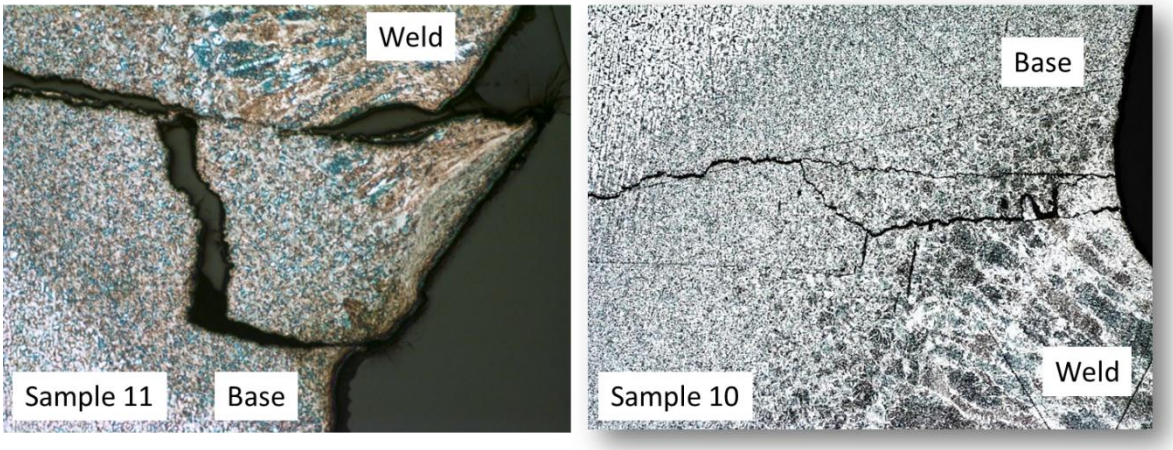

Figure 7.3 Hammer Peened Samples 10 and 11 Showing Crack Initiation in Weld Nugget

7.7 Fatigue Life Estimation Assumptions

For estimation of fatigue life it was assumed that stress and strain were fully elastic and related via Hooke's law for uni-axial loading. In reality there may be some plastic strains that could be considered. The approach of adjusting the entire stress life curve based on the fatigue notch factor, K_f, is conservative. A less conservative approach would be to adjust only the endurance limit of the curve by K_f and construct a new curve with the original stress range intercept at 1000 cycles (Bannantine, 1990). It is not common to use K_f to adjust the strain-life curve. This approach is enabled by the nCode GlyphWorks software and seemed to produce results that match experimental observations. Further investigation should be done to verify the validity of this approach. Another topic that could benefit from further investigation is variation of mesh size and node/element results averaging methods to provide increased insight into the best parameters to use for finite element modeling. It is possible that results may be sensitive to the numerical singularity present at the weld toe.

Figure 7.4 includes fatigue life predictions from the use of experimental data as well as from the finite element methods considered in this research. It is evident from the plot that the fatigue life of the test samples includes cracking from 200,000 cycles to 1 million cycles. The fatigue life prediction methods considered estimate cracking across a range from 90,000 cycles to 420,000 cycles depending on the method. The finite element-based methods considered provided a conservative estimate of 180,000 to 210,000 that aligns well with the minimum sample life observed in testing. Figure 7.4 also shows the sensitivity of fatigue life estimation to the value selected for the fatigue notch factor, K_f. Variation of K_f from 1.63 to 2.2 for strain life analysis using A36 steel strain life material properties resulted in a range of fatigue life predictions from 422,000 cycles to 99,000 cycles, respectively.

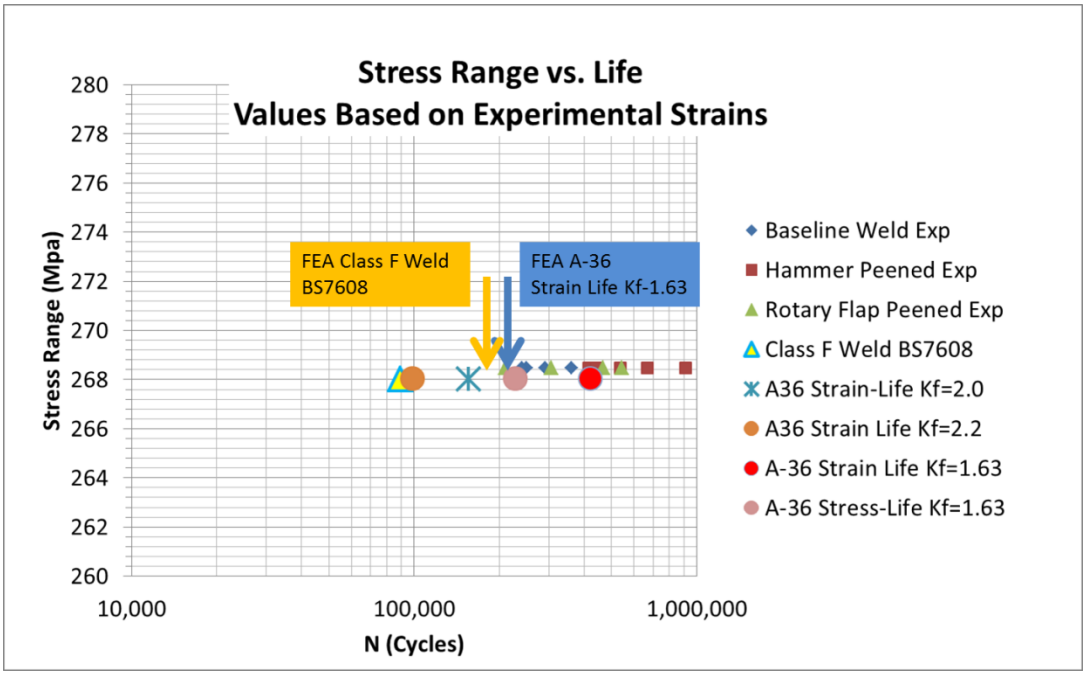

Figure 7.4 Fatigue Life Estimates

Chapter 8 Conclusions and Recommendations

8.1 Conclusions

In heavy truck applications welds are commonly used to join structural steel components that are subjected to cyclical loads. In cases where a weld fatigue issue is discovered in the field the customer desires to have low-cost methods to increase service life. This research was initiated to recommend a process for treating welded joints on heavy trucks that can be accomplished in the field with limited manufacturing resources. Surface peening is a cold working process that introduces beneficial residual compressive stresses in the surface of a work piece. Two different surface peening processes were evaluated for their ability to increase fatigue life in fillet welds. These processes were hammer peening and rotary flap peening. T-shaped fillet weld test samples were fabricated and subjected to cyclic loading in three configurations; as-welded, welded and hammer peened, and welded and flap peened. Metallographic inspection was used to further evaluate the test samples following fatigue testing.

Fatigue life estimation methods were considered based on both experimentally measured strain data and stress/strain results obtained through the use of finite element methods. Stress-life analyses based on weld classifications established by British Standard BS7608 were conducted. Strain-life analyses based on the use of A36 steel fatigue properties with the application of a fatigue notch factor were also conducted. The following conclusions can be drawn from this research.

1. Hammer peening was shown to increase fatigue life by 106% over the baseline un-peened samples at 50% confidence.
2. Rotary flap peening was shown to improve high cycle fatigue life in welded samples by 52% when compared to the un-peened baseline at 50% confidence.

3. It is believed that additional improvements can be made to the flap peening process through the addition of a toe grinding process between the welding and peening processes to smooth the toe of the weld and enable better peening coverage in the region of greatest stress concentration.
4. Additional improvements may be possible in the hammer peening process by ensuring more uniform peening coverage of the weld toe.
5. Stress-life analysis according to the process set forth in BS7608 provided conservative, yet useful fatigue life estimation for both experimentally-measured inputs and for input stresses obtained through numerical simulation.
6. Strain life analysis with the use of A36 steel material properties in combination with a fatigue notch factor provided useful fatigue life predictions for both experimentally-measured strains and for input strains obtained through numerical simulation. The results of this analysis were sensitive to the value of the fatigue notch factor used.
7. Hammer peened test specimens had greater microhardness near the surface, indicating the presence of greater compressive residual stresses than the baseline or flap peened test samples.
8. It would be beneficial to investigate the effects of variable-amplitude loading on fatigue life improvement from hammer or flap peening. The peening conducted in this research was beneficial for high-cycle fatigue and potentially detrimental for low cycle fatigue. Prior to implementation of a recommendation it is important to observe the effects of combined high and low amplitude loading cycles
9. It would be beneficial to quantify the surface roughness of the fatigue test samples after peening and further investigate the relationship between surface roughness and

crack initiation. The test data reported here indicates that low cycle fatigue crack initiation may especially be influenced by the surface roughness after peening.

8.2 Recommendations

1. It is recommended that more investigation be conducted regarding rotary flap peening with the additional process step of weld toe grinding. Further work to quantify the benefits available from this combination of processes may result in improved fatigue performance.
2. It is also recommended that improved peening coverage of the weld toe be investigated for the hammer peen method to investigate further potential fatigue benefits.
3. Based on the comparison of methods conducted in this research effort it is recommended that hammer peening be considered as the most effective method to improve weld fatigue life in the field.
4. Prior to implementation of the hammer peening method of weld treatment it is recommended that the impact of variable-amplitude loading be considered and quantified.

Acknowledgments

I would like to thank the following individuals for their expert support and kind assistance. This project would not have been possible without your help.

- Dave Lyne – PACCAR Technical Center Fabrication – Test sample fabrication
- Tim Silvas – PACCAR Technical Center Fabrication – Test sample fabrication
- PACCAR Technical Center – Funding and laboratory resources
- Odin Kors – PACCAR Technical Center Structures Lab support – load frame operation
- Wes Graham – PACCAR Technical Center Materials Lab support – Microscopy and metallurgy support and expert advice
- Professor Ramulu Mamidala – University of Washington - Advisor and technical guidance
- Hali Diep – Boeing Corporation- Flap peen kit loan

References

3M, "Roto Peen Flap Assemblies TC330" *3M Industrial Business Customer Response Center*, St. Paul, MN (2003).

ASTM A36/A 36M – 08 "Standard Specification for Carbon Structural Steel" ASTM International, West Conshohocken, PA, 2008.

ASTM E140-07, "Standard Hardness Conversion Tables for Metals Relationship Among Brinell Hardness, Vickers Hardness, Rockwell Hardness, Superficial Hardness, Knoop Hardness, and Scleroscope Hardness", ASTM International, West Conshohocken, PA, 2007.

ASTM E606 (2004). "Standard Practice for Strain-Controlled Fatigue Testing" ASTM International, West Conshohocken, PA.

Bailey, P. G., "Manual Peening with the Rotary Flap Process", *The 7th International Conference on Shot Peening*, Institute of Precision Mechanics, Warsaw, Poland (1999) pp405-414.

Bannantine, Julie A., Comer, Jess J., Handrock, James L, "Fundamentals of Metal Fatigue Analysis", Prentice Hall, Upper Saddle River, New Jersey, (1990).

Bell, R., Militaru, D. V., Braid, J. E. M., "The Fatigue Life Improvement of High Strength Steel Welded Joints using Hammer Peening Techniques" *1995 OMAE – Volume III, Materials Engineering*, ASME (1995). pp 313-320.

Bhuvaraghan, Baskaran.,Srinivasan, M. Srinivasan, Maffeo, Bob, "Optimization of the Fatigue Strength of Materials due to Shot Peening: A Survey", *International Journal of Structural Changes in Solids – Mechanics and Applications, Volume 2 Number 2*, (November 2010) pp 33-63.

Branco, C. M., Infante, V. ,Baptista, R. “Fatigue Behavior of Welded Joints with Cracks, Repaired by Hammer Peening” *Fracture Mechanics of Engineering Structures Vol 27.* Blackwell Publishing (2004). pp785-798.

British Standard BS7608 “Code of Practice for Fatigue Design and Assessment of Steel Structures” British Standards Institution, London, (1993)

Fuchs, H. O., Stephens, R. I., “Metal Fatigue in Engineering“ John Wiley and Sons, New York, 1980.

Han, Seung-Ho, Han, Jeong-Woo, Nam, Young-Yun, “Fatigue Life Improvement using Mechanical Post-Treatment for Weldment” *Materials Science Forum*, Vols. 580-582, pp97-100.

Kirkhope, K.J, Bell, R., Caron, L., Basu, R.I., Ma, K.-T., “Weld Detail Fatigue Life Improvement Techniques. Part 1: Review”, *Marine Structures Vol 12*, (1999) pp 447-474.

Kopsov, I.E., “The Influence of Hammer Peening on Fatigue in High Strength Steel” *International Journal of Fatigue Vol 13 No 6*, (Nov. 1991) pp 479-482.

Macdonald, “Fracture and Fatigue of Welded Joints and Structures”, Woodhead Publishing Limited, New Delhi, India (2011).

Maddox, S. J., “Fatigue of Steel Fillet Welds Hammer Peened Under Load” *Welding in the World*. Vol 41 (1998) pp 343-349.

Maddox, S.J., “Fatigue Strength of Welded Structures, Second Edition”, Abington Publishing, Cambridge, England (1991).

Metal Improvement Company, Inc. “Shot Peening Applications” Seventh Edition. Curtiss-Wright Corporation.

Miao, H.Y., Demers, D., Larose, S., Perron, C., Levesque, Martin "Experimental Study of Shot Peening and Stress Peen Forming" *Journal of Materials Processing Technology 210,* (2010) pp2089-2102.

Military Specification MIL-R-81841 (1972) "Rotary Flap Peening of Metal Parts". Naval Air Systems Command, Department of the Navy.

Ministry of Defense "Defense Standard 03-21 Mechanical Methods for the Inducement of Residual Surface Compressive Stresses" Issue 4 Publication Date 22 January 2008. Ministry of Defense, United Kingdom.

Ofsthun, Mark. "When Fatigue Quality Enhancers do not Enhance Fatigue Quality" *International Journal of Fatigue,* Vol25 (2003) pp 1223-1228.

Parkes, L. R. "Rotary Technique Fills a Gap in the Shot-Peening Spectrum." *Welding and Metal Fabrication,* (1975) pp 519-520.

Pilkey, W., Pilkey, D., "Peterson's Stress Concentration Factors (3rd Edition) John Wiley & Sons, Hoboken, New Jersey, 2008.

Appendices

This page intentionally left blank

Appendix 1 Test Sample Drawings

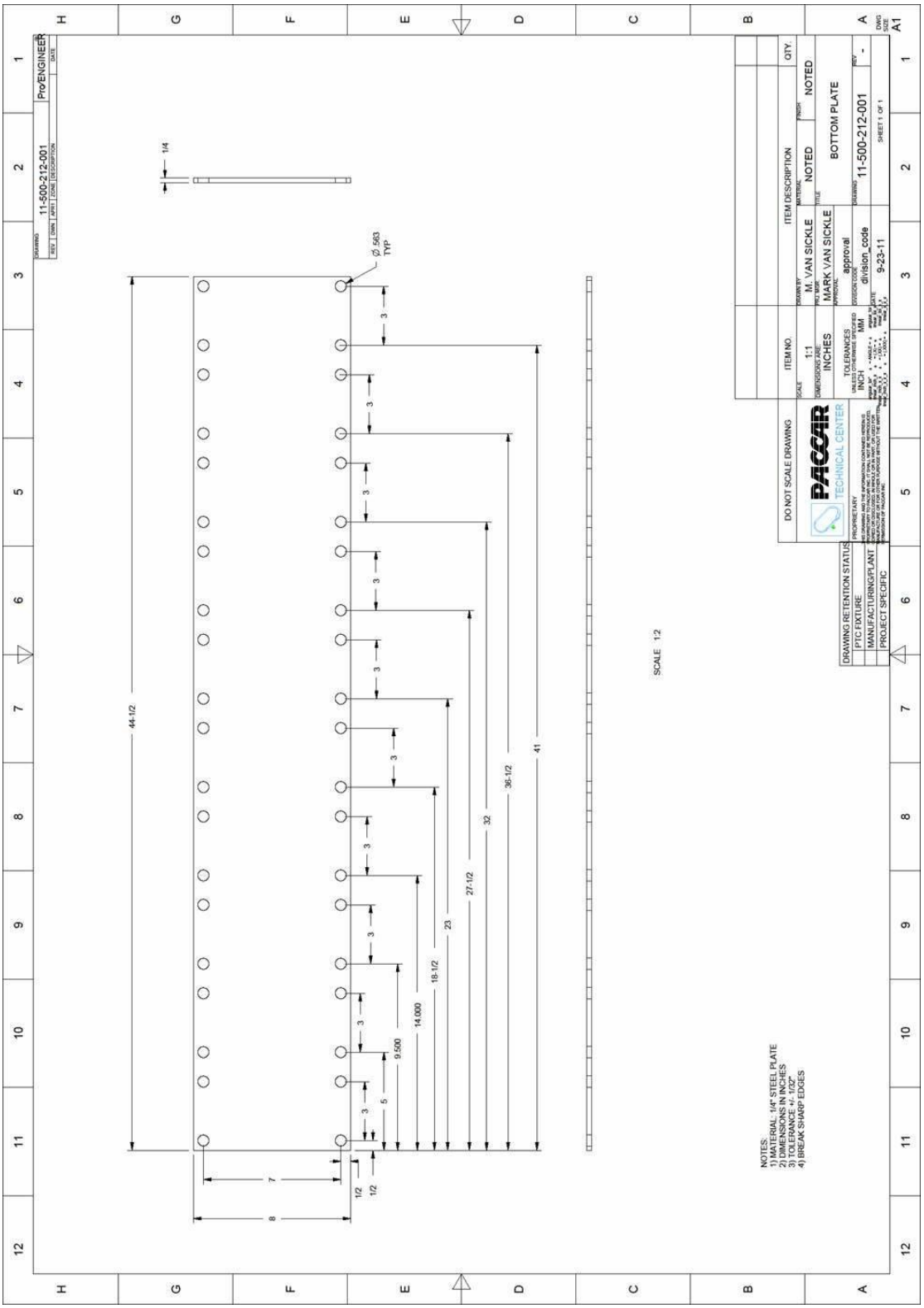

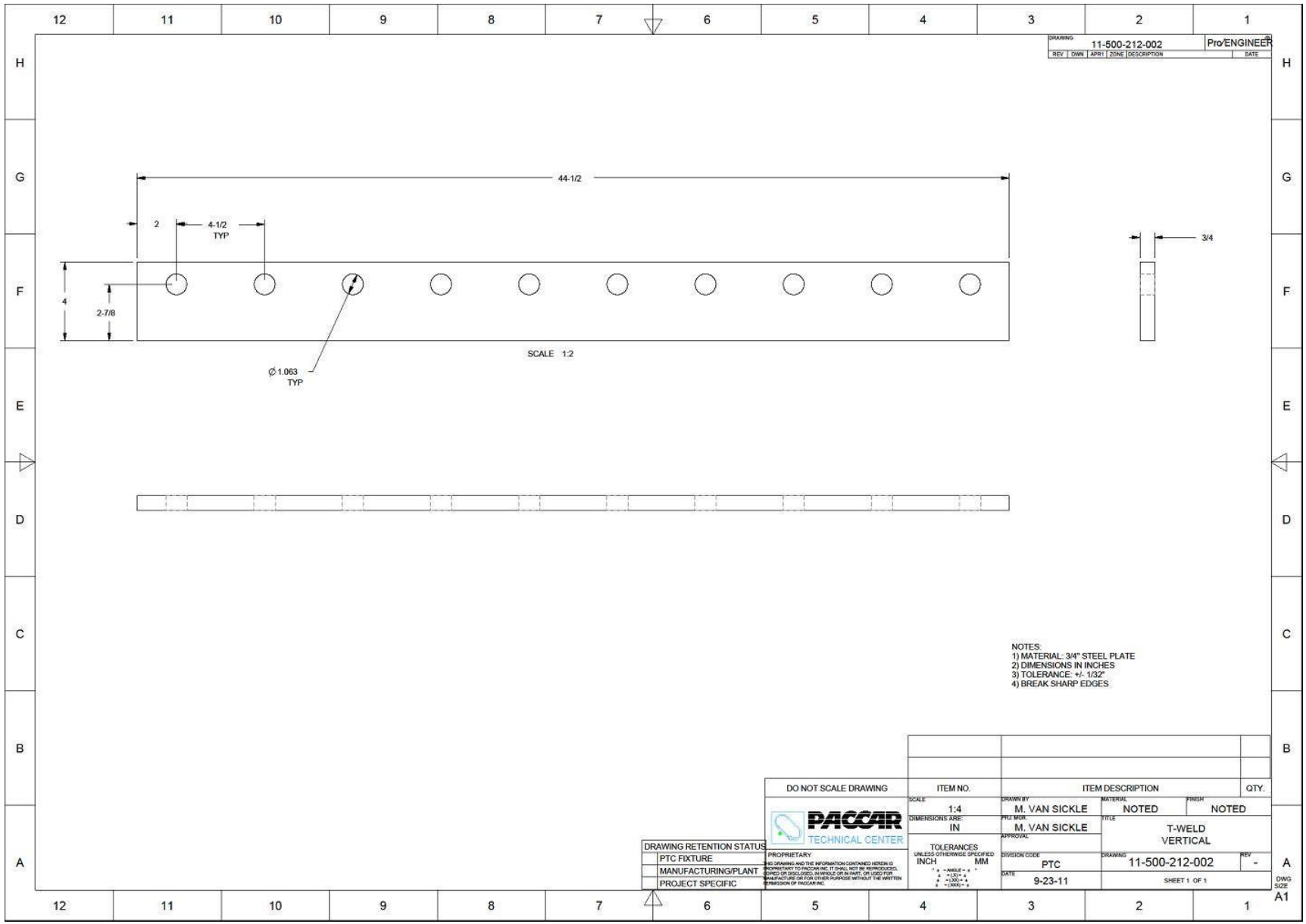
DRAWING
11-500-212-002
Pro/ENGINEER
REV | DWN | APR1 | ZONE | DESCRIPTION | DATE
44-1/2
2
4-1/2
TYP
4
2-7/8
Ø1.063
TYP
SCALE 1:2
3/4
NOTES:
1) MATERIAL: 3/4" STEEL PLATE
2) DIMENSIONS IN INCHES
3) TOLERANCE: +/- 1/32"
4) BREAK SHARP EDGES
DO NOT SCALE DRAWING
ITEM NO.
ITEM DESCRIPTION
QTY.
PACCAR
TECHNICAL CENTER
SCALE
1:4
DRAWN BY
M. VAN SICKLE
MATERIAL
NOTED
FINISH
NOTED
DIMENSIONS ARE:
IN
PRJ. MGR.
M. VAN SICKLE
TITLE
T-WELD
VERTICAL
APPROVAL
TOLERANCES
UNLESS OTHERWISE SPECIFIED
INCH MM
DIVISION CODE
PTC
DRAWING
11-500-212-002
REV
-
DATE
9-23-11
SHEET 1 OF 1
DWG SIZE
A1
DRAWING RETENTION STATUS
PTC FIXTURE
MANUFACTURING/PLANT
PROJECT SPECIFIC
PROPRIETARY:
THIS DRAWING AND THE INFORMATION CONTAINED HEREIN IS PROPRIETARY TO PACCAR INC. IT SHALL NOT BE REPRODUCED, COPIED OR DISCLOSED, IN WHOLE OR IN PART, OR USED FOR MANUFACTURE OR FOR OTHER PURPOSE WITHOUT THE WRITTEN PERMISSION OF PACCAR INC.

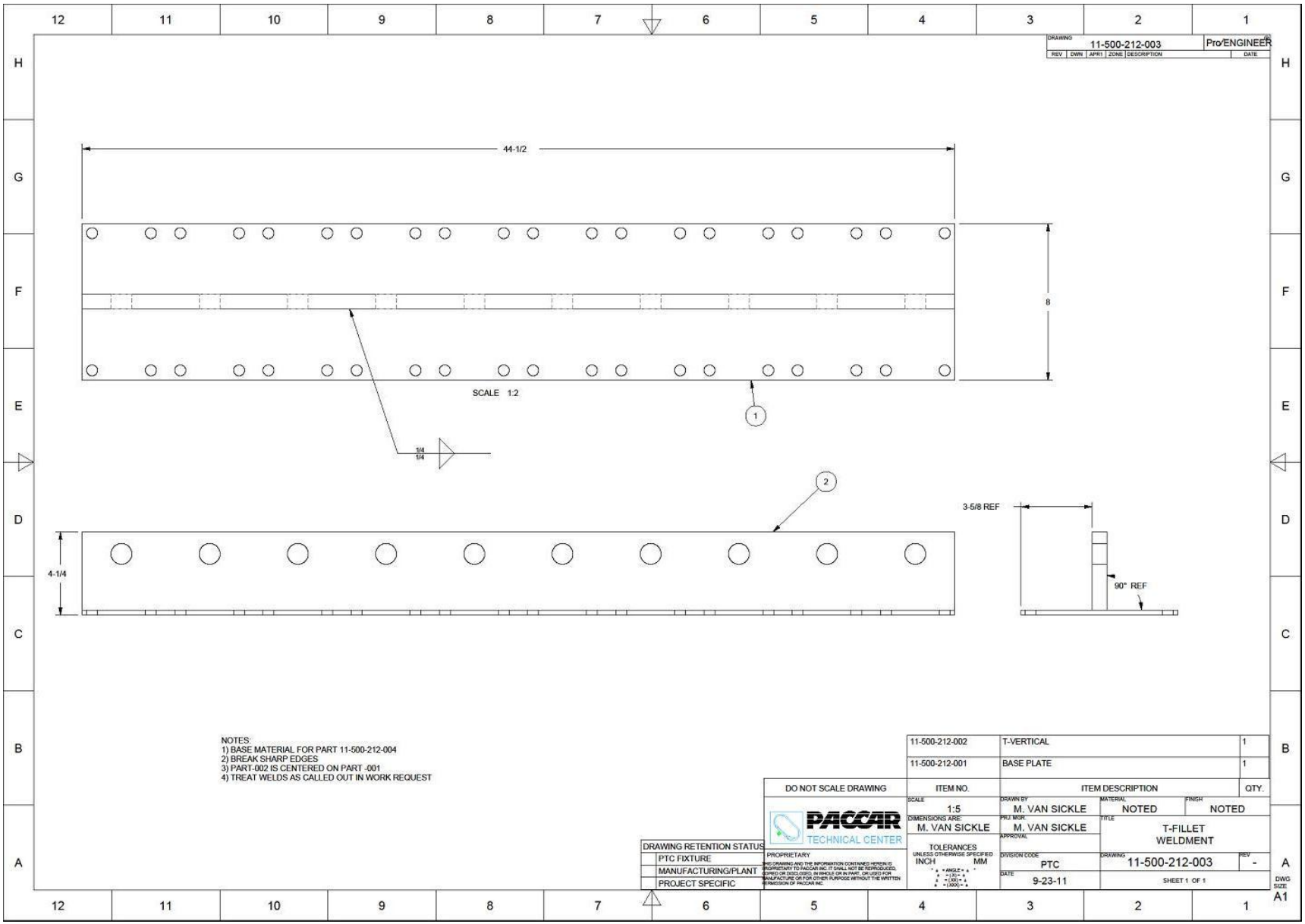
DRAWING 11-500-212-003
Pro/ENGINEER
REV | DWN | APR1 | ZONE | DESCRIPTION | DATE
44-1/2
8
SCALE 1:2
1
1/4
1/4
2
3-5/8 REF
90° REF
4-1/4
NOTES:
1) BASE MATERIAL FOR PART 11-500-212-004
2) BREAK SHARP EDGES
3) PART-002 IS CENTERED ON PART -001
4) TREAT WELDS AS CALLED OUT IN WORK REQUEST
11-500-212-002 | T-VERTICAL | 1
11-500-212-001 | BASE PLATE | 1
DO NOT SCALE DRAWING | ITEM NO. | ITEM DESCRIPTION | QTY.
SCALE 1:5
DRAWN BY M. VAN SICKLE
MATERIAL NOTED
FINISH NOTED
DIMENSIONS ARE: M. VAN SICKLE
PRJ MGR M. VAN SICKLE
TITLE T-FILLET WELDMENT
APPROVAL
TOLERANCES UNLESS OTHERWISE SPECIFIED INCH MM
DIVISION CODE PTC
DRAWING 11-500-212-003
REV -
DATE 9-23-11
SHEET 1 OF 1
DWG SIZE A1
PACCAR TECHNICAL CENTER
DRAWING RETENTION STATUS
PTC FIXTURE
MANUFACTURING/PLANT
PROJECT SPECIFIC
PROPRIETARY
THIS DRAWING AND THE INFORMATION CONTAINED HEREIN IS PROPRIETARY TO PACCAR INC. IT SHALL NOT BE REPRODUCED, COPIED OR DISCLOSED, IN WHOLE OR IN PART, OR USED FOR MANUFACTURE OR FOR OTHER PURPOSE WITHOUT THE WRITTEN PERMISSION OF PACCAR INC.

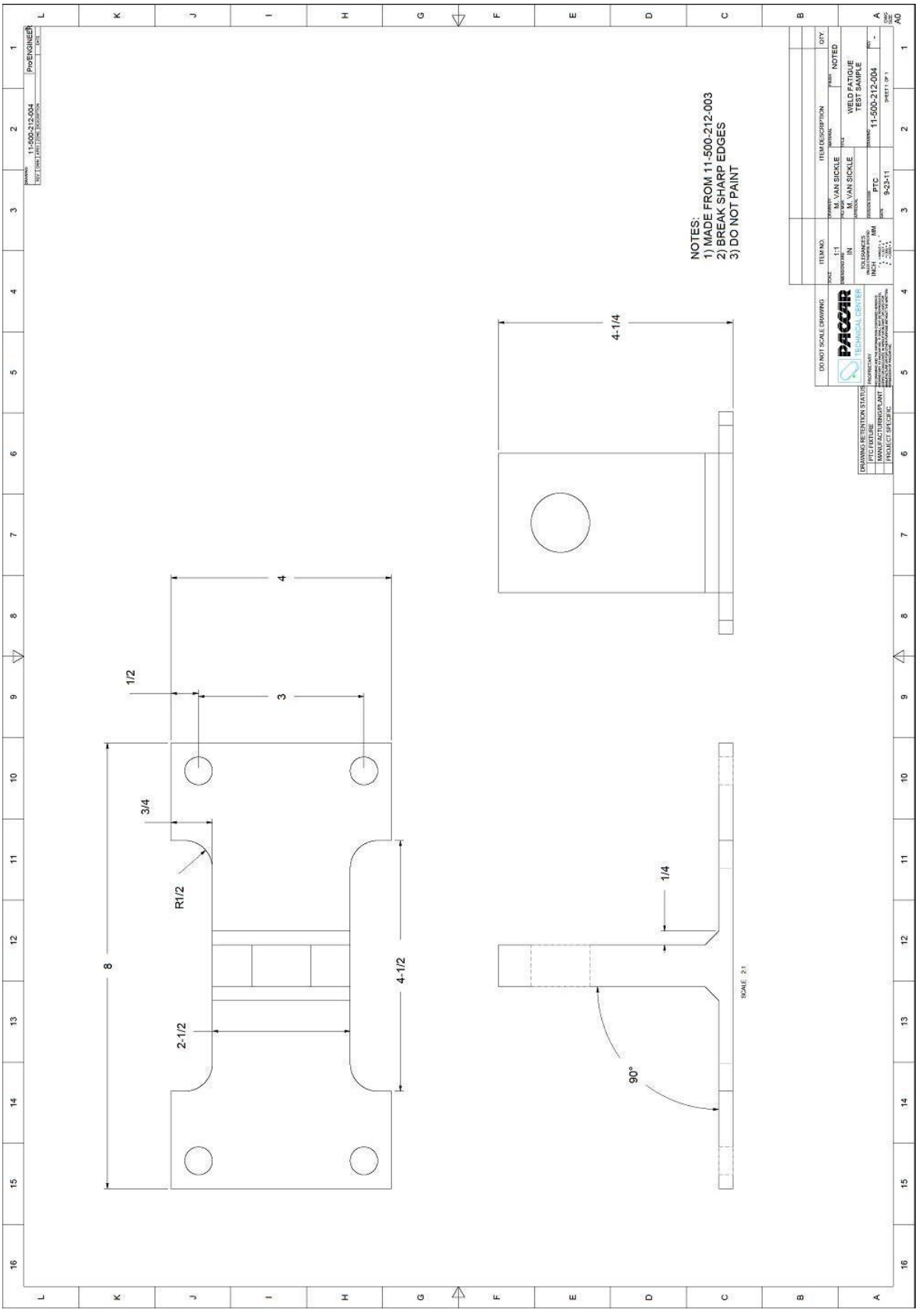
NOTES:
1) MADE FROM 11-500-212-003
2) BREAK SHARP EDGES
3) DO NOT PAINT
4
1/2
3
3/4
R1/2
8
2-1/2
4-1/2
4-1/4
1/4
90°
SCALE 2:1
WELD FATIGUE TEST SAMPLE
11-500-212-004
M. VAN SICKLE
9-23-11
NOTED
PTC
PACCAR

Appendix 2 Strain Gage Installation

TC11-500-212

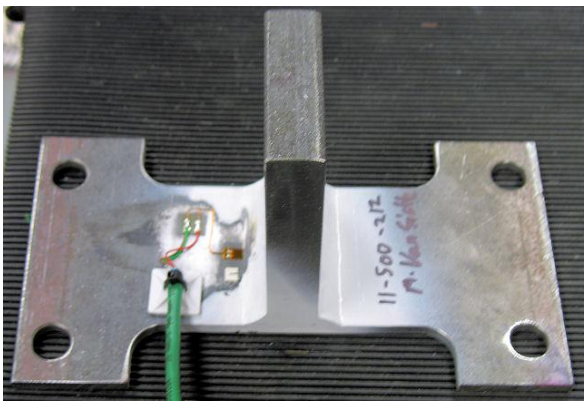

Assessment of Field Treatments for Prolonging the Life of Steel Welded Joints Subjected to Fatigue Loading

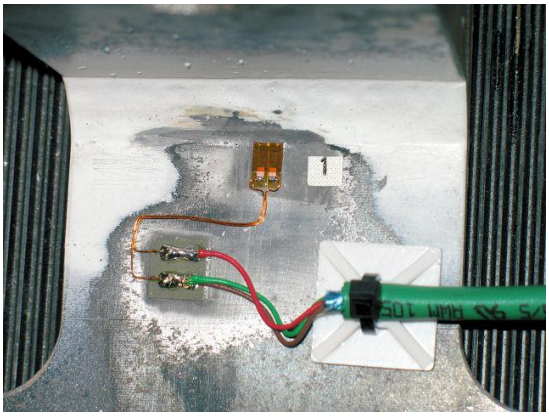

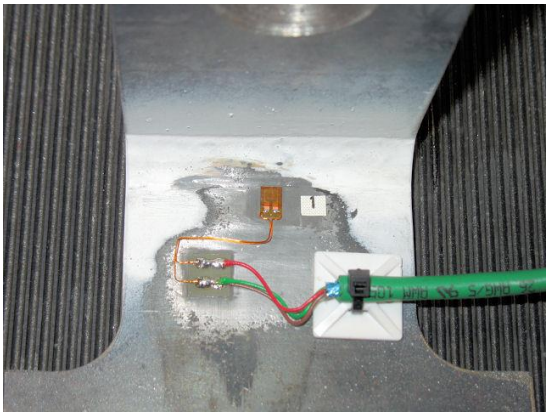

TC11-500-212

Assessment of Field Treatments for Prolonging the Life of Steel Welded Joints Subjected to Fatigue Loading

Gage 1	CEA-06-062UW-350
Gage Factor:	2.15
Kt =	(.9 ± .2)%
Adhesive:	M Bond 200
Engineer:	Mark Van Sickle
Technician:	Rocky Long

February 16,2012

Appendix 3 Almen Intensity Conversion (3M, 2003)

Peening a flat surface

Roto peening is a systematic process of essential steps. Each step is necessary for optimum results. To demonstrate the process, each step on this and the following pages is based on the example at right.

Flat surface 2" x 2 ¼" peened to 12 Almen "A" intensity with a 9/16" x 1 ¼" flap.

HINT: Spot of paint on the back side of the flap, opposite the shot, will help ensure that you are peening the surface with the shot and not the flap.

Step 1

Convert to 3M™ Almen Strip Holder intensity.

Conversion is necessary since the Almen strip bends more when using the 3M Almen Strip Holder than with the conventional screw-down holder.

In the chart at far right, Standard Almen "A" 12, for example, converts to 3M Almen A-17.

The magnetic grip of the 3M Almen Strip Holder eliminates hold-down screws for easier measurement. Plus, the same Almen strip can be used to measure intensity and then used to check for saturation.

3M™ Magnetic Almen Strip Holder

With the chart, you can readily make your own conversions.

Almen "A" intensity desired_____

3M Almen Strip Holder intensity desired _____

Almen "A" Intensity	3M Holder Intensity
3	3
4	4
5	5
6	6
7	7
8	10
9	12
10	14
11	15
12	17
13	18
14	20
15	22
16	23
17	25
18	26
19	28
20	30

Range generally used

Step 2

Determine area to be peened.

For a flat surface, area is length times the width. If the area to be peened is a hole, then the area is equal to 3.14 times the hole diameter times the hole depth.

Flat surface example:

L x W = A

2" x 2 ¼" = 4.5 in^2

With the same formula, calculate your own flat surface sample.

L.____ x W____= Area_____

Hole example:

3.14 x Dia. x Depth = A

3.14 x .75" x 1.25" = 2.94 in^3

Calculate your own sample.

3.14 x Dia. ____

x Depth _____=

Area_____

Step 3

Determine appropriate flap size.

(A) If the area to be peened is flat with no obstructions or restrictions, use a 1" x 2" TC 330 flap.

(B) If peening a hole, use the 9/16" x 1" for a ½" to ¾" diameter. Use the 9/16" x 1 ¼" for diameters over ¾".

(C) In restricted areas use whatever size fits. For narrow slots or radius down to 1/16", cut the flaps narrower with scissors.

Go to Step 4A for 9/16" x 1" and 9/16" x 1 ¼" flaps.

Go to Step 4B for 1" x 2" flaps.

6

Appendix 4 A36 Steel Strain-Life Material Properties

INTERIM REPORT TC07-500-248A: DURABILITY CORRELATION: A36 STEEL STRAIN LIFE PROPERTIES	Publication date: 16 July 2007 Division number: -- Division contact:
PROJECT TC07-500-248 DURABILITY CORRELATION	Authorized signature on file Author: Mark Van Sickle
	Authorized signature on file Approved by: Alan L. Whitmyer

ABSTRACT

The purpose of this project was to perform strain-life and monotonic testing on specimens of A36 steel. Five specimens were pulled to failure in a monotonic tensile test.

Nineteen A36 steel samples were cycled under strain control at five different strain levels. Two of the specimens at the lowest strain level were suspended without failure. Strain-life fatigue parameters were computed from the data recorded for the remaining specimens cycled to failure. The following table lists monotonic strength and cyclic fatigue properties for the material.

A36 monotonic properties	US customary units	SI units
Elastic Modulus *E*	32,440,000 psi	217,700 MPa
Ultimate strength, *Su*	83,400 psi	575 MPa
0.2% yield strength, *Sy*	56,500 psi	390 MPa
Strain at fracture ε	0.2223	
Monotonic strength coefficient, *K*	159,300	1,122
Monotonic strain hardening exponent, *n*	0.2538	
Tensile toughness	16700 psi	115 MPa
A36 cyclic properties		
*Cyclic strength coefficient *K'*	128,900 psi	890 MPa
*Cyclic strain hardening exponent *n'*	0.149	
Cyclic (0.2%) yield strength *Sy'*	50,900 psi	350 MPa
Fatigue ductility coefficient $\varepsilon'f$	0.6262	
Fatigue ductility exponent *c*	–0.544	
Fatigue strength coefficient $\sigma'f$	152,400 psi	1,050 MPa
Fatigue strength exponent *b*	–0.103	
Assumed elastic modulus *E*	29,500 ksi	203.4 GPa

*Values obtained from curve fit of data points, not power law approach

PACCAR
Technical Center

12479 Farm-to-Market Road
Mount Vernon, WA 98273
Telephone (360) 757-8311

INTERIM REPORT TC07-500-248A:
DURABILITY CORRELATION: A36 STEEL STRAIN LIFE PROPERTIES

PROJECT TC07-500-248
DURABILITY CORRELATION

PURPOSE AND SCOPE

The purpose of this project was to perform strain-life and monotonic testing on specimens of A36 steel. Five specimens were pulled to failure in a monotonic tensile test.

Nineteen A36 steel samples were cycled under strain control at five different strain levels. Two of the specimens at the lowest strain level were suspended without failure. Strain-life fatigue parameters were computed from the data recorded for the remaining specimens cycled to failure.

This testing was done to provide material properties for reference in design and analysis for fatigue life estimation of PACCAR designs.

PARTS AND MATERIALS

The specimens for this test were cut from A36 bar stock. All the strain-life specimens were cut and machined at the PACCAR Technical Center. The monotonic specimens were of the same geometry as the strain-life samples. All test specimens were machined according to drawing TC92-032-04. (See Attachment 1.)

METHOD

Monotonic Testing

Five specimens were pulled to failure in a MTS Model 810 22-kip hydraulic load frame. The procedure was in accordance with ASTM E8-00, *Standard Test Methods for Tension Testing of Metallic Materials.* Tensile test specimens were identical to strain-life specimens. The rate of loading was approximately 43 lbf/sec. The load, displacement, and strain were sampled at 20 Hz. The data were exported to Microsoft Excel for plotting and curve-fitting. Strain was measured using an MTS 632-12B-20 extensometer.

Strain-life Testing

Specimens were tested in accordance with ASTM E606-92, *Standard Practice for Strain-Controlled Fatigue Testing,* with the exception of the specimen design. The specimens were machined according to the drawing in Attachment 1. The specimens were polished in accordance with the ASTM standard. Each specimen was polished in the longitudinal direction with 240-, 320-, 400-, and 600-grit sandpaper in succession. The specimens were cyclically loaded one at a time under strain control in a MTS Model 810 22-kip hydraulic load frame. The specimen was held in MTS model 646.10 Hydraulic Collet Grips. Strain was measured by an MTS 632-26 Extensometer. The load frame was aligned according to PACCAR Technical Center Work Instruction SL441-014-1 *Structures Lab Manual – Non-Structural Tests.*

Strain-gaged solder tabs were affixed to the specimen to provide protection from the knife-edges of the extensometer. The test was run in fully reversed axial load, R = -1, from tension to compression. The drive waveform was triangular, and the starting position was positive (tension). The frequency of testing ranged from 0.29 Hz for the high-strain tests to 4 Hz for the low-strain tests. Typical strain rates were 2000 microstrain per second. Failure was defined as 30% reduction in load. The test environment was laboratory ambient air. The strain-life tests were controlled by an MTS TestStar IIs version 2.4C controller using MTS 759.20 Low-cycle Fatigue Test software. Figure 1 shows the strain-life load frame. Figure 2 is a close-up of a strain-life specimen in the collet grips. The data reduction was done in accordance with ASTM E739-91, *Standard Practice for Statistical Analysis of Linear or Linearized Stress-life (S-N and Strain-Life (ε-N) Fatigue Data.*

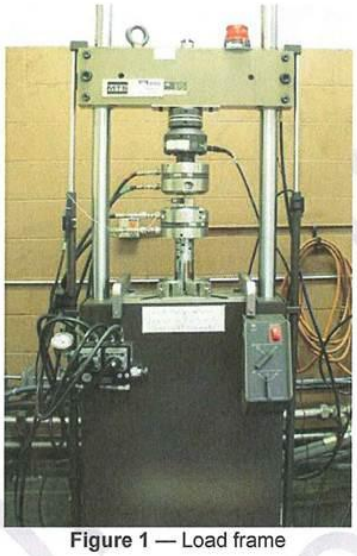

Figure 1 — Load frame

Figure 2 — Sample

RESULTS

Monotonic Test Results

Five specimens were pulled to failure. Table 1 lists the results.

Table 1 — A36 monotonic test results

US customary units									
Sample number	20	22	23	24	25	Average	Maximum	Minimum	Std dev.
Elastic Modulus (psi)	31,574,336	31,701,591	30,821,295	31,367,333	32,440,462	31,581,003	32,440,462	30,821,295	586,529
Ultimate strength, *Su* (psi)	83,703	84,231	81,852	84,132	83,001	83,384	84,231	81,852	984
0.2% yield strength, *Sy* (psi)	57,294	54,426	53,446	60,618	56,769	56,511	60,618	53,446	2,797
Strain at fracture	0.2221	0.2229	0.2233	0.2215	0.2219	0.2223	0.2233	0.2215	0.0008
Monotonic strength coefficient, *K*	160,442	162,704	157,011	159,944	156,465	159,313	162,704	156,465	2,578
Monotonic strain hardening exponent, *n*	0.2550	0.2579	0.2549	0.2528	0.2486	0.2538	0.2579	0.2486	0.0034
Tensile toughness (psi)	16,800	16,908	16,533	16,746	16,690	16,735	16,908	16,533	139
Si units									
Sample number	20	22	23	24	25	Average	Maximum	Minimum	St. dev.
Elastic Modulus (N/mm)	217,698	218,576	212,506	216,271	223,670	217,744	223,670	212,506	4,044
Ultimate strength, *Su* (N/mm)	577	581	564	580	572	575	581	564	7
0.2% yield strength, *Sy* (N/mm)	395	375	368	418	391	390	418	368	19
Strain at fracture	0.2221	0.2229	0.2233	0.2215	0.2219	0.2223	0.2233	0.2215	0.0008
Monotonic strength coefficient, *K*	1,106	1,122	1,083	1,103	1,079	1,098	1,122	1,079	18
Monotonic strain hardening exponent, *n*	0.2550	0.2579	0.2549	0.2528	0.2486	0.2538	0.2579	0.2486	0.0034
Tensile toughness (N/mm)	116	117	114	115	115	115	117	114	1

The parameters for the Ramberg-Osgood equation (E, K and n) were determined by least-squares curve fit. The Ramberg-Osgood equation is as follows:

$$\varepsilon_T = \varepsilon_e + \varepsilon_p = (\sigma/E) + (\sigma/K)^{1/n} \quad [1]$$

where

ε_T = total strain
ε_e = elastic strain
ε_p = plastic strain
σ = stress
E = elastic modulus
K = strength coefficient
n = hardening exponent

The elastic modulus (E) was computed from a least-squares curve fit of the stress-strain data from 12,000 psi to 45,000 psi using engineering stress as the independent variable and engineering strain as the dependent variable. Engineering stress and strain are the measured values based on original area and gauge length of the specimen. True stress and strain are based on the instantaneous length and area of the gauge section. True strain and true stress were computed from the measured engineering values using the following relationships:

$$\varepsilon = ln\,(1 + e) \quad [2]$$

where

ε = "true" strain
e = engineering strain

and

$$\sigma = S(1 + e) \quad [3]$$

where

σ = "true" stress
S = engineering stress

At low strain levels in the elastic stress-strain area, the difference between true and engineering stress-strain is small enough to be neglected.

The 0.2% offset yield point was computed from the intersection of a 0.2% offset strain line and the engineering stress-strain line. The 0.2% offset yield line was drawn parallel to the elastic modulus curve fit line and intercepts the zero stress axis at 0.002 strain. The ultimate strength was the maximum engineering stress measured during the test.

The strength coefficient (K) and the strain-hardening coefficient (n) were computed from a least-squares curve fit of the true plastic stress-strain data using log of the true plastic strain as the dependent variable and log of true stress as the independent variable. The least squares curve fit for plastic strain was calculated for the data between the 0.2% offset yield stress and the ultimate stress. Tensile toughness was also calculated from the stress-strain data for each specimen. Tensile toughness is the area under the entire engineering stress-strain curve up to the point of fracture. Tensile toughness is a measure of the ability of the material to absorb energy without fracture. Tensile toughness should not be confused with fracture toughness, which is resistance to failure in the presence of a crack.

Strain-life Test Results

Raw data from all strain-life tests is included in Attachment 2. Of the 19 A36 specimens cycled, two were suspended at 2 million cycles without failure. Table 2 lists the key strain-life parameters with 95% confidence limits. Figures 3 through 6 plot the strain-life data. Figure 3 is the elastic strain-life (Basquin's) data. Figure 4 is the plastic strain-life curve (Coffin-Manson). Figure 5 is the full strain-life data set, and Figure 6 is the cyclic stress-strain curve. The 95% confidence limits on the fatigue strength coefficient, fatigue strength exponent, fatigue ductility coefficient and fatigue ductility exponent, are also shown in Figures 3 through 5.

The strain-life (Manson-Coffin) curve shown in Figure 4 relates total cyclic strain amplitude to fatigue life as follows:

$$\Delta\varepsilon/2 = \sigma'_f/E(2N_f)^b + \varepsilon'_f(2N_f)^c \qquad [4]$$

where

$2N_f$ = reversals to failure
σ'_f = fatigue strength coefficient
b = fatigue strength exponent (Basquin's exponent)
ε'_f = fatigue ductility coefficient
c = fatigue ductility exponent

The curve-fit parameters in Figures 3 through 5 were calculated using the least-squares algorithm with log of true strain amplitude as the independent variable and log of reversals to failure as the dependent variable. The elastic modulus used to calculate the fatigue strength coefficient was assumed to be 29,500,000 psi. Both the plastic and elastic strain life curves met the F statistic Linearity Test specified in ASTM E739-91.

None of the failures appeared to be directly associated with the damage caused by extensometer knife edges, indicating that the solder tabs were effective in protecting the sample from extensometer knife-edge contact.

RESULTS—Strain-life Test Results

Table 2 — Strain-life parameters with 95% confidence limits and cyclic stress-strain parameters

A36 cyclic properties	Mean	Lower 95% confidence limit	Upper 95% confidence limit	Units
*Cyclic strength coefficient *K'*	128,900	—	—	psi
*Cyclic strain hardening exponent *n'*	0.149	—	—	
**Cyclic strength coefficient *K'*	166,500	—	—	psi
**Cyclic strain hardening exponent *n'*	0.189	—	—	
Cyclic (0.2%) yield strength *Sy'*	50,900	—	—	psi
Fatigue ductility coefficient *ε'f*	0.6262	0.4634	0.88	
Fatigue ductility exponent *c*	–0.5437	–0.5161	–0.5744	
Fatigue strength coefficient *σ'f*	152,434	137,295	173,397	psi
Fatigue strength exponent *b*	–0.1028	–0.0931	–0.1148	
Assumed elastic modulus *E*	29,500	—	—	psi

*Values obtained from curve fit of data points
** Values obtained through application of power law relationship

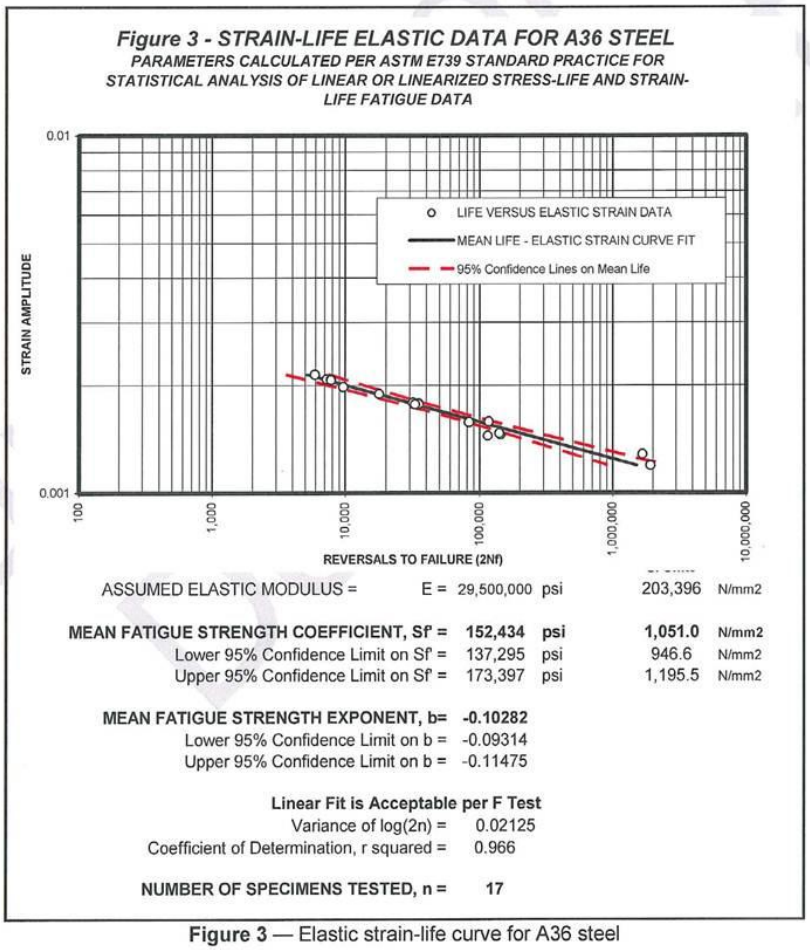

Figure 3 — Elastic strain-life curve for A36 steel

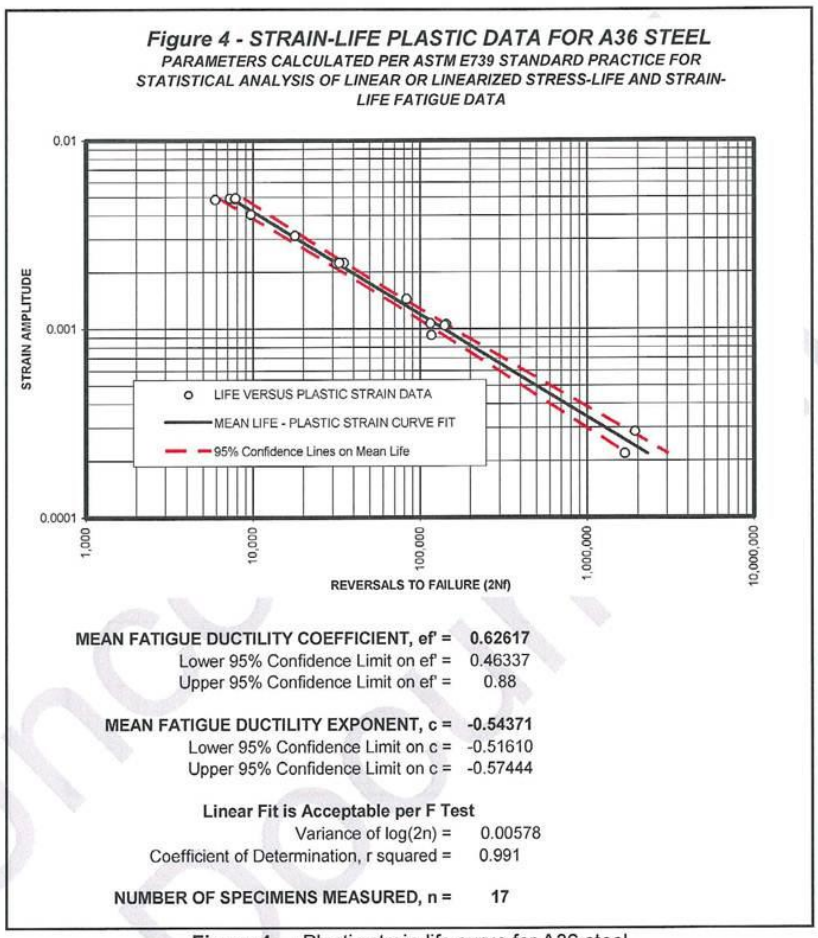

Figure 4 — Plastic strain-life curve for A36 steel

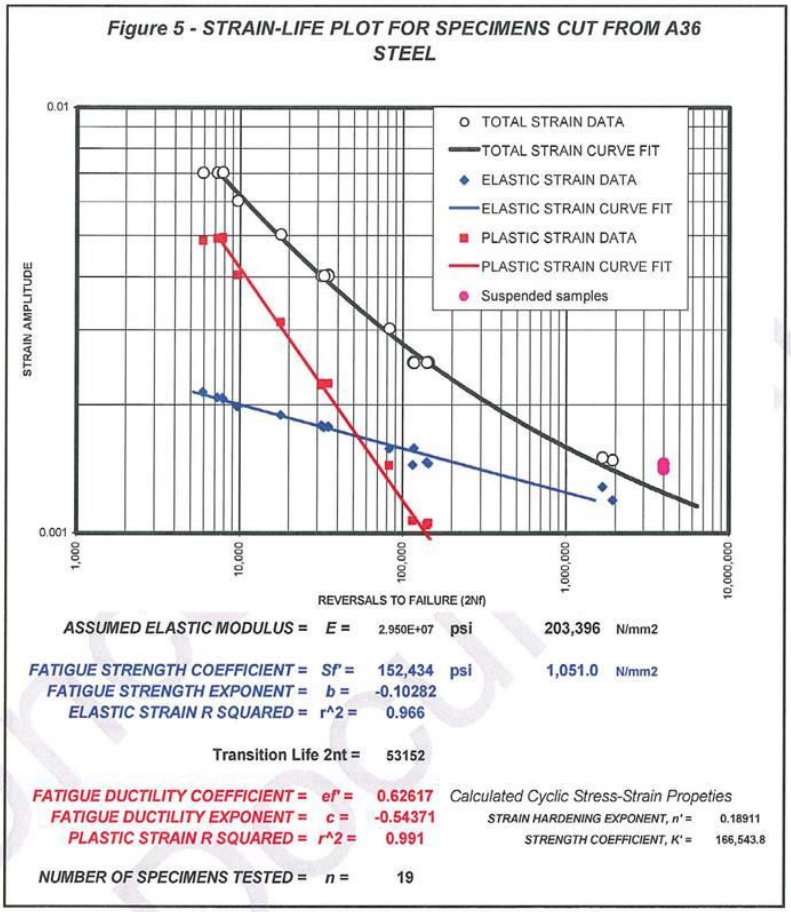

Figure 5 — Total strain-life curve for A36 steel

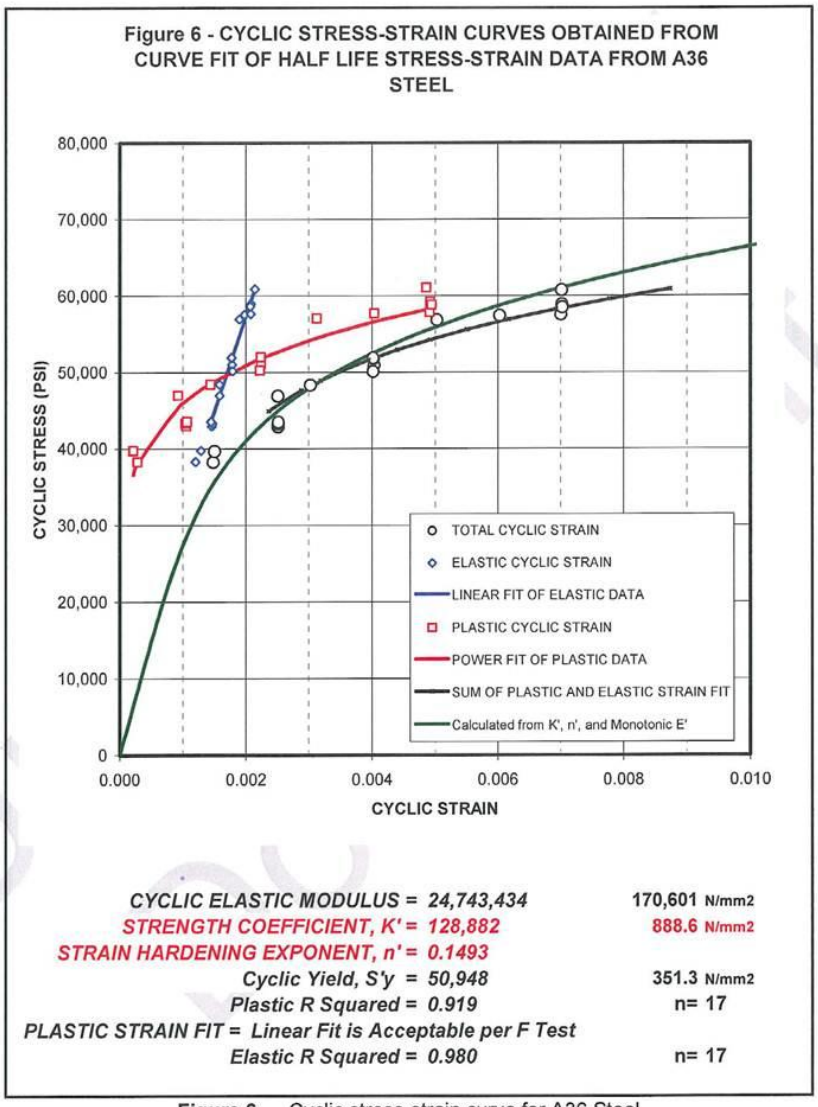

Figure 6 — Cyclic stress-strain curve for A36 Steel

Cyclic Stress-strain

The plastic strain should follow the power-law function:

$$\sigma = K'(\varepsilon_p)^{n'} \quad [5]$$

where

σ = cyclically stable true stress amplitude
K' = cyclic strength coefficient
n' = cyclic strain hardening exponent
ε_p = cyclically stable true plastic strain amplitude

The cyclic plastic curve met the F statistic Linearity Test specified in ASTM E739-91. The values for cyclic strength coefficient (K') and cyclic strain hardening exponent (n') should be related to the strain-life parameters as follows:

$$K' = \sigma_f/(\varepsilon_f)^{n'} \quad [6]$$

and

$$n' = b/c \quad [7]$$

The values from the above equations are only approximately equivalent to the values obtained from the power-law linearized curve fits.

Figure 6 shows the cyclic stress-strain curve for A36 steel.

Elastic modulus: Neither the strain-life test procedure nor the monotonic test procedure was designed to definitively measure the elastic modulus. However, the average first-quarter elastic modulus measured during the strain-life testing for A36 was 31,400,000 psi, which compares well with the assumed value of 29,500,000 psi.

Sample Size and Replication

Nineteen specimens were used for the A36 plots, resulting in an effective replication rate of 74 percent. (% replication = 100[1 – (total number of different stress or strain levels used in testing/total number of specimens tested)]). Sampling and replication guidelines are given in ASTM E739. This standard states that 12 to 24 specimens and 75% to 88% replication are the minimum for reliability data. A minimum of 50% to 75% replication with 12 to 24 specimens is recommended for design allowable data. A minimum replication of 33% to 50% with 6 to 12 specimens is recommended for research and development testing. The sample size and replication rate for this study indicate that the results are suitable for design allowable data.

Hardness, chemistry, and microstructure were not measured as part of this material characterization.

CONCLUSIONS

This data set represents reasonable strain-life fatigue properties for A36 steel.

Attachment 1

Drawing TC94-032-04

Attachment 1: Drawing TC94-032-04

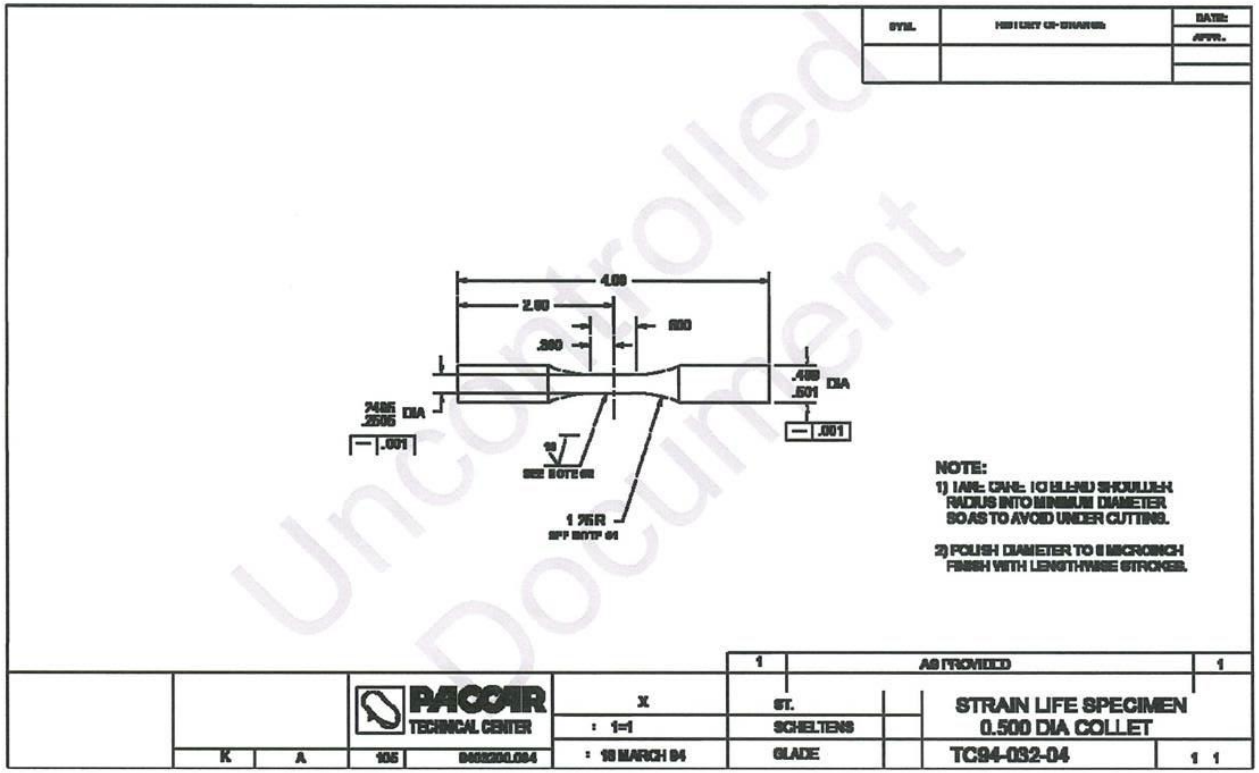

Attachment 2

Raw Data

Appendix 2

A36 Steel Raw Fatigue Data - Tested to 30% Reduction in Load

Specimen I.D.	Strain Amplitude	DIA (inch)	Frequency (Hertz)	Loading Modulus (psi)	Unloading Modulus (psi)	1st 1/4 Cycle Elastic Modulus (psi)	Mid Life Mod (psi)	Maximum Stress (psi)	Minimum Stress (psi)	Maximum Strain	Minimum Strain	Calculated Inelastic Strain Range	Calculated Elastic Strain Range	Measured Inelastic Strain Amplitude	Measured Elastic Strain Amplitude	Reversals to Failure	Cyclic Stress (psi)	Total Strain Amplitude
a36-02	0.0060	0.2464	0.34	31,535,700	31,477,100	31,524,100	28,930,100	56,635	-57,485	0.00602	-0.00604	0.00812	0.00395	0.00405	0.00199	9,668	57,426	0.00603
a36-01	0.0040	0.2469	0.50	9,776,250	13,494,900	30,451,200	28,544,200	49,949	-50,509	0.00397	-0.00409	0.00454	0.00352	0.00225	0.00179	34,908	50,951	0.00403
a36-03	0.0030	0.2440	0.50	31,761,800	31,801,800	31,821,700	30,558,900	46,137	-46,760	0.00302	-0.00303	0.00301	0.00304	0.00144	0.00158	82,792	48,324	0.00302
a36-04	0.0050	0.2458	0.40	32,174,700	32,153,900	31,785,000	29,942,900	55,400	-56,189	0.00499	-0.00507	0.00633	0.00373	0.00313	0.00190	17,834	56,832	0.00503
a36-05	0.0025	0.2475	0.80	31,014,000	30,938,700	30,909,700	29,372,600	41,700	-42,281	0.00247	-0.00256	0.00217	0.00286	0.00106	0.00146	143,526	42,899	0.00252
a36-06	0.0015	0.2443	1.30	32,637,600	32,848,000	32,699,100	31,958,800	37,583	-38,079	0.00146	-0.00151	0.00060	0.00237	0.00029	0.00120	1,929,498	38,255	0.00148
a36-07	0.0070	0.2440	0.29	31,496,900	31,603,400	31,729,200	28,229,400	59,263	-60,336	0.00702	-0.00703	0.00981	0.00424	0.00494	0.00209	7,244	58,858	0.00702
a36-08	0.0025	0.2465	0.80	31,098,600	31,156,700	31,084,300	29,401,500	42,349	-42,608	0.00250	-0.00253	0.00214	0.00290	0.00104	0.00147	140,084	43,250	0.00252
a36-09	0.0070	0.2465	0.29	31,210,000	31,100,400	31,078,400	27,649,500	58,651	-59,257	0.00697	-0.00704	0.00975	0.00426	0.00493	0.00208	7,788	57,539	0.00701
a36-11	0.0040	0.2445	0.50	31,220,700	31,567,200	31,244,000	29,151,000	50,686	-51,260	0.00403	-0.00402	0.00454	0.00350	0.00224	0.00178	35,006	51,769	0.00402
a36-12	0.0070	0.2432	0.29	31,910,000	31,900,800	31,661,600	28,208,600	59,154	-60,451	0.00703	-0.00703	0.00982	0.00424	0.00496	0.00207	7,628	58,491	0.00703
a36-13	0.0025	0.2450	0.80	31,698,400	31,902,100	31,907,700	30,023,800	42,718	-43,113	0.00251	-0.00253	0.00218	0.00286	0.00107	0.00145	114,946	43,469	0.00252
a36-14	0.0040	0.2445	0.50	30,355,100	30,278,600	30,419,900	27,972,600	49,778	-50,120	0.00401	-0.00403	0.00447	0.00357	0.00223	0.00179	31,764	50,127	0.00402
a36-15	0.0015	0.2432	4.00	32,184,200	31,207,200	31,757,200	30,879,400	42,288	-36,330	0.00149	-0.00152	0.00046	0.00255	0.00022	0.00129	1,674,760	39,711	0.00150
a36-17	0.0040	0.2420	0.50	31,051,100	31,182,800	31,308,200	29,236,900	50,849	-51,381	0.00400	-0.00403	0.00454	0.00350	0.00224	0.00177	32,872	51,666	0.00402
a36-18	0.0070	0.2447	0.29	30,823,200	31,192,500	31,182,800	28,293,500	60,651	-61,651	0.00701	-0.00703	0.00971	0.00433	0.00487	0.00215	5,910	60,746	0.00702
a36-19	0.0025	0.2455	0.80	30,394,000	30,682,400	30,514,700	29,568,900	45,763	-46,421	0.00251	-0.00252	0.00191	0.00312	0.00093	0.00159	116,884	46,911	0.00251
			Average	30,137,779	30,380,500	31,357,576	29,289,565											
			Std Dev	5,283,365	4,391,743	598,367	1,138,600											

A36 Samples Suspended Without Failure

Specimen I.D.	Strain Amplitude	DIA (inch)	Frequency (Hertz)	Loading Modulus (psi)	Unloading Modulus (psi)	1st 1/4 Cycle Elastic Modulus (psi)	Mid Life Mod (psi)	Maximum Stress (psi)	Minimum Stress (psi)	Maximum Strain	Minimum Strain	Calculated Inelastic Strain Range	Calculated Elastic Strain Range	Measured Inelastic Strain Amplitude	Measured Elastic Strain Amplitude	Reversals to Failure*	Cyclic Stress (psi)	Total Strain Amplitude
a36-10	0.0015	0.2450	4.00	31,574,500	31,722,800	31,891,300	31,855,600	43,717	-45,748	0.00139	-0.00144	0.00002	0.00281	0.00000	0.00141	4,000,000	45,028	0.00141
a36-16	0.0015	0.2420	4.00	31,370,500	31,462,600	31,517,900	30,908,500	36,606	-36,892	0.00144	-0.00147	0.00053	0.00238	0.00025	0.00121	4,000,000	37,291	0.00146
																*did not fail		

Attachment 3

Instrumentation

Attachment 3: Instrumentation

PACCAR TECHNICAL CENTER

Save this sheet as: IDS_*Proj#_Configuration.xls*

Data Systems
Instrumentation Data Sheet (IDS)

Project number:	TC07-500-248		**Sample rate:**	409.6	**Filter rate:**	80hz			
Project Title:	Durability Correlation		**Transaction#:**						
Project Manager:	Mark Van Sickle		**Truck#:**		**Axle**	**Steer**	**Drive**	**Trailer**	**Total**
Data Systems Technician:			**Trailer#:**		**Weights:**				0
Vehicle Op's Technician:			**Test notes:**						
Structures Lab Technician:	Ralph Beaufort		Strain-life testing done in the MTS model 810 hydraulic load frame						
Date sheet saved:	06 07 2007								

TEST CH #'s	DATA ACQU. CH. NO.	LOCATION/ DESCRIPTION	SENSOR TYPE	MIN VALUE	MAX VALUE	SHUNT RES	CAL VALUE	GAGE/trans PTC DIRECTION	GAGE/trans PTC NUMBER	DATA ACQU. PTC NO.	OTHER
1	NA	Load frame load cell (5k)	Load Cell	-5k	5k					3939	
2	NA	Monotonic testing extensometer MTS model 632-12B-20 - cal per use	Extensometer							0909	SN 386
3	N/A	Strain-life testing extensometer MTS model 632-26 - cal per use	Extensometer							6104	SN 442
4											

Appendix 5 Chart 2.30a From Peterson's Stress Concentration Factors (Pilkey, 2008)

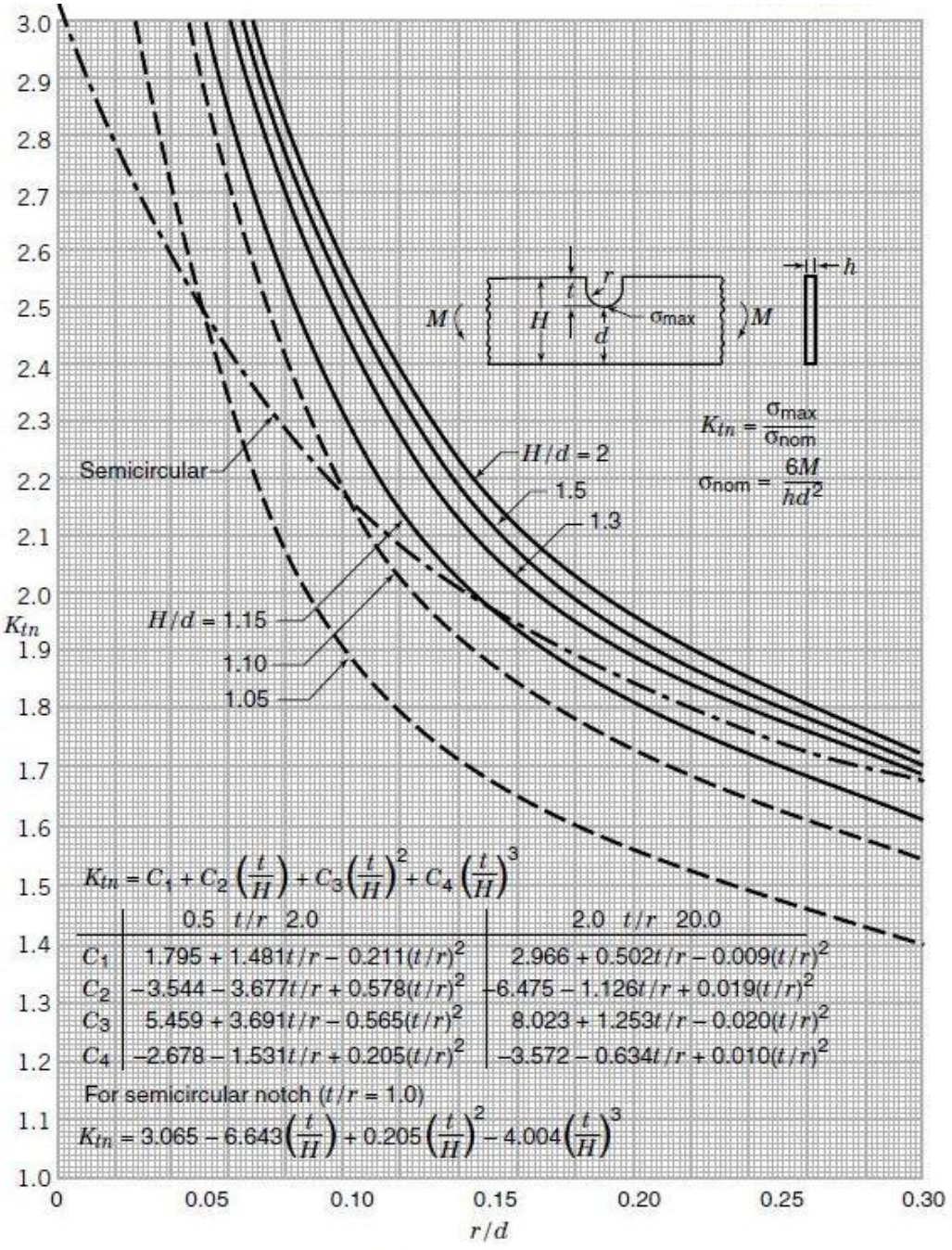

Chart 2.30a Bending of a thin beam element with a notch on one side (Leven and Frocht 1953): stress concentration factors K_{tn} for a U-shaped notch.

Appendix 6 Interim Materials Lab Report – Baseline and Hammer Peened Samples

INTEROFFICE COMMUNICATION
TECHNICAL CENTER

REF: ML12-132
9 July 2012

TO: Mark Van Sickle, PACCAR Technical Center

FROM: Wes Graham

SUBJECT: Analysis of Fillet Weld Characteristics Before and After Hammer Peening
TC11-500-212

TESTS CONDUCTED

- Overall photographs, as received
- Macro-photography
- Microhardness testing
- Metallography

BACKGROUND

A PACCAR Technical Center (PTC) structures project was initiated to evaluate the potential fatigue life benefit of field-capable shot or hammer peening of structural weld joints. Two steel samples made from ASTM A36 and configured as fillet welded T-joints that had undergone fatigue testing were submitted to the Materials Laboratory for analysis. One of the samples was cycled in the unpeened condition to represent a baseline, while the second sample had been hammer peened. The two samples represented distinctly different fatigue lives, and that is the focus of the analysis.

SUMMARY and CONCLUSIONS

- The two samples arrived for analysis as shown in Figure 1. Also see Figures 2 and 3.
  - The unpeened sample had fractured at the weld toe, initiating in the base metal HAZ.
  - The hammer peened sample arrived unbroken with crack initiation in the weld nugget.
- The hammer peened sample showed an improved strength based on hardness, compared with the unpeened. This is judged to be the consequence of work hardening; results are plotted in Figure 4.
- An informal summary was provided to the requester earlier, and is included as an attachment in this report.

RECOMMENDATIONS

It will be useful to obtain a similar comparison of fatigue benefit related to flap or shot peening of the weld toe. Flap (or shot) peening would be expected to produce a higher compressive stress at the surface, while hammer peening likely drives the maximum compressive stress to a greater subsurface depth, presumed to produce a surface less protected by the objective: a high compressive residual stress.

Approval signature on file
Wes Graham
Metallurgical Engineer
(360) 757-5347

Approval signature on file
Kirk Dunn
Supervisor – Structural Materials
(360) 757-5317

TO: Mark Van Sickle
REF: ML12-132

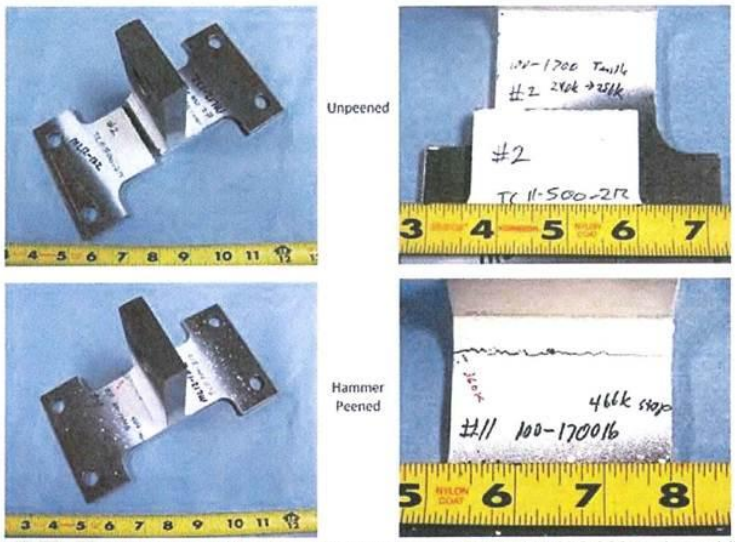

Figure1 — The reference unpeened fillet welds shown at the top fractured in 256,000 cycles, while the hammer peened welds at the bottom were cycled to 466,000 before cracking.

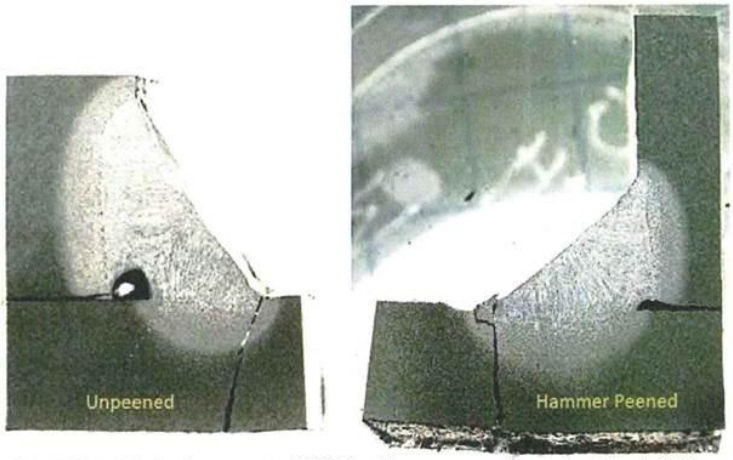

Figure 2 — Cracking initiated in the base material HAZ of the unpeened sample at the left. It appears that cracking initiated near the weld toe in the weld nugget before deviating, as shown for the hammer peened sample at the right.

TO: Mark Van Sickle
REF: ML12-132

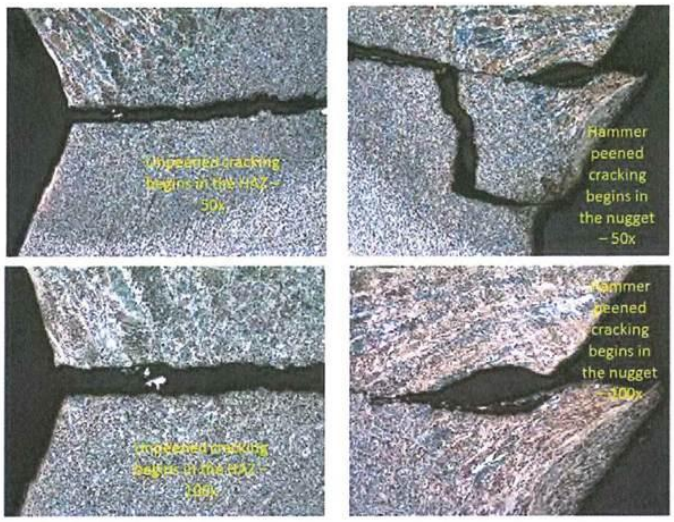

Figure 3 — Close-ups of the unpeened and hammer peened fracture paths are shown at the left and right, respectively. Etched in 2% Nital and originally imaged at 50x (top) and 100 x (bottom).

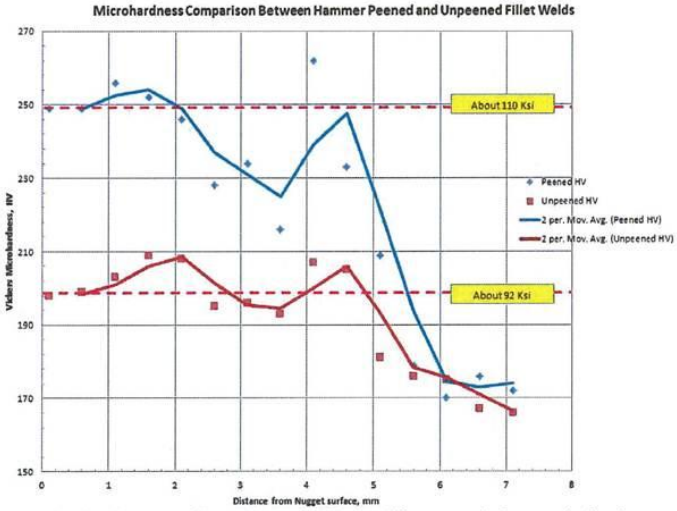

Figure 4 — Vickers microhardness profiles reflect significant differences before and after hammer peening.

Attachment 1 is a PowerPoint summary of analytical results previously shared with the requester.

TO: Mark Van Sickle
REF: ML12-132

Attachment 1: Summary of Analytical Results

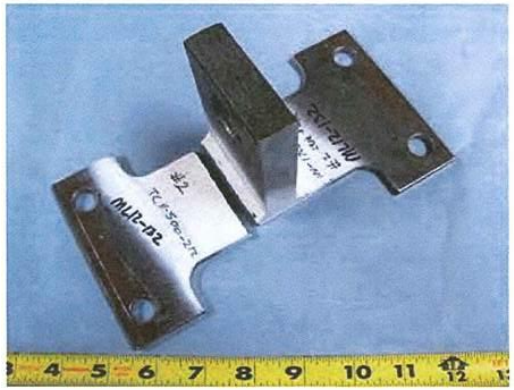

Unpeened

Hammer Peened

TO: Mark Van Sickle
REF: ML12-132

Attachment 1: Summary of Analytical Results

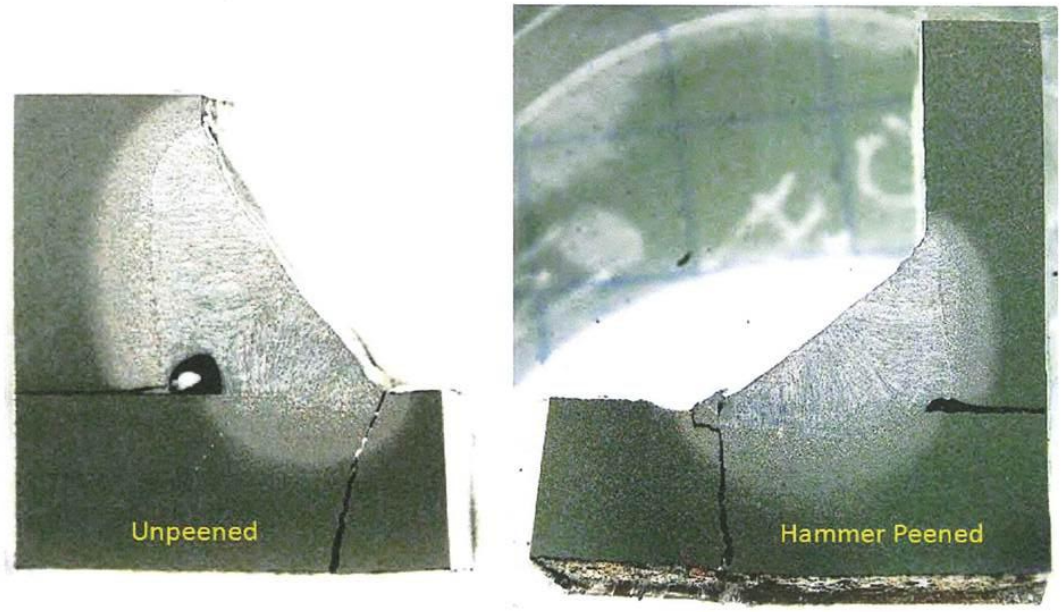

TO: Mark Van Sickle
REF: ML12-132

Attachment 1: Summary of Analytical Results

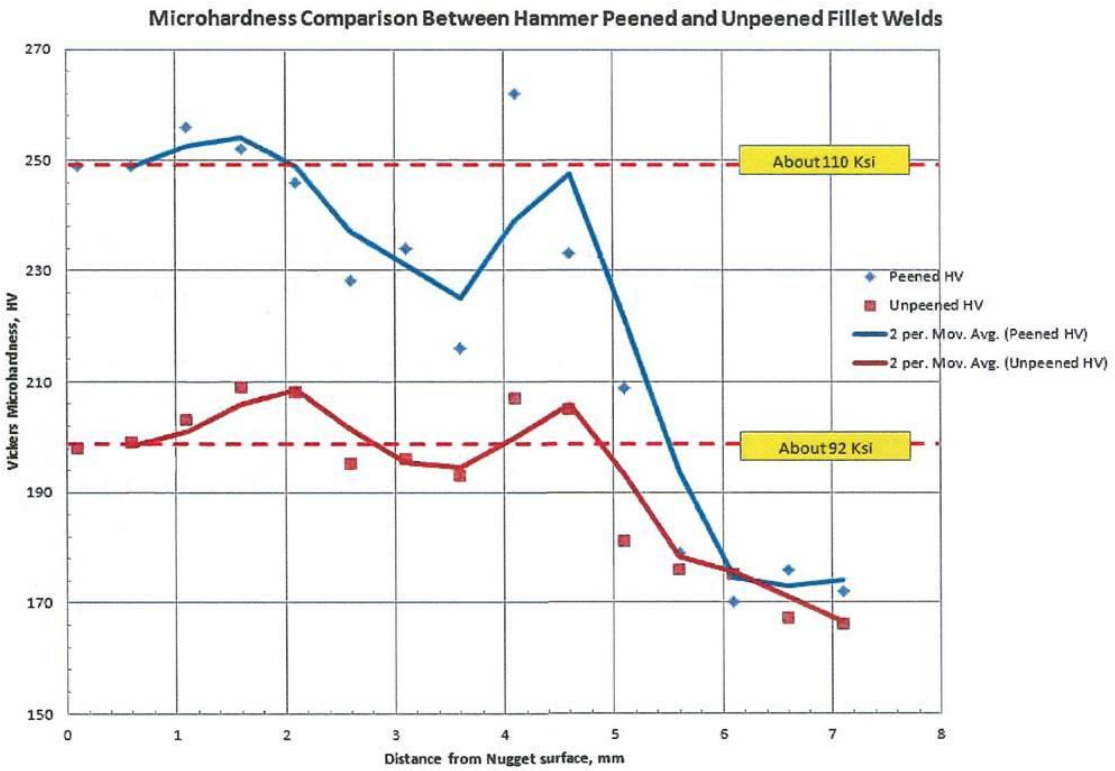

TO: Mark Van Sickle
REF: ML12-132

Attachment 1: Summary of Analytical Results

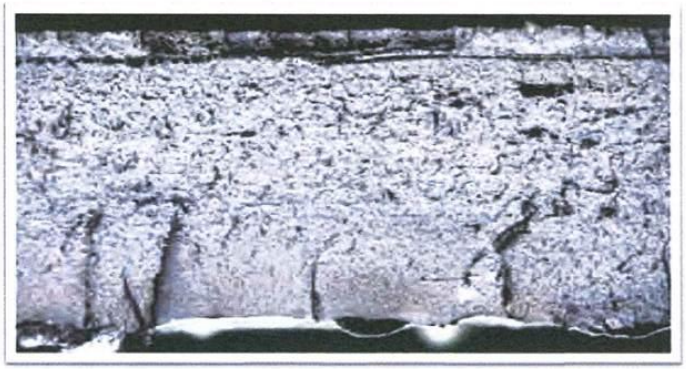

It appears that slow fatigue growth extended deeper into the weld toe area when hammer peened (above) than that when unpeened (below). This may be associated with work hardening that increased the fatigue strength of the weld nugget from ~ 92 Ksi to ~110 Ksi (see Vickers hardness data).

Originally photographed approximately at mid-width of the fracture at 20x magnification. Crack growth was upward in the photos.

TO: Mark Van Sickle
REF: ML12-132

Attachment 1: Summary of Analytical Results

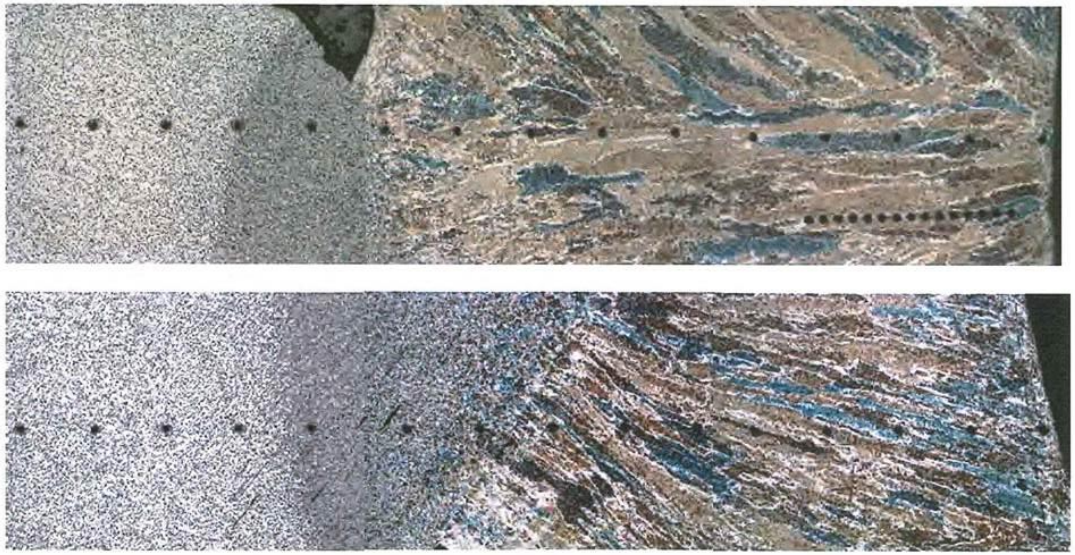

Here are the Vickers microhardness traces for the hammer peened (upper) and unpeened samples. The traces and plots begin at the surface of the nugget and traverse L to R through the HAZ to base metal. One can associate spikes with the indent locations here, and so noting that the HAZ and transition areas are harder. I can't say with certainty if the harder nugget after peening is the result of work hardening, but that is a possibility.

TO: Mark Van Sickle
REF: ML12-132

Attachment 1: Summary of Analytical Results